NEW SUBGRID MODELS FOR INERTIAL PARTICLES IN LARGE-EDDY SIMULATIONS OF TURBULENT FLOWS

A Dissertation

Presented to the Faculty of the Graduate School

of Cornell University

in Partial Fulfillment of the Requirements for the Degree of

Doctor of Philosophy

by

Baidurja Ray

August 2013

NEW SUBGRID MODELS FOR INERTIAL PARTICLES IN LARGE-EDDY SIMULATIONS OF TURBULENT FLOWS

Baidurja Ray, Ph.D.

Cornell University 2013

An initially uniform distribution of inertial particles will spontaneously organize themselves into clusters in a turbulent flow, driven primarily by the small-scale turbulent fluctuations. Accurate prediction of such clustering of inertial particles, along with their relative velocity statistics, is essential for computing their binary collision rates, an important quantity that determines the evolution of the size distribution of these particles, under conditions when collisions lead to agglomeration or coalescence. In large-eddy simulations (LES) of turbulent flows, only the large-scale turbulent fluctuations are represented on the grid whereas the small-scales (or subgrid scales) need to be modeled. None of the existing LES subgrid models are able to accurately predict the particle collision rates across the entire range of particle inertia, where inertia is parameterized by the Stokes number (St) defined as the ratio of the particle response time to the Kolmogorov time-scale (τ_η). In this work, we present new subgrid models designed to recover the clustering and relative velocity statistics of inertial particles. We begin by considering the effect of the subgrid scales on our statistics of interest. We do this by analyzing the exact distribution of particles obtained from direct numerical simulations (DNS) and comparing them with the ones obtained from a filtered DNS (FDNS). FDNS is obtained by filtering out the 'subgrid' scales and represents a 'perfect' LES with an exact representation of the large-scales (free of any subgrid modeling error). This provides a benchmark study and points to the need of incorporating the mech-

anism by which the small-scales affect particle statistics, into the LES subgrid models designed to recover clustering and relative velocities of inertial particles. We then consider a subgrid model based on kinematic simulations of turbulence (so-called KSSGM), and show that it can accurately predict the relative velocity statistics for all St, but can capture clustering only for $St \geq 2.0$. We investigate the reasons for its failure to predict clustering at $St < 2.0$, and identify the important small-scale statistics that a subgrid model needs to predict in order to capture clustering correctly. We conclude that none of the existing subgrid models are capable of recovering the necessary small-scale statistics, and recognize the difficulty in doing so in a single-particle framework. We therefore shift our attention to a two-particle framework, based on the understanding that clustering is driven by two-point dynamics, and the recognition that all of the existing theories of particle clustering and collisions are formulated in this framework. We then develop a novel satellite particle simulation (SPS) methodology that allows us to efficiently simulate pair-wise interactions of particles in turbulence, thereby providing an ideal test-bed for the development and testing of two-particle models. We derive models from existing theories of inertial particle clustering primarily focussing on low St, and test them using the SPS. We analyze a class of models, that are referred to as Drift-Diffusion Models (DDMs), and show how they can be derived from statistical mechanical theories of clustering. We consider the theories by Chun et al. (2005) (CT) and Zaichik and Alipchenkov (2009) (ZT). We show that the DDM-CT gives good results for $St \leq 0.05$, whereas the DDM-ZT works well for $St \leq 0.2$. Such models represent an entirely new framework for subgrid modeling of inertial particle motion in a LES, and the initial results provide strong evidence regarding the viability of such an approach. Finally, we discuss some issues related to implementing these two-particle models in a single-particle tracking framework.

BIOGRAPHICAL SKETCH

Baidurja Ray was born on April 17, 1983 in the city of Kolkata (formerly Calcutta), located on the shores of the Hooghly river in eastern India. His entire schooling was done at South Point (Junior and High) School in the same city. He was fortunate to have had some amazing teachers and talented peers at South Point, who inspired him to seek out the very best in himself. A growing interest in physics and its applications led him to pursue a Bachelors degree in Mechanical Engineering at Jadavpur University, Kolkata. Having narrowed his interest down to thermal and fluid sciences, he went on to pursue a Masters degree at the Indian Institute of Science (IISc), Bangalore. While doing applied combustion research at IISc, he realized that without a deeper fundamental understanding of the science, his engineering capabilities would be constrained. This resulted in applications to U.S. universities for admission to Ph.D. programs, culminating in the acceptance of an offer from Cornell University. For the past (almost) five years at Cornell, he has been engaged in research in the rich and interesting field of particle-laden turbulent flows under the guidance of Prof. Lance Collins.

ACKNOWLEDGEMENTS

The (almost) five years I spent as a graduate student at Cornell, has been a period of growth for me, both in terms of my academic knowledge, experience and perspective, but also in terms of personal development, and there are plenty of people that I have to thank for it.

The Ph.D. advisor is (arguably) the most important determinant of the performance of a Ph.D. student. I am extremely grateful to Professor Lance R. Collins, for acting as an inspirational and motivational figure throughout my time as a Ph.D. student. His deep knowledge, intuition and passion for research, his amazing ability to project calmness under all circumstances, and his trust and support towards his students, have earned my deepest respect. I am grateful to him for the time he devoted towards guiding me in my research despite heavy administrative workloads (first as a chair, and then as a dean). I hope I have incorporated some of his deep, fundamental approach towards engineering problems and his ability to convey a compelling storyline while writing research papers. I sincerely thank him for making my Ph.D. work and life at Cornell, such a cherished and rewarding experience.

I also thank the other members of my Special Committee, Professor Zellman Warhaft and Professor Peter J. Diamessis. In addition to being a pioneering researcher in his field, Professor Warhaft is a wonderful human being and it has been a pleasure interacting with him about work, life and the environment (which he deeply cares about). Professor Diamessis has been a friend and mentor for me. He has always been very kind to me, and has always motivated me by his rootedness and humanity, despite being one of the leading researchers in his field. I have learned so much from the long discussions with him about work and life, and will cherish them always.

I thank the National Science Foundation (NSF) for supporting my research through grants CBET 0756510 and 0967349, and the Texas Advanced Computing Center (TACC) for providing outstanding computing resources on Ranger, Spur, Longhorn and Stampede. I thank the graduate school at Cornell for partially funding my conference travels, and the Sibley School of Mechanical and Aerospace Engineering for providing funding through teaching assistantships and the Olin Fellowship.

I would like to thank Dr. Rajesh Bhaskaran and Dr. Kimberly Williams, for their support and guidance through my work as part of the Graduate Research and Teaching Fellowship (GRTF), and the Center for Teaching Excellence for providing funding. It was an important and enjoyable learning experience for me. I thank Jayasri, and the entire grad group at 'EARS Beginning Training' in Spring 2009, which will remain one of my best memories of Cornell. I have been fortunate to have made some amazing new friends (and continued some old friendships) during my time in the U.S. Thank you to Peter, Michelle, Andy, Varun, Ranjith, Qi, Sayak, Adhiraj, Dwaipayan, Devranjan, Suvajyoti, and Snehaunshu, to name some of them. I also thank Professor Ashim Datta for engaging in frank and honest discussions about life in the U.S., and to Professor Rajarshi Roy at UMD, for an unforgettable series of informal meetings and interactions. I concede the possibility of leaving out someone deserving an acknowledgement, and provide an apology in advance.

I thank my family and my brother for being the extremely supportive and wonderful people that they are. Lastly, and most importantly, I thank my wife Ishita for being the constant source of support, love, inspiration, and guidance. She has been the single most important source of comfort and motivation for me throughout the last five years, which has helped me traverse the journey called

'getting a Ph.D.' successfully.

TABLE OF CONTENTS

LIST OF TABLES

LIST OF FIGURES

CHAPTER 1

INTRODUCTION

1.1 Particle-laden turbulent flow

Particle-laden turbulent flows are ubiquitous in both natural and engineering systems (Crowe et al., 1998; Crowe, 2005). Some examples of natural systems include the turbulent air-flow laden with water and/or ice droplets in clouds (Shaw, 2003), dispersion of smoke and pollutants in the atmosphere, transport of contaminants and/or biological specimens (like algae) in rivers and oceans, transport and deposition of aerosols inhaled into the human airway (Li et al., 1996), and the formation of planets from protoplanetary disks (Johansen et al., 2007). Some common engineering applications include powder manufacturing based on aerosol processes (Moody and Collins, 2003), spray combustion in engines and turbines (Caraeni et al., 2000), transport and deposition of sand and other contaminants in oil pipelines, and gas-solid flows in fluidized bed reactors (Taghipour et al., 2005).

While the results of this work are applicable to a wide range of particle-laden flows, we are especially interested in understanding the role turbulence plays in the evolution of atmospheric clouds. Figure 1.1 shows a typical cumulus cloud, identifying our region of interest. In this work, we will be focussed on the core region of such a cloud, and approximate the flow there as homogeneous, isotropic turbulence simulated on a periodic cube. We will approximate the cloud droplets as point particles with finite inertia, and ignore any thermodynamic effects such as evaporation, condensation, etc. The droplet size distribution in cumulus clouds is known to affect its 'time-to-rain'. It is believed that particle clustering (described below) plays a crucial role in the broadening of the droplet size distribution in

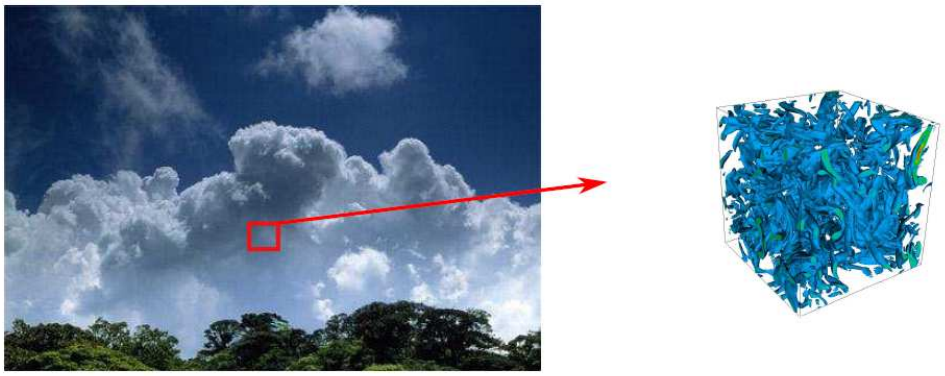

Figure 1.1: A typical cumulus cloud in the atmosphere. We are interested in the core of such a cloud. As indicated in the figure, we approximate the flow there as homogeneous, isotropic turbulence in a periodic cube. *Image credit: http://photography.nationalgeographic.com.*

warm cumulus clouds, during both condensational growth and growth by collision and coalescence (Pinsky and Khain, 1997; Shaw et al., 1998; Reade and Collins, 2000a,b; Falkovich et al., 2002; Shaw, 2003; Devenish et al., 2012; Grabowski and Wang, 2012). Correctly accounting for turbulence induced collisions will improve the predictions of warm rain initiation from cumulus clouds.

1.2 Clustering and collision rate of inertial particles

An initially uniform distribution of particles, suspended in an isotropic turbulent flow organizes themselves into spatial clusters. This phenomena is known as preferential concentration or clustering, and has been observed both experimentally (Fessler et al., 1994; Salazar et al., 2008; Saw et al., 2008; Gibert et al., 2012; Bateson and Aliseda, 2012; Saw et al., 2012) and numerically (e.g., Maxey, 1987; Squires and Eaton, 1991; Wang and Maxey, 1993; Eaton and Fessler, 1994; Sundaram and Collins, 1997) in a variety of turbulent flows, including inhomogeneous and anisotropic flows. Early work on particle clustering (Maxey, 1987; Eaton and

Fessler, 1994) identified the 'centrifuging' as the primary mechanism of clustering, whereby the particles, due to their inertia, cannot follow the highly curved streamlines in regions of high vorticity and are ejected out of those regions by centrifugal forces. They are then found to accumulate in the straining regions of the flow.

In order to demonstrate this mechanism, consider the simple case of a particle-pair subjected to pure strain and pure rotation. We consider a two-dimensional fluctuating pure strain and pure rotation flow fields as follows:
Pure strain:

$$\begin{aligned} u &= \ xsin(\omega t) \\ v &= -\ ysin(\omega t) \end{aligned} \tag{1.1a}$$

Pure rotation:

$$\begin{aligned} u &= -\ ysin(\omega t) \\ v &= \ xsin(\omega t) \end{aligned} \tag{1.1b}$$

We arbitrarily choose the frequency of the fluctuations to be $\omega = 10$ rad/s. Then, the characteristic time-scale of these flows is given by $\tau = 2\pi/\omega$ s. We introduce two particles at random positions in these flow fields, and watch them evolve. Throughout this work, we will use the following equation of motion for inertial particles (Maxey and Riley, 1983)

$$d\boldsymbol{u}^p/dt = (\boldsymbol{u}^f - \boldsymbol{u}^p)/\tau_p\,,$$

where $\boldsymbol{u}^p$ is the particle velocity vector, $\boldsymbol{u}^f = [u \quad v]$ is the fluid velocity vector, and τ_p is the particle response time (for more details, see §2.3.3). We set the particle response time to be equal to the time-scale of the underlying flow, i.e., $\tau_p = \tau$. Then, the evolution of the particle-pair with time is shown in figure 1.2. We see that in a purely rotating flow, the particles diffuse away from each other, whereas in a purely straining flow, they drift towards each other. The qualitative

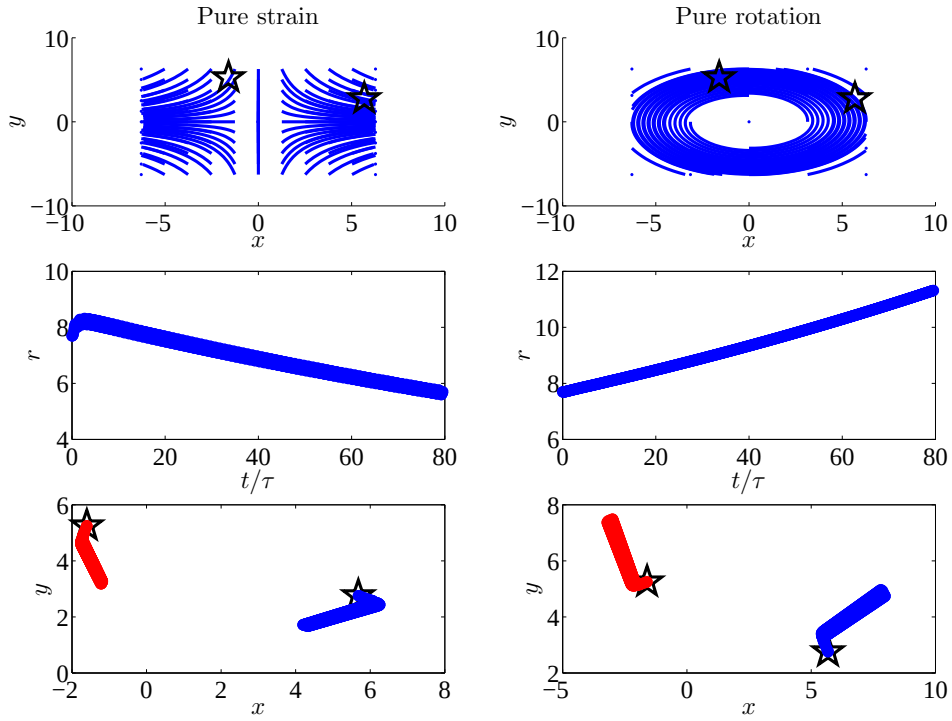

Figure 1.2: The left panel shows results from a pure strain flow, while the right panel shows pure rotation. The black stars denote the initial positions of the two particles. r denotes their separation evolving as a function of time. The bottom panel indicates in blue and red, the evolution of the position of the two particles respectively, starting from their initial position. Here $\omega = 10$ rad/s.

nature of the results are independent of the initial positions of the particles. This conceptually illustrates how inertial particles in turbulence tend to avoid regions of high vorticity, and preferentially accumulate in regions of high strain. We will refer to an 'inward drift' causing particle-pairs to move toward each other and cluster, and an 'outward diffusion' causing particle-pairs to move away from each other.

Although centrifuging is still believed to be the primary mechanism of clustering for small St particles, recent findings (see Bragg and Collins (2013a) and references therein) suggest other mechanisms such as the 'history effect' are important, particularly at higher St. Here, St denotes the Stokes number, defined to be the ratio of the particle response time to the Kolmogorov time-scale. In this work,

the Stokes number is used as a non-dimensional measure of the particle's inertia. We will consider the effect of turbulence on both high and low St particles. High St or 'heavy' particles are ubiquitous in nature and industry. Examples include droplets in *highly* turbulent clouds, pollutants in the atmosphere, and aerosols in powder manufacturing processes. Droplets in warm cumulus clouds typically lie in the low St regime.

An important statistical measure of particle clustering is the radial distribution function or RDF (McQuarrie, 1976). The RDF can be computed from a field of Q particles by sorting them into spherical bins around each particle, and calculating the average number of particles per unit volume in each bin normalized by the total number of particle pairs per unit volume in the system (figure 1.3). Therefore, the

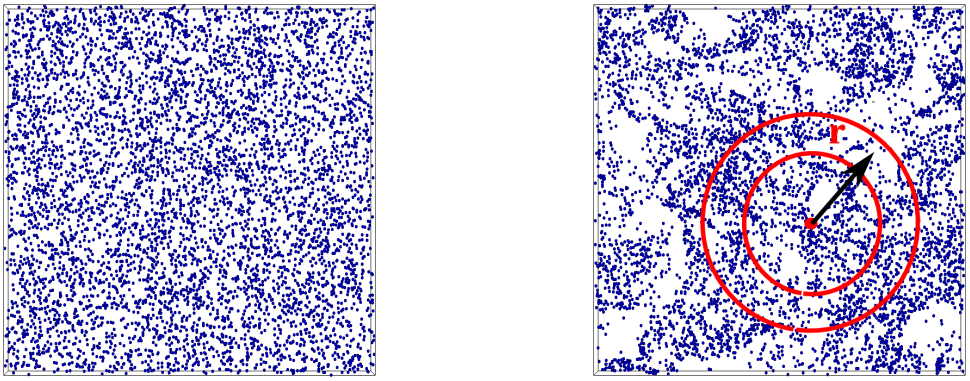

(a) (b)

Figure 1.3: Sketch to illustrate calculation of the RDF. (a) A uniform distribution of particles with RDF of unity. (b) A clustered distribution of particles with a spatially varying RDF. The particle field is divided into spherical bins around each particle. Then the number of particles per unit volume is computed for each bin. This procedure is repeated for all the particles in the system and averaged. This average is normalized by the total number of particle-pairs per unit volume Q_p/V. An RDF of unity indicates uniformly distributed particles, and any value higher than unity indicates clustering.

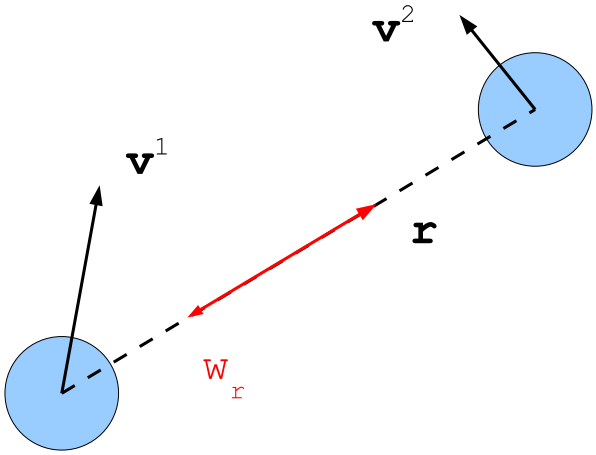

Figure 1.4: Sketch explaining the radial relative velocity w_r between two particles.

RDF at a separation distance r is given by

$$g(r) = \frac{\langle Q_{p,r}/V_r \rangle}{Q_p/V} \quad ,$$

where $Q_p = Q(Q-1)/2$ is the total number of particle pairs in the system, V is the volume of the system, $Q_{p,r}$ is the number of particles in the bin at separation $r = |\boldsymbol{r}|$ from a test particle, V_r is the volume of the bin at separation r and $\langle \cdot \rangle$ denotes an average over all (test) particles in the system. The RDF is a convenient measure of particle clustering, especially in isotropic turbulence. There are other measures of clustering reported in the literature. For example, Eaton and Fessler (1994) used the deviation of the concentration PDF from a Poisson distribution, and Monchaux et al. (2010) used a Voronoï analysis to quantify preferential concentration. Shaw et al. (2002) compares and contrasts the different existing measures of particle clustering, and argues that the RDF is the most suitable for quantifying droplet clustering in clouds. A strong motivation for using the RDF is the fact that the RDF evaluated at particle contact arises in the expression for the collision rate (Sundaram and Collins, 1997). The average collision frequency for a

monodisperse particulate system (here monodisperse implies that all the particles are identical) is given by

$$N_c = \frac{n^2}{2} K(\sigma) \ , \tag{1.2a}$$

where σ denotes the particle diameter, $n \equiv Q/V$ is the particle number density and $K(\sigma)$ is the collision kernel, defined for a statistically stationary suspension as

$$K(\sigma) = 4\pi\sigma^2 g(\sigma) \int_{-\infty}^{0} (-w_r) P(w_r|\sigma)\, dw_r \ . \tag{1.2b}$$

As can be seen from (1.2b), apart from the RDF, the other statistical input to the collision kernel is the probability density function (PDF) of the radial component of the relative velocity w_r (figure 1.4), defined as

$$w_r(\boldsymbol{r}) = [\boldsymbol{v}_2(\boldsymbol{x}+\boldsymbol{r}) - \boldsymbol{v}_1(\boldsymbol{x})] \cdot \frac{\boldsymbol{r}}{|\boldsymbol{r}|} \ , \tag{1.3}$$

where $\boldsymbol{v}_1(\boldsymbol{x})$ and $\boldsymbol{v}_2(\boldsymbol{x}+\boldsymbol{r})$ are the instantaneous velocities of two particles located at $\boldsymbol{x}$ and $\boldsymbol{x}+\boldsymbol{r}$, respectively. The collision kernel $K(\sigma)$ essentially encapsulates the stochastic nature of the particle collision process, being strongly influenced by the underlying fluctuating turbulent flow. Looking closely at equation (1.2b), we find that it is influenced by $w_r \in [-\infty, 0)$. Physically, we have $w_r > 0$ for a particle-pair moving away from each other, whereas $w_r < 0$ for a pair moving towards each other. Therefore, to account for particle-pairs coming into contact with each other, we only need to account for pairs that have $w_r < 0$. We also need to account for the non-uniform spatial distribution of the particles, and this is quantified by the RDF. Therefore, in order to develop a general expression for the collision kernel shown in (1.2b), we must have the means of predicting or computing the RDF and the relative velocity PDF.

1.3 Simulating particle-laden turbulence

There are broadly two different approaches to simulating inertial particles in a turbulent flow. The first approach is called Eulerian statistical modeling (ESM), where continuum equations for particle properties (such as concentration), or their PDF, are formulated and solved on the some computational grid. They have the advantage of giving fast solutions to the steady-state particle field properties, often on the same grid as the fluid. However, they are almost always unclosed, and require closure assumptions that impact their accuracy and validity. The second approach, and the one we adopt in this work, is called Lagrangian particle tracking (LPT). In this approach, a large number of particles are evolved in the turbulent flow field, based on some equation of motion. Then, at any instant of time, we can obtain any property or statistics of the particle field. This method is usually more expensive than ESM, but provides much higher accuracy and flexibility. Assuming that we know the equation of motion with which to evolve the particles in LPT, the accuracy of the particle statistics depends on the accuracy with which we can specify the underlying turbulent flow field. Since a turbulent flow is typically comprised of motions across a large range of spatio-temporal scales, and since inertial particle clustering is driven primarily by the small scales, the prediction of clustering from LPT is sensitive to the description of the small-scale turbulence.

Direct numerical simulations (DNS) of particle-laden turbulence capture all of the turbulent flow scales on the grid, and are therefore able to correctly predict clustering (Salazar et al., 2008). However, the computational cost of DNS limits the Reynolds numbers to values well below what is found in most practical systems (e.g., atmospheric conditions), and hence it is primarily used as a research tool to aid in theoretical understanding and model development. Reynolds-Averaged

Navier-Stokes (RANS) equations represents the other extreme, where only the average turbulent velocity field is solved for, and the impact of the turbulent fluctuations is modeled. RANS calculations are considerably cheaper and are heavily used for practical computations, but contain none of the physics responsible for particle clustering. Consequently, the RANS framework is not suitable for predicting the collision kernel. Large-eddy Simulations (LES) represent a compromise between these two extremes. We give a brief description of the LES in the next paragraph, to motivate our interest in improving its accuracy for particle-laden turbulent flows.

The main idea behind a LES is that only the largest scales of the turbulent fluctuations are resolved by the grid, while the smaller scales are modeled. This is motivated by the fact that if we want to resolve all the scales of turbulent motion, as in a DNS, nearly all of the computational effort will be spent in solving for the smallest scales (Pope, 2000). Now, according to Kolmogorov's hypothesis, these small-scales possess certain universal characteristics that are independent of the details of the outer flow. Based on this idea, the LES simulates the largest scales of motion, which carry most of the energy and are affected by the boundaries, and models the 'universal' small (subgrid) scales. In essence, we decompose the turbulent velocity field as $\boldsymbol{u}(\boldsymbol{x},t) = \tilde{\boldsymbol{u}}(\boldsymbol{x},t) + \boldsymbol{u}^R(\boldsymbol{x},t)$, where $\tilde{\boldsymbol{u}}(\boldsymbol{x},t)$ is the filtered velocity, obtained by applying a filter function to $\boldsymbol{u}(\boldsymbol{x},t)$ and $\boldsymbol{u}^R(\boldsymbol{x},t)$ is the residual. This decomposition is different from the Reynolds decomposition used in RANS approaches, in that the filtered velocity field is not a mean velocity, but represents the scales of motion larger than the applied filter-scale. When we apply a filter to the Navier-Stokes equation, we end up with a residual stress tensor that needs to be modeled. It is worth mentioning here that despite its long history (Smagorinsky, 1963) and popularity, there are still certain outstanding con-

ceptual and computational issues concerning LES (Mason, 1994; Pope, 2004). In terms of computational cost, LES lies somewhere between DNS and RANS, and with increasing availability of computing resources, is beginning to be viable for practical calculations (Kim et al., 1999; Poinsot, 2010). In particle-laden LES with LPT, the error in the particle statistics usually arises from the error in modeling the residual velocity $\boldsymbol{u}^R(\boldsymbol{x}, t)$ seen by the particles. In this work, we will seek a model for $\boldsymbol{u}^R(\boldsymbol{x}, t)$ that will correctly predict the collision kernel. We will also demonstrate an alternative approach to account for the effect of the subgrid scales on particle clustering.

1.4 Goals of this work

The following are the overarching goals of this work:

1. To understand, both qualitatively and quantitatively, the effect of the small-scales (subgrid scales in a LES) on the RDF and w_r statistics (and hence the collision kernel) for all St.
2. To model the effect of subgrid scales on inertial particle motion, in order to accurately predict the RDF and w_r statistics from a LES.
3. To understand, using theory and modeling, the key statistical information needed from the subgrid scales for different St regimes, and use them in developing better modeling strategies.

1.5 Organization of the dissertation

This dissertation is divided into six chapters. The current chapter, Chapter 1, introduces the theme, scope and contents of the dissertation. Each of the chapters 2 through 5 can be read independently, and represents pre-prints of manuscripts that have been published, are under review, or are in preparation for submission to a journal. Chapter 6 summarizes the major findings, contributions and conclusions from this work. The rest of this chapter explains how each of the following chapters relate to each other and represent a progression towards achieving the goals of this work, put forth in the previous paragraph.

Fede and Simonin (2006) explored the effect of LES filtering on inertial particles, and showed the strong influence of the small-scales on certain particle statistics. Jin et al. (2010a) investigated the effect of LES on collision-related statistics of inertial particles. Continuing from these studies, Chapter 2 (Ray and Collins, 2011) explores the effect of filtering on the RDF and relative velocity statistics across the whole range of particle Stokes numbers and particle separation distances. We show that filtering has a strong effect on both the RDF and w_r for both small and large St. We consider a simple model based on defining a scale-shifted St to account for filtering, and discuss its shortcomings. This illustrates the necessity of incorporating the physics behind the mechanism of clustering into the subgrid model. We also consider the effect of filter-scale on particle statistics.

Once we understand the shortcomings of a LES in terms of predicting the RDF and w_r, we can explore the performance of various existing subgrid models. A number of investigators have evaluated particle-laden LES, with emphasis on various particle statistics and use of different subgrid models (Wang and Squires, 1996b,a; Armenio et al., 1999; Boivin et al., 2000; Fede and Simonin, 2006; Mar-

chioli et al., 2008; Pozorski and Apte, 2009). In general, subgrid models that work well for flow statistics are not easily translated to describe inertial particle statistics. Consequently, there have been attempts at developing models specifically aimed towards recovering inertial particle statistics. Shotorban and Mashayek (2005), and Kuerten (2006) used the approximate deconvolution method (ADM) to exactly recover the scales of the turbulence represented on the grid in a LES. But, as has been shown previously (Jin et al., 2010a; Ray and Collins, 2011), exact representation of the larger turbulent fluctuations in a LES is not sufficient to correctly predict particle clustering. Shotorban and Mashayek (2006b,a), Fede et al. (2006), and Pozorski and Apte (2009) constructed stochastic Langevin-type models to recover the subgrid fluctuations seen by inertial particles. But, these models are not able to predict particle clustering accurately. Pozorski and Apte (2009) were able to match the RDF approximately for $St = 2.0$ with their model, only after choosing an appropriate but arbitrary value of their model constant. In fact, Cernick (2013) compared the ADM, and the subgrid models of Fukagata et al. (2004), Shotorban and Mashayek (2006b) and Berrouk et al. (2007) and showed that they contain insufficient physics to recover the correct levels of particle clustering. Jin et al. (2010a), and Ray and Collins (2011, 2013a) have demonstrated the crucial role that the subgrid turbulent fluctuations in a LES play in particle clustering. Therefore, we require a subgrid model that contains sufficiently detailed information regarding the small-scale structure of the turbulence without adding significant computational expense or arbitrary adjustable parameters.

Chapter 3 (Ray and Collins, 2013b) describes such a model, which we call a Kinematic Simulation based SubGrid Model (KSSGM). The central idea of the KSSGM is to recover some information about the subgrid flow structure by approximating the correct subgrid energy (and dissipation) spectrum. In isotropic

turbulence, this means that we capture the Eulerian two-point correlations of the subgrid fluid velocity (and velocity gradient) seen by the inertial particles. We show that the KSSGM can accurately predict the moments of w_r up to order 2 for all St, but can capture the RDF only for $St \geq 2.0$. The KSSGM is relatively inexpensive to compute, and has no arbitrarily adjustable parameters. We also investigate the reason for the failure of the model to predict the RDF for $St < 2.0$. Previous studies (Eaton and Fessler, 1994) have hypothesized the influence of the small-scale coherent structures of the turbulent flow field on inertial particle clustering. The presence of small-scale coherent structures is reflected in the Lagrangian time-scale of rotation-rate ($\mathcal{T}_R^L$) being larger for low St particles, than for high St particles. The KSSGM does not describe these structures accurately and is unable to capture this difference, and hence is unable to predict $\mathcal{T}_R^L$ and the RDF for $St < 2.0$. We conclude that recovering the effect of subgrid coherent structures on particle clustering from a LES is extremely challenging, and remains an open question.

Having identified the difficulty in capturing the clustering of low St particles in a conventional subgrid modeling framework, we opt for a different approach. In this approach, we look to derive models from existing theories for predicting the clustering and collision-rate of inertial particles, and use them in conjunction with a LES. We identify and work with two major theories viz., the theory by Chun et al. (2005) (CT) and the theory by Zaichik and Alipchenkov (2009) (ZT), which have been successful in predicting particle clustering especially in the low St regime. A major feature of both of these theories is the fact that they are formulated for particle-pairs, in a reference frame consisting of the *relative* positions and velocities of particles. Therefore, any model derived from the theories are also formulated in the reference frame moving with a particle. Development and testing of such

models in a conventional LES with particle tracking is impractical. Since we are interested in the relative particle separations in the dissipation range, we require a *very large* number of particles to resolve those separations, increasing the computational cost beyond what is practically feasible. To overcome this issue, we develop a novel satellite particle simulation (SPS) framework based on the work of Brunk et al. (1998), and Chun et al. (2005). The SPS provides an efficient way of investigating particle-pair dynamics at small separations, and is ideal for development and testing of models written in the relative reference frame. Chapter 4 (Ray and Collins, 2013a) documents the development, implementation and results from a SPS. We show that the power-law behaviors of the RDF and w_r statistics at small separations are predicted by the SPS in agreement with DNS and FDNS (filtered DNS, refer to §2.3.2), when the DNS and FDNS velocity gradients are provided to the SPS. This indicates that the results from the SPS are directly transferrable to a DNS or FDNS with particle tracking, and therefore the SPS provides a valid test-bed for *a priori* testing of LES models.

Now that we have validated the SPS framework, we can derive models from CT and ZT and test them using the SPS. Following the nomenclature in Chun et al. (2005) we call these models Drift-Diffusion Models (DDMs) based on their form containing a deterministic drift term, and a stochastic diffusion term. The DDMs considered in this work are valid in the limit of $St \ll 1$. We show that the DDM derived from CT substantially overpredicts the RDF power-law beyond $St = 0.05$. We then derive a DDM from ZT and show that it gives good agreement with DNS data for $St \leq 0.2$. We derive an analytical form for the drift term in the DDM-ZT in the limit of $St \ll 1$, and show that the results can be improved by using a better model for the drift. Chapter 5 (Ray et al., 2013) describes the formulation and results from the DDM derived from the CT and ZT. This represents a new

framework for subgrid modeling in a LES, and the DDMs appear promising as the first subgrid models that can capture clustering of low St particles in a LES.

CHAPTER 2

PREFERENTIAL CONCENTRATION AND RELATIVE VELOCITY STATISTICS OF INERTIAL PARTICLES IN NAVIER-STOKES TURBULENCE WITH AND WITHOUT FILTERING

2.1 Abstract

The radial distribution function (RDF, a statistical measure of preferential concentration), and the relative velocity measured along the line-of-centers of two particles are the key statistical inputs to the collision kernel for finite-inertia particles suspended in a turbulent flow (Sundaram and Collins, 1997). In this paper, we investigate the behavior of these two-particle statistics using direct numerical simulation (DNS) of homogeneous isotropic turbulence. While it is known that the RDF for particles of any Stokes number (St) decreases with separation distance (Sundaram and Collins, 1997; Reade and Collins, 2000a; Salazar et al., 2008), we observe that the peak in the RDF vs St curve shifts to higher St as we increase the separation distance. Here, St is defined as the ratio of the particle's viscous relaxation time to the Kolmogorov time-scale of the flow. Furthermore, as found in a previous study (Wang et al., 2000), the variance of the radial relative velocity (w_r) is found to increase monotonically with increasing separation distance and increasing Stokes number; however, we show for the first time that the parameteric variation of the skewness of w_r with St and r/η is qualitatively similar to that of the RDF, and points to a connection between the two. We then apply low-pass filters (using three different filter-scales) on the DNS velocity field in wavenumber space in order to produce 'perfect' large-eddy simulation (LES) velocity fields without any errors associated with subgrid scale modeling. We present visual evidence of

the effect of sharp-spectral filtering on the flow structure and the particle field. We calculate the particle statistics in the filtered velocity field and find that the RDF decreases with filtering at low St and increases with filtering at high St, similar to Fede and Simonin (2006). We also find that the variation of the RDF with St shifts toward higher St with filtering at all separation distances. The variance of w_r is found to decrease with filtering for all St and separation distances, but the skewness of w_r shows a non-monotonic response to filtering that is qualitatively similar to the RDF. We consider the variation of the RDF and moments of w_r with filter-scale and find that they are approximately linear in the inertial range. We demonstrate that a simple model consisting of a redefinition of the St based on the time-scale of the filtered velocity field cannot recover the unfiltered statistics. Our findings provide insight on the effect of subgrid scale eddies on the RDF and w_r, and establish the requirements of a LES model for inertial particles that can correctly predict clustering and collisional behaviour.

2.2 Introduction

The behaviour of aerosol particles suspended in a turbulent gas is of importance to a wide variety of industrial (diesel engine spray and combustion, two-phase reactors) and atmospheric (pollutant transport, cloud formation) processes. Numerical simulations of inertial particles in turbulence have shown that the particles tend to cluster outside of vortices, in the high-strain regions of the flow (Squires and Eaton, 1991; Eaton and Fessler, 1994; Sundaram and Collins, 1997). Such preferential concentration can influence a broad range of aerosol processes, such as particle settling (Wang and Maxey, 1993; Aliseda et al., 2002), evaporation/condensation (Shaw et al., 1998; Vaillancourt and Yau, 2000) and interparticle collisions (Sun-

daram and Collins, 1997). It also has been hypothesized that particle clustering is responsible for the broadening of the droplet size distribution during condensational growth in cumulus clouds (Shaw et al., 1998; Reade and Collins, 2000a; Falkovich et al., 2002). The radial distribution function (RDF) has been established as a measure of particle clustering in isotropic turbulence and is defined as the ratio of the average number of particle pairs per unit volume found at a given separation distance to the expected number if the particles were uniformly distributed (McQuarrie, 1976). The RDF can be computed from a field of Q particles by binning the particles according to their separation distance and calculating

$$g(r) = \frac{Q_{p,r}/\Delta V_r}{Q_p/V} \ , \tag{2.1}$$

where $Q_{p,r}$ is the average number of particles found in an elemental shell volume ΔV_r at a distance $r = |\boldsymbol{r}|$ from a test particle, V is the total volume and $Q_p = Q(Q-1)/2$ is the total number of particle pairs in the system. Sundaram and Collins (1997) showed that the RDF evaluated at particle contact precisely corrects the collision kernel for particle clustering. The average collision frequency for a monodisperse particulate system is given by

$$N_c = \frac{n^2}{2} K(\sigma) \ , \tag{2.2a}$$

where σ denotes the particle diameter, n is the particle number density and $K(\sigma)$ is the collision kernel, defined for a statistically stationary suspension as

$$K(\sigma) = 4\pi\sigma^2 g(\sigma) \int_{-\infty}^{0} (-w_r) P(w_r/\sigma)\, dw_r \ . \tag{2.2b}$$

As can be seen from equation (2.2b), apart from the RDF, the other statistical input to the collision kernel is the PDF of the radial relative velocity (w_r) defined as

$$w_r(\boldsymbol{r}) = [\boldsymbol{v}_2(\boldsymbol{x}+\boldsymbol{r}) - \boldsymbol{v}_1(\boldsymbol{x})]\cdot\hat{\boldsymbol{r}} \ , \tag{2.3}$$

where $\boldsymbol{v}_1(\boldsymbol{x})$ and $\boldsymbol{v}_2(\boldsymbol{x}+\boldsymbol{r})$ are the velocities of two particles located at $\boldsymbol{x}$ and $\boldsymbol{x}+\boldsymbol{r}$, respectively, and $\hat{\boldsymbol{r}}$ is a unit vector pointing along their line-of-centers. The effect of inertia on the radial relative velocity statistics has been investigated in the context of predicting the collision kernel (Wang et al., 2000; de Jong et al., 2010; Bec et al., 2010) and also for modeling the particle motion that leads to clustering (Zaichik and Alipchenkov, 2003; Chun et al., 2005; Zaichik and Alipchenkov, 2009). Recently, it has been found that inertial particle relative velocities can be multi-valued in the limit of zero separation due to the formation of caustics (Wilkinson et al., 2006; Falkovich and Pumir, 2007; Salazar and Collins, 2012), which tends to enhance the collision rate. In this work, we explore the parametric behavior of the RDF and the radial relative velocity PDF in some detail, and also identify a relation between them.

Direct numerical simulation (DNS) provides a very accurate basis on which to describe the Lagrangian motion of particles in a turbulent flow. However, its computational cost limits its applicability to simple geometries and low-to-moderate Reynolds numbers. We can relax these restrictions in a large-eddy simulation (LES) where only the large scales are explicitly calculated, while the small scales are modeled. Therefore, it is better suited to describing real world flows at arbitrary Reynolds numbers, including the flow in the atmosphere. However, LES introduces models for the so-called 'subgrid-scale' (SGS) stresses (Pope, 2000). In the context of high-Reynolds-number turbulence, the class of models known as dynamic subgrid models (Germano et al., 1991) perform reasonably well for arbitrary geometries. Extensions of these and other models for Lagrangian simulations of particles exist and are able to reproduce the mean kinetic energy, two-way coupling, and dispersive properties of the particles (see, for example Wang and Squires, 1996b; Armenio et al., 1999; Boivin et al., 2000). However, since the dynamics

responsible for inertial particle clustering occur at the small (unresolved) scales, these models are not able to capture this physics accurately (Fede and Simonin, 2006; Marchioli et al., 2008; Pozorski and Apte, 2009). The unresolved fluctuations profoundly affect binary processes such as collision (Jin et al., 2010a), as well as aerosol processes that are sensitive to fluctuations in particle concentrations (e.g., evaporation/condensation, toxicity). While numerous SGS models for inertial particles have been proposed recently, focused primarily on capturing particle dispersion using a Langevin type formulation (Shotorban and Mashayek, 2006b,a; Fede et al., 2006; Berrouk et al., 2007; Bini and Jones, 2007; Jin et al., 2010b), and also some attempts have been made towards accounting for the subgrid scales using de-filtering (Shotorban and Mashayek, 2005; Kuerten, 2008), there currently is no modeling framework for particulate systems that can account for clustering of arbitrary-inertia particles.

The work presented in this paper represents a first step towards the development of a LES subgrid model for particles that would correctly capture clustering and collision rates. To provide an ideal testbed for a LES model, we apply a low-pass filter to a high-resolution DNS (512^3) as described in §2.3.2. The resultant filtered velocity field can be thought of as a 'perfect' LES velocity field, free of any subgrid modeling errors. We then calculate the RDF and the PDF of w_r for particles advected by the filtered velocity field and compare them to those for particles advected by the unfiltered velocity, yielding direct evidence of the effect of the sub-grid scales on those quantities. Fede and Simonin (2006) investigated the effect of filtering on various Eulerian and Lagrangian statistics of particles and more recently Jin et al. (2010a) reported the errors in the RDF, w_r and the collision kernel incurred in a LES and a filtered DNS. Here, we consider the effect of filtering on the RDF and w_r over a wider range of r/η. Also, we examine the

variation of the statistics as a function of filter scales that roughly span the inertial range, and provide visual evidence of the response of the flow and the particle field to the filtering operation. We use our filtered DNS to provide further support for the previously unexplored relation between the RDF and w_r.

2.3 Direct Numerical Simulation

In this section, we present details of the DNS used to solve the three-dimensional time-dependent Navier Stokes equations for the fluid phase with and without filtering, and the equations of motion for each inertial particle suspended in the fluid.

2.3.1 Fluid Phase

The governing equations for a three-dimensional incompressible flow are the continuity and the Navier Stokes equation. In rotational form, the equations are

$$\frac{\partial u_i}{\partial x_i} = 0 \quad , \tag{2.4a}$$

$$\frac{\partial u_i}{\partial t} + \epsilon_{ijk}\omega_j u_k = -\frac{\partial(p/\rho + \frac{1}{2}u^2)}{\partial x_i} + \nu\frac{\partial^2 u_i}{\partial x_j \partial x_j} + F_i \quad , \tag{2.4b}$$

where u_i is the velocity vector, $u \equiv \sqrt{u_i u_i}$ is the magnitude of the velocity vector, ρ is the fluid density, ν is the kinematic viscosity, ϵ_{ijk} is the alternating unit tensor, $\omega_i = \epsilon_{ijk}\frac{\partial u_k}{\partial x_j}$ is the vorticity, p is the pressure and F_i is a time-dependent deterministic forcing function that injects energy into the first two wavenumbers in Fourier space in order to maintain a statistically stationary isotropic turbulence (Witkowska et al., 1997). Equations (2.4) are solved using a pseudo-spectral algorithm with de-aliasing based on a combination of truncation and phase-shift

Variable	Unfiltered DNS 1	Unfiltered DNS 2	Filter 1 ($\kappa_c\eta$=0.154)	Filter 2 ($\kappa_c\eta$=0.112)	Filter 3 ($\kappa_c\eta$=0.077)
N	512	128	512	512	512
R_λ	227	95	-	-	-
$\kappa_{max}\eta$	1.67	1.60	-	-	-
k	1.255	1.178	1.193	1.157	1.105
ϵ	0.256	0.232	0.056	0.035	0.020
η	0.007	0.028	0.010	0.011	0.013
τ_η	0.058	0.139	0.121	0.154	0.205
L	1.404	1.490	-	-	-

Table 2.1: Turbulence parameters for DNS and filtered DNS. N is the number of grid points in each of the 3 dimensions, R_λ is the Reynolds number based on the Taylor micro-scale, $k = \int_0^{\kappa_{max}} E(\kappa)\, d\kappa$ is the kinetic energy, $\epsilon = 2\nu \int_0^{\kappa_{max}} \kappa^2 E(\kappa)\, d\kappa$ is the dissipation rate, $\eta = \frac{\nu^{3/4}}{\epsilon^{1/4}}$ is the Kolmogorov length scale, $\tau_\eta = \sqrt{\frac{\nu}{\epsilon}}$ is the Kolmogorov time scale and $L = \frac{3\pi}{2k} \int_0^{\kappa_{max}} \frac{E(\kappa)}{\kappa}\, d\kappa$ is the integral length scale; For the filtered DNS, k, ϵ, η and τ_η are computed by replacing κ_{max} by the cut-off filter scale κ_c.

(Patterson and Orszag, 1971; Johnson, 1998; Brucker et al., 2007) on a flow domain comprised of a cube with each side of length 2π (in arbitrary units). We use 512 grid points in each direction and achieve a moderate Reynolds number based on the Taylor microscale ($R_\lambda = 227$). The time step was chosen so that the CFL number is less than 0.5. We evolve the flow-field for about thirteen eddy turnover times to reach statistical stationarity. Additional details of simulation parameters and resolution are given in table 2.1.

2.3.2 Filtering

We perform low-pass filtering of the DNS velocity field in Fourier space so that all the Fourier modes of velocity beyond a certain cutoff wavenumber κ_c are removed from the flow and only the remaining 'large scales' are retained. The filtering operation we perform is defined below. We apply a sharp spectral filter which

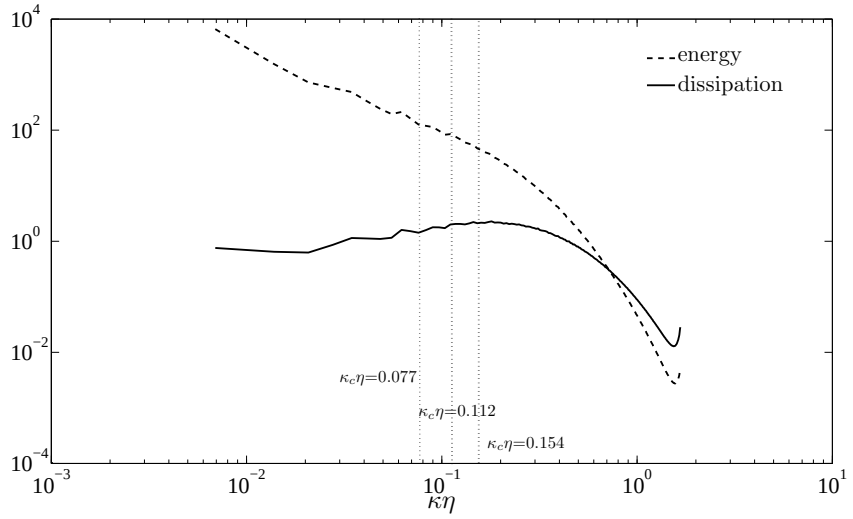

Figure 2.1: Filter cut-off scales ($\kappa_c\eta$) superimposed on the energy ($E(\kappa)/\eta {u_\eta}^2$) and dissipation ($2\nu\kappa^2 E(\kappa)/{u_\eta}^3$) spectra at R_λ=227. Notice that $\kappa_c\eta$ are well within the inertial subrange.

removes all wavenumbers above a critical wavenumber κ_c, yielding the following definition of the filtered velocity

$$\tilde{\boldsymbol{u}}(\boldsymbol{k},t) = \begin{cases} \boldsymbol{u}(\boldsymbol{k},t) & \text{if } |\boldsymbol{k}| \leq \kappa_c \\ \boldsymbol{0} & \text{otherwise} \end{cases} , \tag{2.5}$$

where the cutoff wavenumber was varied over the non-dimensional range: $\kappa_c\eta$=0.154, 0.112 and 0.077. Figure 2.1 shows the energy and dissipation spectra obtained from our DNS as a function of wavenumber. Notice that the cutoff wavenumbers (or filter scales) roughly span the inertial range. The turbulent kinetic energy, dissipation rate and the Kolmogorov length and time-scales are computed for the filtered velocity field using the standard definitions shown in table 2.1, with κ_{max} replaced by κ_c.

We find that if we choose the filter scale to the right of the peak in the dissipation spectrum (i.e., in the dissipation range), the filtering has very little effect on clustering. On the other hand, when it is chosen to the left of the peak in the dissipation spectrum, i.e., in the inertial sub-range (consistent with a LES),

there is a significant impact of filtering on the two-particle statistics relevant for clustering and collision.

2.3.3 Inertial Particle Motion

We assume a very dilute suspension of inertial particles which allows us to neglect the feedback of particle motion on the carrier fluid (Sundaram and Collins, 1999). We also consider particles whose radius a is much smaller than the Kolmogorov length scale η and simulate them as point-particles. Furthermore, we assume that the particles are much denser than the surrounding fluid ($\rho_p/\rho_f \gg 1$), the particle Reynolds numbers are small, and collisions and gravitational settling are negligible. Under these assumptions, the equations of motion for the particles reduce to (Maxey and Riley, 1983)

$$\frac{d\boldsymbol{x}_p^{(i)}}{dt} = \boldsymbol{v}_p^{(i)}\,, \tag{2.6a}$$

$$\frac{d\boldsymbol{v}_p^{(i)}}{dt} = \frac{\boldsymbol{u}\left[\boldsymbol{x}_p^{(i)}\right] - \boldsymbol{v}_p^{(i)}}{\tau_p^{(i)}}\,, \tag{2.6b}$$

where the superscript 'i' denotes the i^{th} particle, $\boldsymbol{x}_p^{(i)}$ is the inertial particle position, $\boldsymbol{v}_p^{(i)}$ is the particle velocity, $\tau_p^{(i)} = (2/9)\frac{\rho_p a^2}{\rho_f \nu}$ is the particle response time and $\boldsymbol{u}\left[\boldsymbol{x}_p^{(i)}\right]$ denotes the fluid velocity at the inertial particle location. We use $10,400,000$ particles divided equally into 13 different Stokes numbers. These particles are introduced into the stationary flow field at random positions and with the fluid velocity at those points. Heun's method (two-stage second order Runge-Kutta) is used to advance the particles in time according to equations (2.6). Fluid velocities at particle locations are obtained using eighth-order Lagrangian interpolation (Berrut and Trefethen, 2004). We allow sufficient time (four eddy turnover times) for the particles to equilibriate with the flow before taking statistics. Parti-

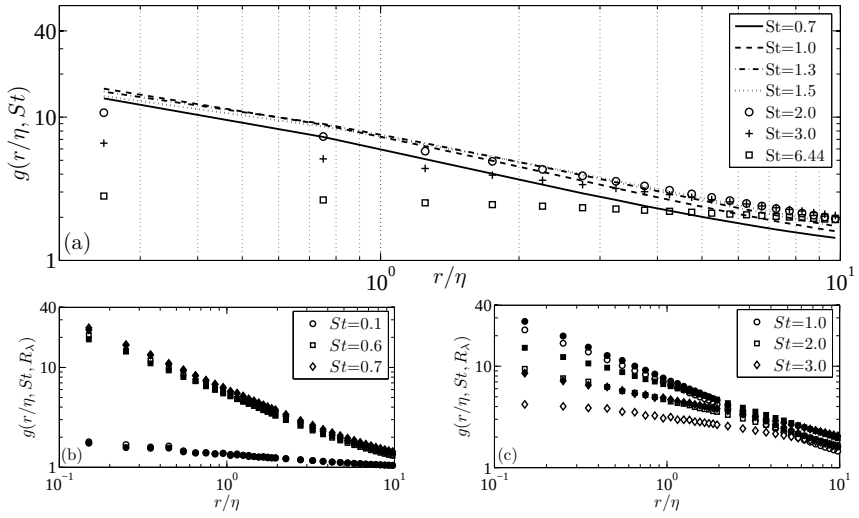

Figure 2.2: (a) Variation of the RDF with r/η for R_λ=227 and at the indicated values of St. Reynolds number dependence of the RDF, where open symbols represent R_λ=95 and filled symbols represent R_λ=227 for (b) low and (c) high Stokes numbers, as indicated.

cle statistics are averaged over several eddy turnover times. In order to investigate the effect of filtering, the particles are similarly advanced using the filtered velocity field. Details of the unfiltered and filtered flow fields are provided in table 2.1.

2.4 Results and Discussion

In this section, we present the results of our simulations with and without filtering for the RDF (§2.4.1) and the radial relative velocity (§2.4.2). In §2.4.3, we combine these two statistics to calculate the collision kernel.

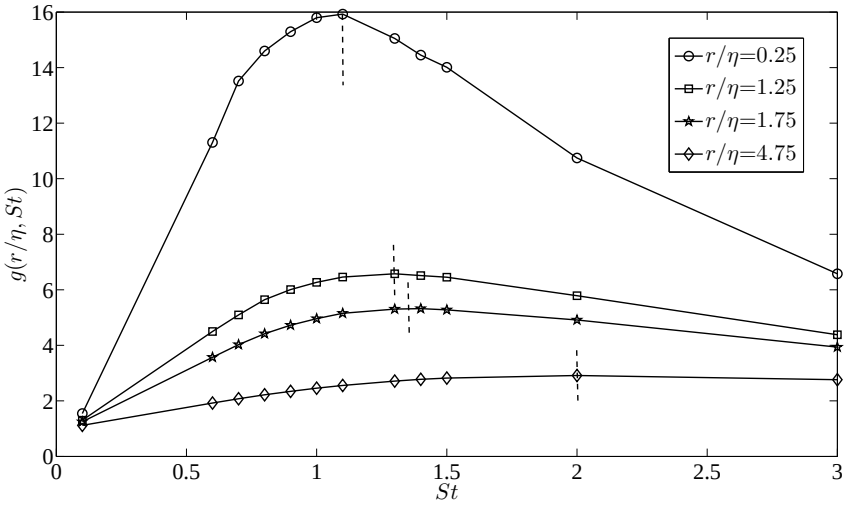

Figure 2.3: Variation of the RDF with St at the indicated values of r/η. Vertical dashed lines are at the approximate maximum in each curve.

2.4.1 Radial distribution function

We begin by looking at the RDF in the fully resolved, unfiltered DNS in order to identify its important characteristics and set the stage for a discussion on the effect of filtering. Figure 2.2(a) shows the variation of the RDF as a function of separation distance at different St. We observe that for all St, the RDF decreases with increasing separation distance whereas for very high and very low (not shown) St, the RDF is small and almost independent of separation. Maxey (1987) has shown that the divergence of the particle velocity is positive in regions of high rotation and negative in regions where the strain rate dominates. This implies that clustering is driven primarily by small-scale vortices that 'centrifuge' inertial particles out of the rotating regions into the straining regions of the flow. Therefore, the effect is weak for very heavy particles (having large response times) that are unable to respond to the small-scale vortices, and for very light particles that tend to follow fluid particles faithfully. For particles of intermediate inertia (having intermediate Stokes numbers), clustering is most significant. Another more subtle observation

that can be made from figure 2.2(a) is that the curves for different St cross each other at different values of r/η. This indicates that the extent of preferential concentration depends also on the separation distance of interest. This is illustrated more clearly in figure 2.3, which shows the RDF as a function of St at different separation distances. Notice that the peak in the RDF (indicated with a vertical dashed line) shifts to higher values of St with increasing separation distance. It is plausible that clustering at larger separations is driven by large (slower) eddies that 'resonate' with particles of higher St. This observation is consistent with the model for the 'residual' RDF ($h(r) \equiv g(r) - 1$) proposed by Reade and Collins (2000a), which found the expression $h(r/\eta, St) = c_0(St)(\frac{r}{\eta})^{-c_1(St)} \exp\left(-c_2 \frac{r}{\eta}\right)$, where c_0 and c_1 are functions of St and c_2 is a constant. Expressions for the coefficients c_0 and c_1 were derived empirically in Reade and Collins (2000a) using least squares minimization. c_0 was found to peak around St=0.9 while c_1 decreased monotonically with St, which together causes the peak in the RDF to shift to higher St with increasing r/η. In figure 2.2(b) and 2.2(c), we consider the Reynolds number dependence of the RDF by comparing the results of our 512^3 ($R_\lambda = 227$) simulations with a lower resolution simulation (128^3 at $R_\lambda = 95$). Our goal is to test the conclusion reached by Collins and Keswani (2004) that the RDF eventually saturates with increasing R_λ. In agreement with their study, we observe the dependence of the RDF on R_λ is weak for low St. However for $St \geq 1$, we see a very significant variation with R_λ at small r/η (the regime of importance for predicting the collision kernel) indicating that a more careful study is necessary to determine the nature of this dependence across the whole range of St.

Next we consider the effect of filtering on particle clustering. Figure 2.4 shows the effect of filtering on the distribution of vorticity magnitude in a $898\eta \times 898\eta \times 14\eta$ slice of the solution domain along with the particle distribution for St=0.9 and

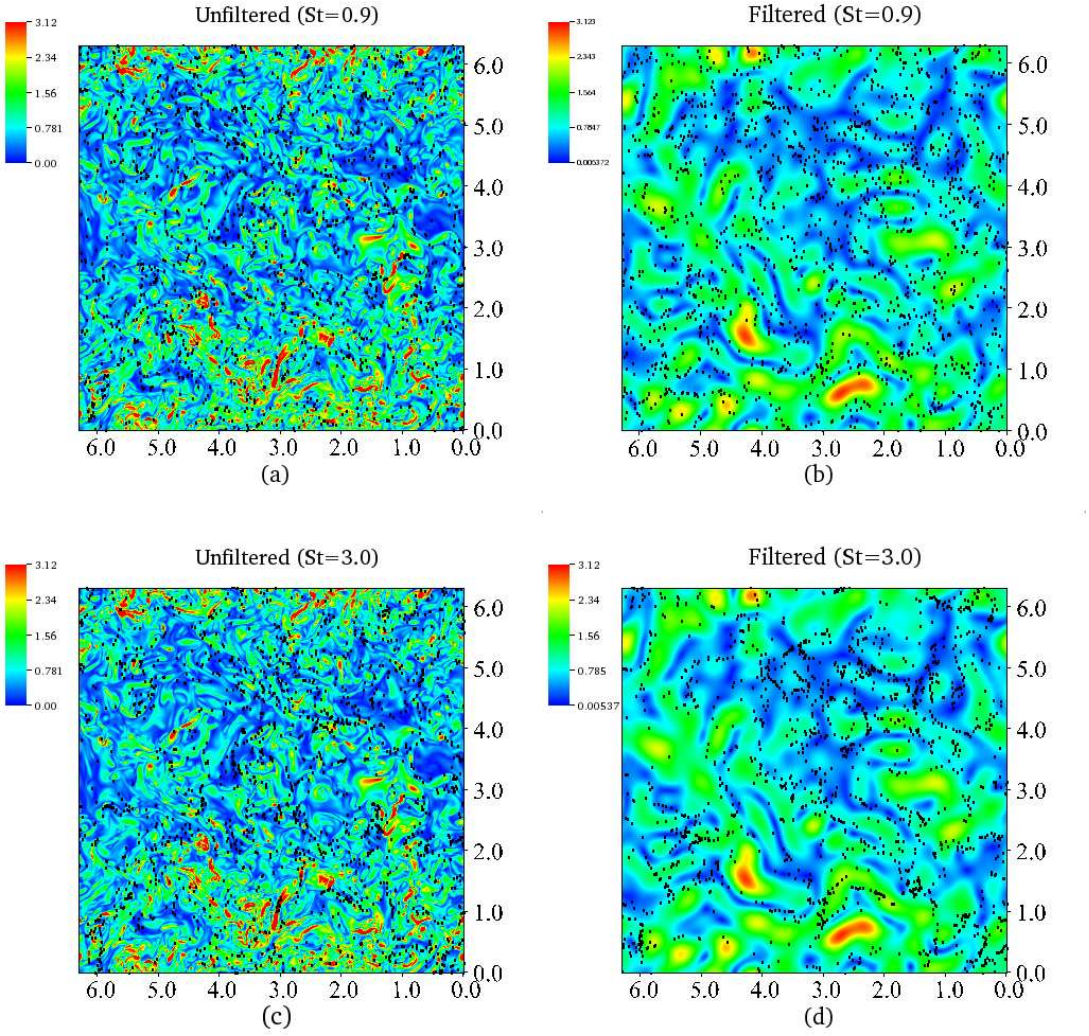

Figure 2.4: (Color online) Particle field for (a) and (b) $St = 0.9$, and (c) and (d) $St = 3.0$ superimposed on top of the contours of vorticity magnitude in a $898\eta \times 898\eta \times 14\eta$ slice of (a) and (c) unfiltered, and (b) and (d) filtered ($\kappa_c\eta = 0.077$) flow fields. Legends correspond to vorticity magnitude normalized by the root mean square (RMS) vorticity. Unfiltered vorticity contours above 3.12 times the RMS not shown for clarity.

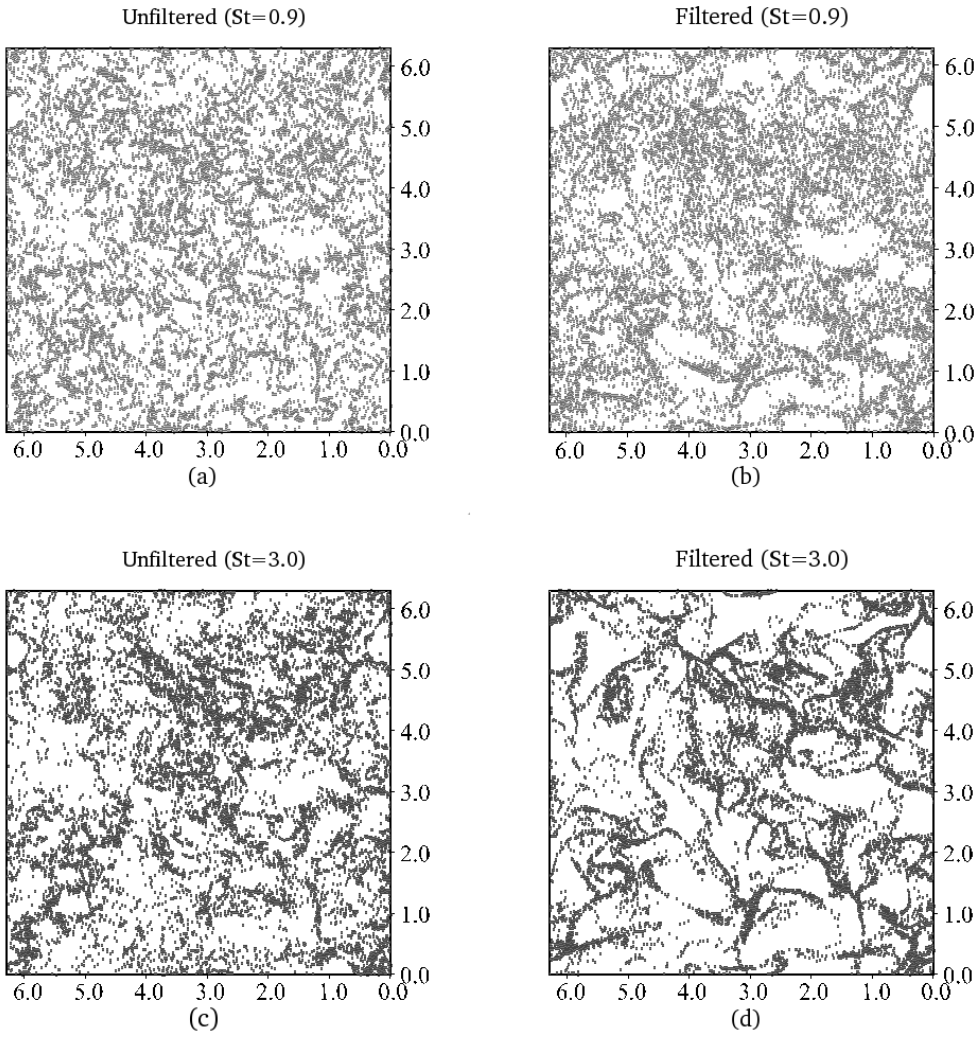

Figure 2.5: Particle field in a $898\eta \times 898\eta \times 14\eta$ slice as in figure 2.4 without the vorticity contours for clarity.

St=3.0 superimposed on it. Notice that the sharp spectral filter washes out the fine structure in the vorticity field and retains only the large-scale structure. This is similar to previous flow visualizations of LES fields (Metais and Lesieur, 1992; Wang et al., 1996), but the results shown here are for more substantial filtering of the inertial range. The dots superimposed on the images show the particle locations for St = 0.9 (low) and 3.0 (high) cases. Notice the particles in the lower Stokes number case are highly clustered in the unfiltered DNS, whereas they are more uniformly distributed in the filtered DNS. The exact opposite is true for the high Stokes number case, i.e., the clustering is greater in the filtered DNS as the particles seek to avoid the larger vortical regions of the filtered velocity. We can see evidence of the randomizing effect of the subgrid scales at the higher St when we compare figures 2.4(c) and 2.4(d). To see this more clearly, figure 2.5 shows the same slices of the solution cube now with only the particle field. Figure 2.5(d) shows that the absence of subgrid scales creates 'gaps' in the filtered particle field, the length of which are twice those for the unfiltered case (figure 2.5(c)) in agreement with the ratio of their effective Kolmogorov scales (see table 2.1). This results in the filtered field being more clustered for St=3.0, in agreement with figure 2.4. For St=0.9, shown in figures 2.5(a) and 2.5(b), we can see that although the filtered particle field contains larger 'gaps' compared to the unfiltered case, the number of such gaps are larger in the unfiltered particle field. This is a clear indication that for the low St particles, the sub-grid scale eddies that are absent in the filtered velocity field are driving the clustering of these particles.

Figure 2.6 shows the effect of filtering on the spatial variation of RDF for different St. Consistent with the visual images shown in figures 2.4 and 2.5, we find that the effect of filtering is different for low and high St. At low St, filtering reduces the RDF while at high St, it increases the RDF. This behavior has been

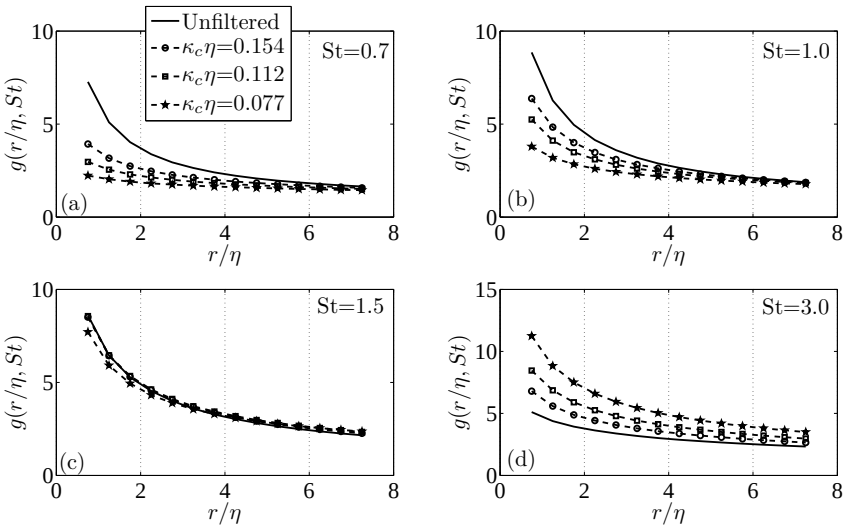

Figure 2.6: Effect of three levels of filtering ($\kappa_c\eta$ = 0.154, 0.112 and 0.077) on the spatial variation of the RDF for Stokes numbers: (a) 0.7, (b) 1.0, (c) 1.5 and (d) 3.0.

observed in previous studies (Fede and Simonin, 2006; Pozorski and Apte, 2009; Jin et al., 2010a) and can be explained as follows. As discussed in the previous section, for low St particles, clustering is driven by the small-scale eddies due to the centrifuging effect. Hence, when we filter out these small scales, the RDF decreases. However, the large St particles have higher response times than the filtered eddies and hence those eddies act to randomize the motion of the particles, which tends to cause particle pairs to diffuse away from each other, thereby reducing the clustering. Therefore, removing the small scales by filtering results in an increase in the RDF for high St particles. At an intermediate Stokes number ($St \approx 1.5$), these two effects cancel and the filtered and unfiltered RDFs are nearly the same, as can be seen in figure 2.6(c). Figure 2.6 also shows that the qualitative behavior of the RDF does not change by varying the filter-scale in the inertial range. Therefore we can look at the effect of filtering by considering filter 1 (refer to table 2.1) as a representative filter-scale.

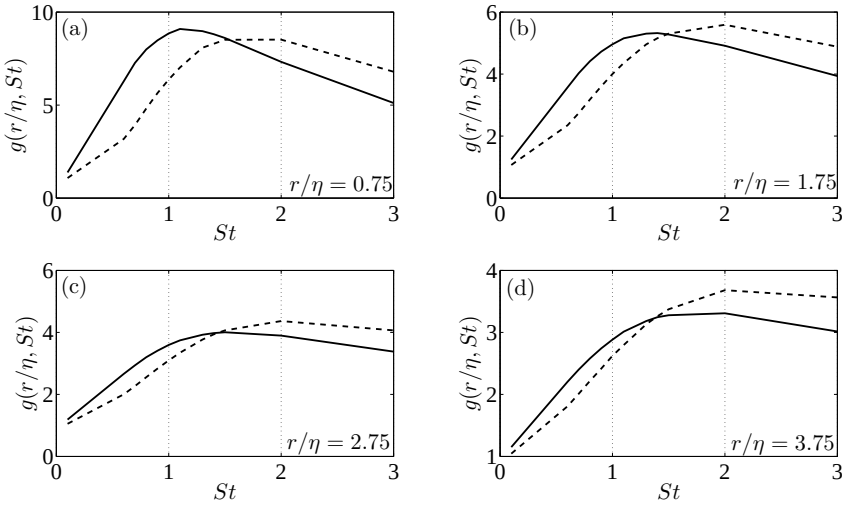

Figure 2.7: Effect of filtering ($\kappa_c\eta$=0.154) on the variation of the RDF with St at r/η of (a) 0.75, (b) 1.75, (c) 2.75 and (d) 3.75. Solid lines are the unfiltered RDF and dashed lines are the filtered RDF.

Figure 2.7 shows the effect of filtering on the Stokes number dependence of the RDF at fixed separation distances. We observe that for all separations, the filtered curves are shifted to the right. This behavior has been reported earlier by Fede and Simonin (2006) at one particular separation distance using a different measure of clustering. Jin et al. (2010a) also found this trend while evaluating the RDF at contact using both a filtered DNS and a LES, and attributed the shift in the peak of the filtered curve to the larger time-scale of the filtered velocity field. They also implied that the RDF is dependent not only on the vorticity intensity (which is a measure of the frequency or the time-scale) but also on the vorticity distribution (which is dependent on the spatial structure) of the flow. We show later in this section that a simple rescaling of the Stokes number based on the time scales of the DNS and the filtered DNS cannot predict the RDF accurately.

In order to illustrate the quantitative effect of the filter scale on the RDF, we

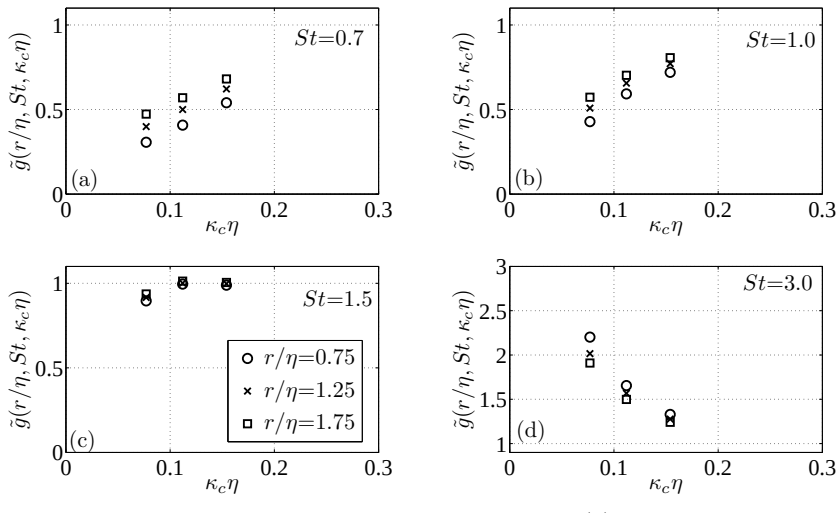

Figure 2.8: Variation of the RDF ratio with filter-scale at the indicated values of r/η and for Stokes numbers of (a) 0.7, (b) 1.0, (c) 1.5 and (d) 3.0.

define the ratio

$$\tilde{g}(r/\eta, St, \kappa_c\eta) = g_f(r/\eta, St, \kappa_c\eta)/g(r/\eta, St) \tag{2.7}$$

where $g_f(r/\eta, St, \kappa_c\eta)$ denotes the filtered RDF and $g(r/\eta, St)$ denotes the unfiltered RDF. Figure 2.8 shows the variation of the RDF ratio as a function of the cut-off wavenumber (or filter-scale) for different r/η and St. We find that the effect of filtering increases as the filter-scale gets smaller. Also, away from the cross-over St ($\approx$1.5), the variations look approximately linear. This can be verified by considering the absolute value of the correlation coefficient between $\tilde{g}(\kappa_c\eta, r/\eta, St)$ and $\kappa_c\eta$, which is found to be very close to unity for all St, indicating that to a very good approximation, the RDF ratio varies linearly with filter-scale in the inertial range (for particles on either side of the crossover St).

The simplest 'subgrid' model for the particles would be to replace the Kolmogorov time in the definition of St by the Kolmogorov time for the filtered velocity field. The filtered velocity field, by definition, is devoid of the sub-filter scale eddies and hence inherently has a different Kolmogorov time-scale as compared to

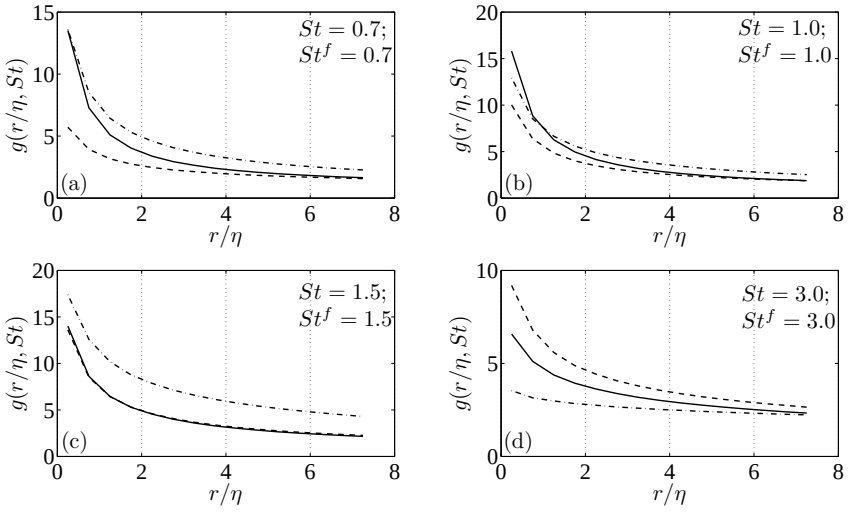

Figure 2.9: Effect of filtering ($\kappa_c\eta$=0.154) on the spatial variation of the RDF for Stokes numbers (a) 0.7, (b) 1.0, (c) 1.5 and (d) 3.0. Solid lines are the unfiltered RDF, dashed lines are the filtered RDF and dashed-dot lines are the filtered RDF based on the modified Stokes number (St^f).

the unfiltered velocity field (see table 2.1). Let us call this time-scale ${\tau_\eta}^f$, and note that ${\tau_\eta}^f > \tau_\eta$. Therefore, we can define an effective Stokes number St^f as

$$St^f = \frac{\tau_p}{{\tau_\eta}^f} = \frac{\tau_\eta}{{\tau_\eta}^f}\frac{\tau_p}{\tau_\eta} = \frac{\tau_\eta}{{\tau_\eta}^f} St\,, \tag{2.8a}$$

$$\Rightarrow St^f < St\,. \tag{2.8b}$$

Computing the statistics in terms of St^f can thus be thought of as the simplest model to account for the filtering. The results are shown in figures 2.9 and 2.10. Figure 2.9 shows that for the spatial variation of RDF, such a model overcompensates for the effect of filtering at all St. The same conclusion holds for all separation distances in figure 2.10, where we plot the variation of RDF with St. For the purpose of illustration, we can compute the relative errors in the prediction of the RDF using this simple model. For r/η=2.0 in figure 2.9, the relative errors for St = 0.7, 1.0, 1.5 and 3.0 are 0.222, 0.064, 0.600 and -0.250, respectively. For $St = St^f = 1.0$ in figure 2.10, the relative errors for r/η = 0.75, 1.75, 2.75 and 3.75 are -0.059, 0.222, 0.250 and 0.321, respectively. From these representative

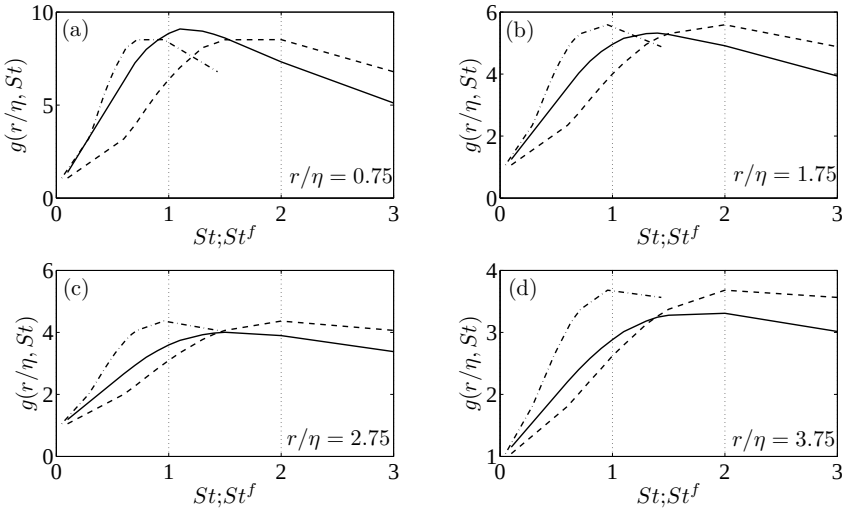

Figure 2.10: Effect of filtering ($\kappa_c\eta$=0.154) on the variation of the RDF with Stokes number at r/η of (a) 0.75, (b) 1.75, (c) 2.75 and (d) 3.75. Solid lines are the unfiltered RDF, dashed lines are the filtered RDF and dashed-dot lines are the filtered RDF based on the modified Stokes number (St^f).

numbers, we can see that this simple model is inadequate for predicting the RDF. More importantly, it is apparent that the very nature of the variation of the filtered RDF is different from that of the unfiltered RDF so that a model based on only a time scale shift cannot capture the correct behaviour. Clearly, we need to incorporate more of the physics of the small scales to accurately predict clustering.

2.4.2 Radial relative velocity

Let us now look at the other major component of the collision kernel for particles, the radial relative velocity (w_r). Figure 2.11(a) shows the PDF of w_r normalized by the Kolmogorov velocity scale u_η as a function of St at a particular separation distance (r/η=0.75). As has been observed both experimentally and numerically by de Jong et al. (2010), the PDF becomes broader as St increases. Figure 2.11(b) shows the PDF for St=1.0 as a function of separation distance, where we observe

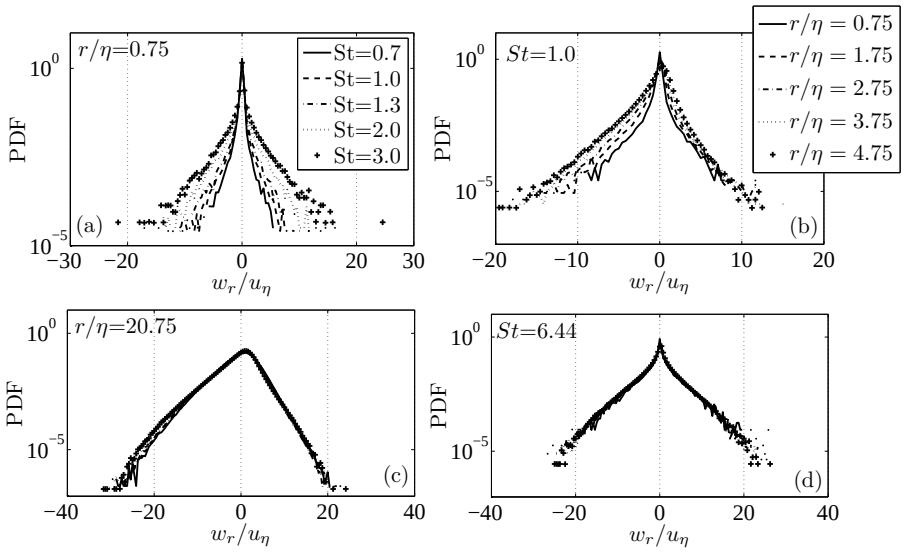

Figure 2.11: Variation of the PDF of the radial relative velocity at the indicated values of Stokes number and at r/η of (a) 0.75 and (c) 20.75; variation of the same at the indicated values of r/η and Stokes numbers of (b) 1.0 and (d) 6.44.

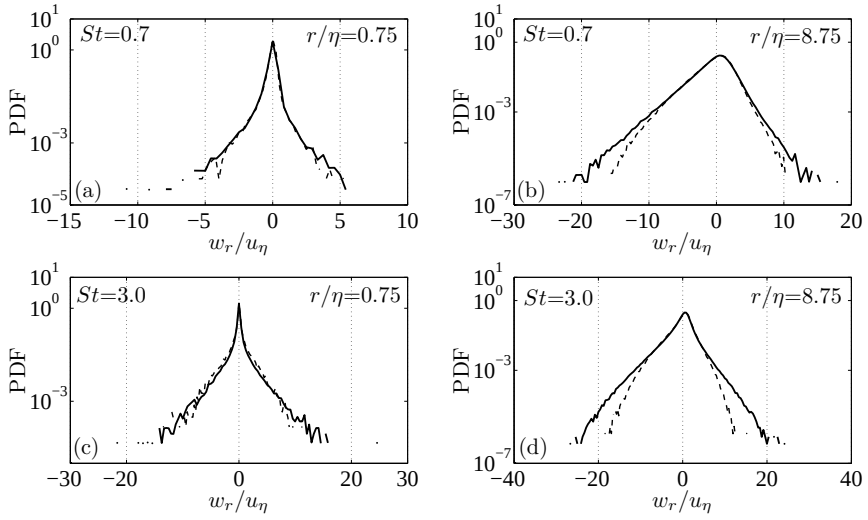

Figure 2.12: Reynolds number dependence of the PDF of the radial relative velocity at: $St = 0.7$ and r/η (a) 0.75 and (b) 8.75; and $St = 3.0$ and r/η (c) 0.75 and (d) 8.75. Solid lines represent $R_\lambda = 227$ and dashed lines represent $R_\lambda = 95$.

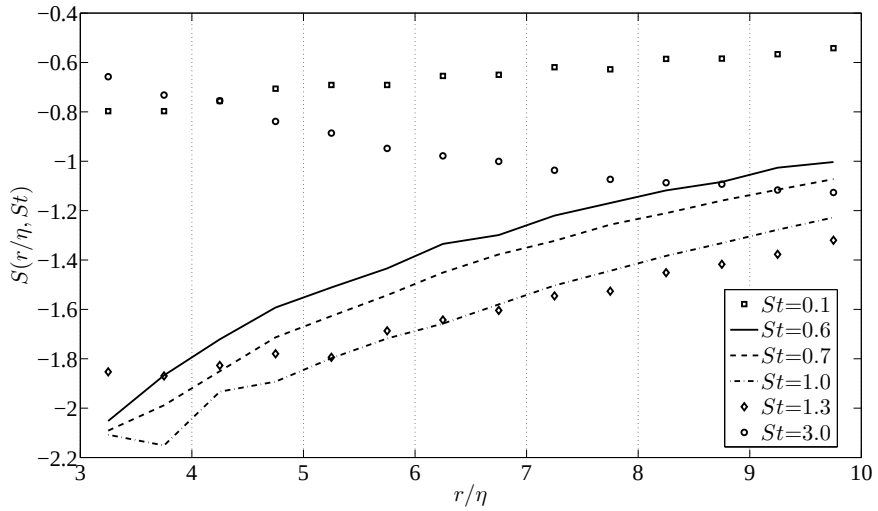

Figure 2.13: Variation of the skewness of the PDF of the radial relative velocity as a function of r/η at the indicated values of St.

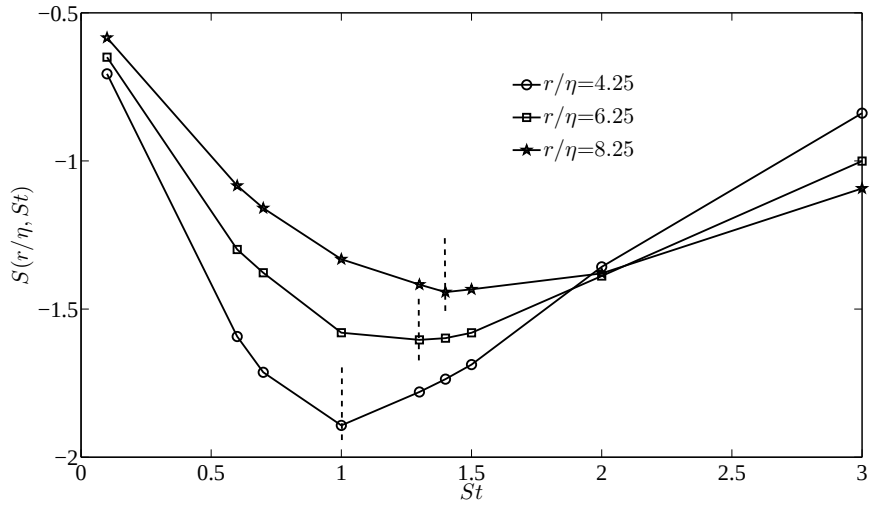

Figure 2.14: Variation of the skewness of the PDF of the radial relative velocity as a function of St at the indicated values of r/η. Dashed vertical lines show approximate peaks.

a broadening of the PDF with increasing separation distance. Bec et al. (2010) and Salazar and Collins (2012) observe a similar trend in their simulations by considering different moments of w_r. Both of these trends can be explained by recognizing that both with increasing particle inertia and increasing separation distance between particles, the particle velocities become increasingly decorrelated with each other, and this leads to broader PDFs. However, the effect eventually saturates at larger r/η or St, as shown in figures 2.11(c) and 2.11(d), where we see no effect of further variation in either parameter. Wang et al. (2000) had earlier considered PDFs of w_r (normalized by its standard deviation) at particle contact at different Reynolds numbers and found no dependence on R_λ over the range they simulated (R_λ=24-75). In figure 2.12, we verify their conclusion over a larger range of R_λ (227 and 95). We use the Kolmogorov velocity scale u_η to normalize w_r and find that for small separations, the PDFs are nearly independent of Reynolds number. However, as we increase the separation distance, the PDFs show a stronger dependence on the Reynolds number in the tails. This is likely due to the fact that internal intermittency increases with Reynolds number, leading to the broader tails in the PDF. Furthermore, neighboring inertial particles are affected by the 'sling effect' (Falkovich et al., 2002) or 'caustics' (Wilkinson et al., 2006), whereby inertial particles are flung together from uncorrelated regions of the flow. This leads to an increase in the probability of neighboring particles having uncorrelated velocities (Salazar and Collins, 2012). With increasing Reynolds number, we would expect increased intermittency in the flow to enhance the rate of occurrence of casutics leading to higher relative velocities between particles. However, our results also confirm the findings of Wang et al. (2000) that showed that low-order moments, which primarily reflect the central part of the PDF and only weakly depend on the tails, show very little Reynolds number dependence.

It is self evident that the relative velocity between two particles along their line-of-centers affects their radial separation and hence must be related to the RDF. Close inspection of figure 2.11 reveals that the PDFs are skewed towards negative values of w_r (Wang et al., 2000). Since $w_r < 0$ corresponds to particles moving towards each other, it is plausible that the skewness ($S(r/\eta, St) = \langle {w_r}^3 \rangle / (\langle {w_r}^2 \rangle^{3/2})$) of the PDF is related to clustering. Wang et al. (2000) hinted at this correspondence by showing that at particle contact, low St particles show higher negative skewness in w_r than both fluid tracers and high St particles. Here we probe the issue more closely by considering the parametric dependence of S on r/η and St. Figure 2.13 shows the spatial variation of $S(r/\eta, St)$ at different St, and indeed it shows some qualitative resemblance to the RDF. Similar to the RDF, the skewness decreases monotonically with separation distance (except at high St) and the magnitude of skewness for low St particles are higher than those of high St. We also observe the crossover between different St curves, and when we plot $S(r/\eta, St)$ as a function of St in figure 2.14, we see the peaks in the skewness curves shift to the right with increasing r/η, similar to the RDF. We conclude there is a very close qualitative correspondence between the RDF and the skewness of the radial relative velocity PDF. We can understand this finding a little more if we consider the theoretical arguments presented in Chun et al. (2005), which showed that low St particles undergo a net inward drift (i.e.,$\langle w_r \rangle_p < 0$) in isotropic turbulence leading to clustering. However, as the particle field approaches equilibrium, this inward drift eventually will be balanced by an outward diffusion flux, such that $\langle w_r \rangle_p = 0$. Hence the signature for this balance of drift and diffusion will manifest in the next odd-order moment, i.e., the skewness.

As we did with the RDF, let us now look at the effect of filtering on the statistics of w_r. Figure 2.15 compares the filtered and unfiltered PDF of w_r at two separation

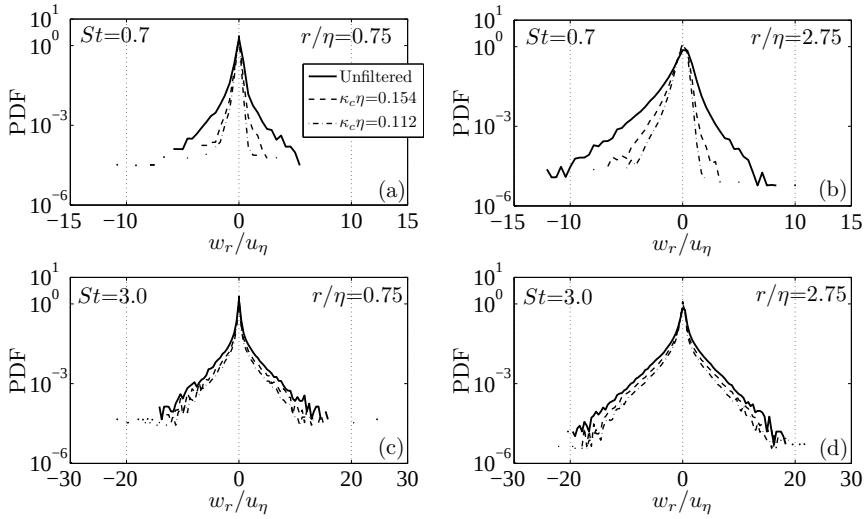

Figure 2.15: Effect of filtering on the radial relative velocity PDF at: $St = 0.7$ and r/η (a) 0.75 and (b) 2.75; and $St = 3.0$ and r/η (c) 0.75 and (d) 2.75. Solid lines are the unfiltered case, dashed lines are $\kappa_c\eta$=0.154 and dash-dot lines are $\kappa_c\eta$=0.112.

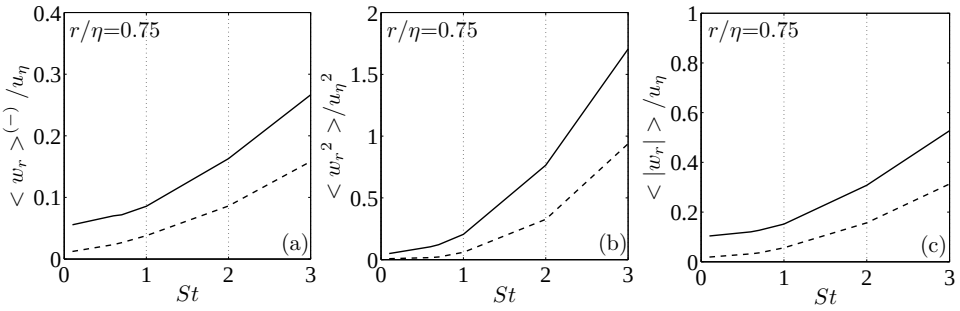

Figure 2.16: Effect of filtering ($\kappa_c\eta = 0.154$) on the mean inward component, variance and mean of the absolute value of w_r. Solid lines are the unfiltered case and dashed lines are the filtered case.

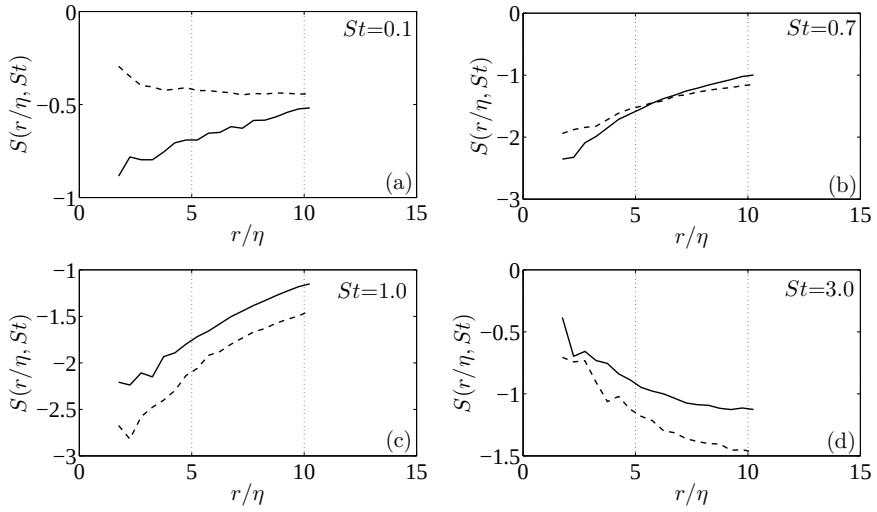

Figure 2.17: Effect of filtering ($\kappa_c\eta$=0.154) on the spatial variation of skewness of the PDF of the radial relative velocity at Stokes numbers: (a) 0.1, (b) 0.7, (c) 1.0 and (d) 3.0. Solid lines are the unfiltered case and dashed lines are the filtered case.

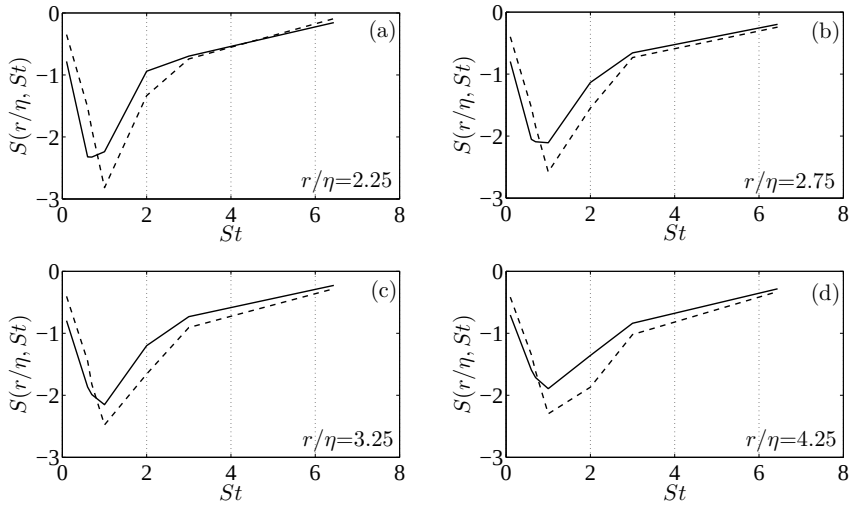

Figure 2.18: Effect of filtering ($\kappa_c\eta$=0.154) on the variation of skewness of the PDF of the radial relative velocity with St at r/η: (a) 2.25, (b) 2.75, (c) 3.25 and (d) 4.25. Solid lines are the unfiltered case and dashed lines are the filtered case.

distances for St=0.7 and St=3.0 and for two different filter scales. For both the St and r/η considered, we observe that filtering narrows the PDF. This is true for all St, as can be seen in figure 2.16(b), which shows the variance normalized by ${u_\eta}^2$. Figure 2.16(c) shows the absolute mean $\langle|w_r|\rangle$ normalized by u_η which is used in some collision kernel models (Wang et al., 2000; Bec et al., 2005; Ayala et al., 2008a) and behaves similarly to the variance. This behavior is similar to that reported in Jin et al. (2010a), where the reduction in $\langle|w_r|\rangle$ with filtering is attributed to the loss of enstrophy in the flow field due to filtering. w_r enters into the collision kernel through the mean radial inward velocity $\langle w_r\rangle^{(-)} = \int_{-\infty}^{0} -w_r P(w_r/\sigma)\, dw_r$ (de Jong et al., 2010) and figure 2.16(a) shows that filtering reduces $\langle w_r\rangle^{(-)}$ for all St considered in this study. An important observation from figure 2.16 is that all of the above trends are monotonic with St as opposed to what was found for the RDF. However, if we now look at the skewness, we find something different. Figure 2.17 shows the effect of filtering on skewness for different St as a function of separation distance. We find that at low St, the skewness is reduced by velocity filtering, but at high St, it increases with filtering with a crossover at around St=0.7. Although the crossover points for the RDF and the skewness of w_r differ, we find that the skewness has a qualitatively similar, non-monotonic response to filtering as did the RDF. Furthermore, if we plot the effect of filtering on the variation of skewness with St at different separation distance (figure 2.18), we find that the filtered curves shift to the right for all the cases, consistent with the RDF. Hence, the non-monotonic response of the RDF to filtering appears to be connected to the skewness of the radial relative velocity.

At this point, it might be instructive to look at the variation of the statistics of w_r as a function of the cut-off filter-scale ($\kappa_c\eta$). Fede and Simonin (2006) looked at the variance of w_r normalized by the unfiltered variance as a function of cut-

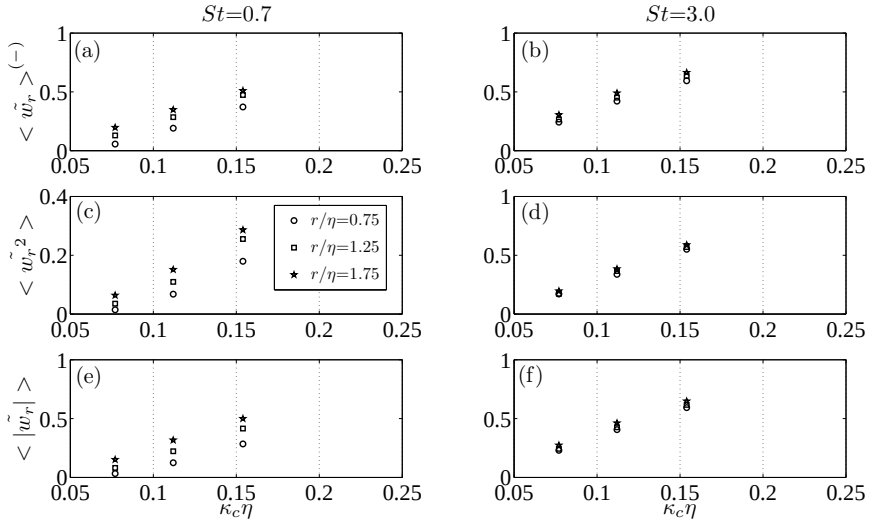

Figure 2.19: Variation of the mean inward component, variance and mean absolute value of w_r, normalized by their unfiltered values, with filter-scale at the indicated values of St and r/η.

off wavenumber and showed that it smoothly asymptotes to 1 as the cut-off scale extends into the dissipation range. Here, we consider cut-off wavenumbers in the inertial range (table 2.1) and consider the variation of $\langle w_r \rangle^{(-)}$, $\langle {w_r}^2 \rangle$ and $\langle |w_r| \rangle$ normalized by their unfiltered values as a function of $\kappa_c \eta$. Figure 2.19 shows that for all separation distances and St, their behavior is approximately linear with slopes and intercepts that are functions of both St and r/η.

Let us now consider the simple model discussed in §2.4.1 and recalculate the statistics of w_r in terms of the modified Stokes number St^f (equations (2.8)). Figure 2.20 shows that such a model overcompensates for the effect of filtering. Figure 2.21 plots the variation of the mean inward relative velocity and the variance and absolute mean of w_r and reiterates the findings of §2.4.1, namely that the very nature of variation of the filtered statistics is different from the unfiltered ones. As a result, a scale shift can at best match the original value at one St, but does not contain the required physics of the filtered scales to recover the behavior of the unfiltered curves. We can compute the maximum error incurred in computing

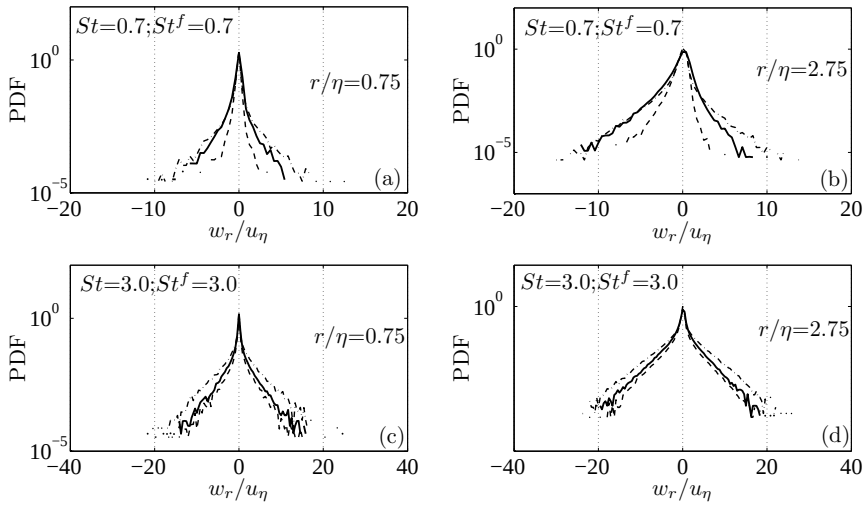

Figure 2.20: Effect of filtering on the radial relative velocity PDF at: $St = 0.7$ and r/η (a) 0.75 and (b) 2.75; and $St = 3.0$ and r/η (c) 0.75 and (d) 2.75. Solid lines are the unfiltered case, dashed lines are the filtered case ($\kappa_c\eta = 0.154$) and dash-dot lines are the filtered case based on the modified Stokes number, St^f.

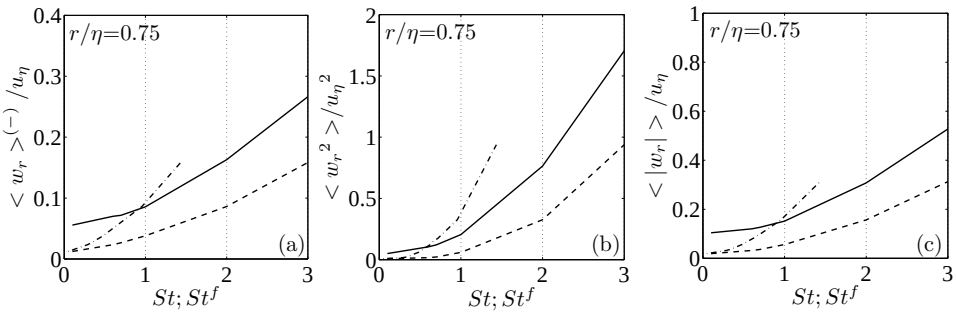

Figure 2.21: Effect of filtering ($\kappa_c\eta = 0.154$) on the mean inward component, variance and mean of the absolute value of w_r. Solid lines are the unfiltered case, dashed lines are the filtered case and dash-dot lines are the filtered case based on the modified Stokes number, St^f.

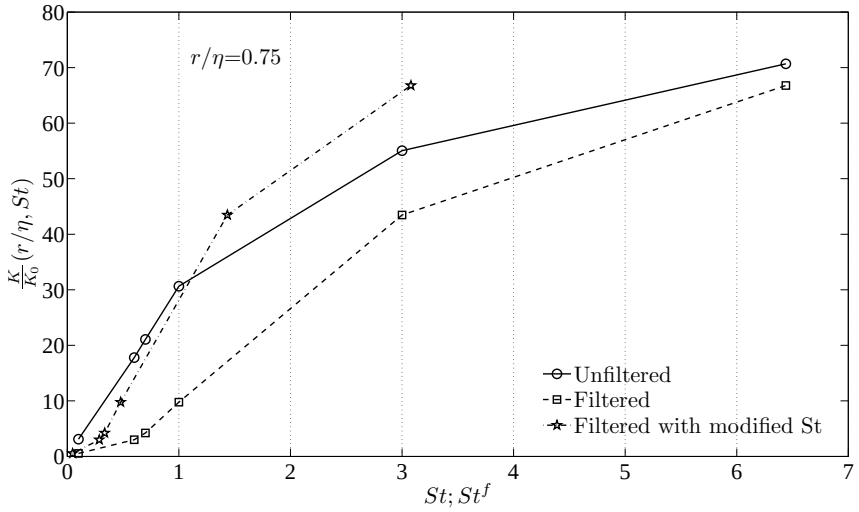

Figure 2.22: Effect of filtering on the variation of the non-dimensional collision kernel with Stokes number. Solid lines are the unfiltered case, dashed lines are the filtered case ($\kappa_c\eta = 0.154$) and dash-dot lines are the filtered case based on the modified Stokes number, St^f.

these statistics with the simple model. For r/η=0.75, the maximum relative error in prediction of $\langle w_r \rangle^{(-)}/u_\eta$, $\langle w_r \rangle^2/{u_\eta}^2$ and $\langle |w_r| \rangle/u_\eta$ are -0.875, 0.500 and -0.900 respectively, well above what is required for an accurate collision model.

2.4.3 Collision kernel

Let us now use the RDF and the PDF of w_r discussed in the previous two sections and construct the collision kernel for particles following equation (2.2b). We normalize it by the collision kernel for fluid elements defined as $K_0(r) = (8\pi/15)^{1/2} r^3 u_\eta/\eta$ (Saffman and Turner, 1956). For predicting collision frequency, we require the RDF and w_r measured at contact. In the framework of our point-particle simulations, we set $r/\eta = 0.75$ to compute the collision kernel. We could not go to smaller r/η due to statistical considerations. Figure 2.22 shows the variation of the collision kernel as a function of St at $r/\eta = 0.75$. We observe that

it increases with St, which indicates that the broadening of the PDF of w_r with St dominates the reduction in RDF up to at least $St = 6.44$. Also, we see that filtering reduces the kernel for all St up to 6.44 and that a simple rescaling of the Stokes number does not recover the original curve. The reduction in the average particle collision rate with filtering has recently been reported in Jin et al. (2010a) for $St < 3$. They found that for $St > 3$, the filtered DNS can predict the collision kernel accurately. We also observe the filtered collision kernel approaches the unfiltered kernel with increasing Stokes number; however, the rate of approach here is slower than was found in Jin et al. (2010a). This may be due to differences in the Reynolds number of the DNS, the filter cutoff scale, and/or the relatively large collision diameter ($r/\eta = 0.75$) chosen here for illustrative purposes. What is clear is that a better subgrid model is required to accurately predict the collision kernel (and related quantities such as the particle size distribution with coalescence) in a LES with particles of arbitrary Stokes number.

2.5 Conclusions

In this work, we have studied the radial distribution function and the radial relative velocity statistics of inertial particles in homogeneous, isotropic turbulence using DNS (R_λ=227). In addition to the well-known result of a decrease in the RDF with separation distance at all St, we have found that the St at which clustering is peaked, depends upon the spatial separation considered and increases with increasing separation distance. We have confirmed the Reynolds number independence of the RDF at low St found by Collins and Keswani (2004), but demonstrated that a stronger dependence is found at higher St. The radial relative velocity between two particles drives their spatial separation (and hence the RDF) but the relation

between the two is not yet well-established. Here we show that the first and second moments of w_r increase with both separation distance and St due to decorrelation between the particles. However, the skewness decreases in magnitude with separation distance (for low St) and the skewness vs St curve shows a peak which shifts to higher St with increasing separation, in qualitative agreement with the RDF. We have also considered the Reynolds number dependence of w_r and confirmed the result of Wang et al. (2000) that the PDF of w_r is independent of Reynolds number for small separations, although we do observe significant variations in the tails of the PDF for $r/\eta \geq 8.75$.

We then systematically studied the effect of filtering on the RDF and w_r by applying a sharp spectral cut-off filter to the DNS velocity field. The filtered velocity field is an 'ideal' LES velocity field free of subgrid modeling assumptions. We find that at all separation distances, the RDF decreases with filtering for low St and increases with filtering for high St, with a cross-over around St=1.5, which is independent of the filter-scale in the inertial range. We show, for the first time, visual evidence of the above effect of filtering on particle clustering. We also show that even in a strongly filtered velocity field, the particles tend to avoid regions of high vorticity and therefore show significant preferential concentration. Also, the RDF vs St curves shift to the right with filtering at all separation distances. We observe a narrowing of the PDF of w_r with filtering at all St and separation distances, which is reflected in a decrease in the absolute mean and the variance. However, the skewness of w_r shows qualitatively, the same non-monotonic response to filtering as the RDF, providing further support for the relationship between the two. We also find that the RDF and the moments of w_r vary approximately linearly with filter-scale in the inertial range, with their slopes and intercepts being functions of both St and separation distance. We have tested a simple model for the

subgrid scales and showed that redefining the St using the time-scale of the filtered velocity field cannot recover the unfiltered statistics. The nature of variation of the filtered statistics differs from that of the unfiltered ones and hence any model involving only a scale-shift in St cannot capture the particle behaviour accurately. Rather, we need to incorporate the physics of the subgrid scales. Our results help establish the requirements that a LES subgrid model for particles should satisfy in order to capture clustering and collisional behaviour correctly.

2.6 Acknowledgments

This study was supported by the National Science Foundation under grant number CBET 0756510. The authors gratefully acknowledge the Texas Advanced Computing Center (TACC) at The University of Texas at Austin for providing HPC resources on Ranger that have contributed to the research results reported within this paper.

CHAPTER 3

A SUBGRID MODEL FOR CLUSTERING OF HIGH-INERTIA PARTICLES IN LARGE-EDDY SIMULATIONS OF TURBULENCE

3.1 Abstract

Clustering (or preferential concentration) of inertial particles suspended in a homogeneous, isotropic turbulent flow is strongly influenced by the smallest scales of the turbulence. In particle-laden large-eddy simulations (LES) of turbulence, these small scales are not captured by the grid and hence their effect on particle motion needs to be modeled. In this paper, we use a subgrid model based on kinematic simulations of turbulence (Kinematic Simulation based SubGrid Model or KSSGM), for the first time in the context of predicting the clustering and the relative velocity statistics of inertial particles. We show that the KSSGM gives excellent predictions for clustering in *a priori* tests for inertial particles with $St \geq 2.0$, where St is the Stokes number, defined as the ratio of the particle response time to the Kolmogorov time-scale. To the best of our knowledge, the KSSGM represents the first model that has been shown to capture the effect of the subgrid scales on inertial particle clustering for $St \geq 2.0$. We also show that the mean inward radial relative velocity between inertial particles ($\langle w_r \rangle^{(-)}$, which enters into the formula for their collision kernel) is accurately predicted by the KSSGM for all St. We explain why the model captures clustering at higher St but not for lower St , and provide new insights into the key statistical parameters of the turbulence that a subgrid model would have to describe, in order to accurately predict clustering of low St particles in a LES.

3.2 Introduction

Inertial particles in turbulence have been shown to cluster outside of vortices, in the high-strain regions of the flow using both numerical simulations (Maxey, 1987; Squires and Eaton, 1991; Wang and Maxey, 1993; Eaton and Fessler, 1994; Sundaram and Collins, 1997) and experiments (Fessler et al., 1994; Salazar et al., 2008; Saw et al., 2008; Gibert et al., 2012; Bateson and Aliseda, 2012; Saw et al., 2012). Such clustering can influence a broad range of aerosol processes, such as particle settling (e.g., Wang and Maxey, 1993), evaporation/condensation (e.g., Shaw et al., 1998) and interparticle collisions and coagulation (e.g., Sundaram and Collins, 1997; Reade and Collins, 2000b). It has been hypothesized that particle clustering plays a crucial role in the broadening of the droplet size distribution in warm cumulus clouds, during both condensational growth and growth by collision and coalescence (Shaw et al., 1998; Falkovich et al., 2002; Shaw, 2003; Devenish et al., 2012; Grabowski and Wang, 2013). High-inertia particles, i.e., particles with response times greater than the Kolmogorov time-scale, are ubiquitous in natural and industrial applications. Some examples include cloud droplets in *highly* turbulent clouds (e.g., see table 3 in Ayala et al., 2008b), planetesimal formation in protoplanetary disks (Pan and Padoan, 2010; Pan et al., 2011), motion of aerosols inhaled into the human airway (Khan et al., 2010), and most industrial and atmospheric gas-solid flows.

The radial distribution function or RDF (McQuarrie, 1976), an important measure of particle clustering in isotropic turbulence, is defined as the ratio of the average number of particle pairs per unit volume found at a given separation distance to the expected number if the particles were uniformly distributed. The RDF can be computed from a field of Q particles by binning the particles according to

their separation distance and calculating

$$g(r) = \frac{Q_{p,r}/\Delta V_r}{Q_p/V} \ , \tag{3.1}$$

where $Q_{p,r}$ is the average number of particles found in an elemental shell volume ΔV_r at a distance $r = |\boldsymbol{r}|$ from a test particle, V is the total volume and $Q_p = Q(Q-1)/2$ is the total number of particle pairs in the flow. Sundaram and Collins (1997) showed that the RDF evaluated at particle contact precisely corrects the collision kernel for particle clustering. The average collision frequency for a monodisperse particulate system is given by

$$N_c = \frac{n^2}{2} K(\sigma) \ , \tag{3.2a}$$

where σ denotes the particle diameter, $n \equiv Q/V$ is the particle number density and $K(\sigma)$ is the collision kernel, defined for a statistically stationary suspension as

$$K(\sigma) = 4\pi\sigma^2 g(\sigma) \int_{-\infty}^{0} (-w_r) P(w_r|\sigma)\, dw_r \ . \tag{3.2b}$$

As can be seen from (3.2b), apart from the RDF, the other statistical input to the collision kernel is the probability density function (PDF) of the radial component of the relative velocity, w_r, defined as

$$w_r(\boldsymbol{r}) = [\boldsymbol{v}_2(\boldsymbol{x}+\boldsymbol{r}) - \boldsymbol{v}_1(\boldsymbol{x})] \cdot \frac{\boldsymbol{r}}{|\boldsymbol{r}|} \ , \tag{3.3}$$

where $\boldsymbol{v}_1(\boldsymbol{x})$ and $\boldsymbol{v}_2(\boldsymbol{x}+\boldsymbol{r})$ are the velocities of two particles located at $\boldsymbol{x}$ and $\boldsymbol{x}+\boldsymbol{r}$, respectively. In equation (3.2b), we are interested in the mean inward radial relative velocity $\langle w_r \rangle^{(-)}(\Delta) = -\int_{-\infty}^{0} w_r P(w_r|\Delta)\, dw_r$. The effect of inertia on the radial relative velocity statistics has been investigated in the context of predicting the collision kernel (Wang et al., 2000; Ayala et al., 2008b,a; de Jong et al., 2010; Bec et al., 2010) and also for modeling the particle motion that leads to clustering (Chun et al., 2005; Zaichik and Alipchenkov, 2009; Pan and Padoan, 2010).

As the RDF and the PDF of w_r are strongly influenced by the details of the small-scale turbulent fluctuations, RANS based turbulence models are inadequate in capturing them. Direct numerical simulations (DNS) resolve all of the turbulent scales and hence can accurately predict the particle statistics, but DNS is still much too expensive for simulations of practical applications at realistic Reynolds numbers. Large-eddy simulations (LES) provide a compromise by accurately simulating the larger scales of the turbulent fluctuations, while the smaller subgrid scales need to be modeled. As the availability of computing power increases, LES is increasingly becoming an attractive choice for performing practical turbulent flow calculations more accurately than RANS-based methods. Consequently, particle-laden LES has emerged as a viable tool for computing particle statistics in turbulence, and has received considerable attention recently (Wang and Squires, 1996b,a; Armenio et al., 1999; Boivin et al., 2000; Fede and Simonin, 2006; Marchioli et al., 2008; Pozorski and Apte, 2009). However, subgrid models that work well for flow statistics are not easily translated to describing inertial particle statistics. Consequently, there have been attempts at developing models specifically aimed towards recovering inertial particle statistics. Shotorban and Mashayek (2005) and Kuerten (2006) used the approximate deconvolution method to exactly recover the scales of the turbulence represented on the grid in a LES. But, as we will show in §3.5, and as has been shown previously (Jin et al., 2010a; Ray and Collins, 2011), an exact representation of the larger turbulent fluctuations in a LES does not necessarily yield the correct particle clustering. Shotorban and Mashayek (2006b,a), Fede et al. (2006), and Pozorski and Apte (2009) constructed stochastic Langevin-type models for the subgrid fluctuations seen by inertial particles. But, these models were not able to predict particle clustering across the whole range of St (Cernick, 2013). In fact, Pozorski and Apte (2009) were only able to match the RDF approximately

for $St = 2.0$, after choosing an appropriate but arbitrary value of their model constant. Jin et al. (2010a), and Ray and Collins (2011, 2013a) have demonstrated the crucial role that the small-scale turbulent fluctuations play in particle clustering. Therefore, we seek a subgrid model that contains sufficiently detailed information regarding the small-scale structure of the turbulence without adding significant computational expense, and is devoid of arbitrarily adjustable parameters.

Such a model, which we call a Kinematic Simulation based SubGrid model (KSSGM), is described in §3.4. The central idea of the KSSGM is to predict some information about the subgrid flow structure based on a good estimate of the subgrid energy (and dissipation) spectrum. In isotropic turbulence, this implies that we have captured the Eulerian two-point correlations of the subgrid fluid velocity (and velocity gradient) seen by the inertial particles. We then show in §3.5 that the KSSGM gives excellent results for the RDF at $St \geq 2.0$, and for $\langle w_r \rangle^{(-)}$at all St. The KSSGM is relatively inexpensive to compute, and it is free of arbitrarily adjustable parameters, since the only input to the model viz. the energy spectrum can be specified by well-known model spectra (Pope, 2000). We also discuss why the KSSGM is less effective in predicting the RDF for inertial particles with $St < 2.0$, which sheds light on a path forward for that regime.

This paper is organized as follows. In §3.3.1 we describe the details of the numerical methods used to evolve the isotropic turbulent flow field and track a large number of inertial particles. In §3.3.2 we describe the filtering of a DNS velocity field to obtain an 'exact' LES velocity field, which can be used for *a priori* testing of our model. Section 3.4 describes the theory and implementation of KSSGM in detail. In §3.5, we present the results from an *a priori* test of the KSSGM for the RDF and $\langle w_r \rangle^{(-)}$. Section 3.6 provides some concluding remarks.

3.3 Numerical simulations

This section provides an overview of all of the simulation tools we have used in the course of this investigation.

3.3.1 Direct Numerical Simulation

We perform DNS of homogeneous, isotropic turbulence in a periodic cube that contains inertial particles. Below we describe the numerical techniques used to solve for the flow field and the particle motion.

Fluid phase

The governing equations for a three-dimensional incompressible flow are the continuity and the Navier Stokes equation. In rotational form, the equations are

$$\frac{\partial u_i}{\partial x_i} = 0 \quad , \tag{3.4a}$$

$$\frac{\partial u_i}{\partial t} + \epsilon_{ijk}\omega_j u_k = -\frac{\partial (p/\rho + \frac{1}{2}u^2)}{\partial x_i} + \nu \frac{\partial^2 u_i}{\partial x_j \partial x_j} \quad , \tag{3.4b}$$

where u_i is the velocity vector, $u \equiv \sqrt{u_i u_i}$ is the magnitude of the velocity vector, ρ is the fluid density, ν is the kinematic viscosity, ϵ_{ijk} is the alternating unit symbol, ω_i is the vorticity, and p is the pressure. Equations (3.4) are solved using a pseudo-spectral algorithm with de-aliasing based on a combination of truncation and phase-shift (Patterson and Orszag, 1971; Johnson, 1998; Brucker et al., 2007) on a flow domain comprised of a cube with each side of length 2π (in arbitrary units). Periodic boundary conditions are imposed on each of the cube faces. We use 128 grid points in each direction and achieve a Reynolds number based on the

Taylor microscale (R_λ) of 95. The time-step was chosen so that the CFL number is less than 0.5. At each time-step, we use a deterministic forcing function to inject energy into the first two wavenumbers in Fourier space, in order to maintain a statistically stationary isotropic turbulence (Witkowska et al., 1997). We evolve the flow-field for about thirteen eddy turnover times to reach statistical stationarity. Additional details of simulation parameters and resolution are given in table 1.

Inertial particle motion

We assume a dilute suspension of inertial particles, which allows us to neglect the feedback of particle motion on the carrier fluid (Sundaram and Collins, 1999). We also consider particles whose radius a is much smaller than the Kolmogorov length scale η and simulate them as point-particles. Furthermore, we assume that the particles are much denser than the surrounding fluid ($\rho_p/\rho_f \gg 1$), the particle Reynolds numbers are small, and collisions and gravitational settling are neglected. Under these assumptions, the equations of motion for the particles reduce to (Maxey and Riley, 1983)

$$\frac{d\boldsymbol{x}(t)}{dt} = \boldsymbol{v}(t) \ , \tag{3.5}$$

$$\frac{d\boldsymbol{v}(t)}{dt} = \frac{\boldsymbol{u}\left[\boldsymbol{x}(t)\right] - \boldsymbol{v}(t)}{\tau_p} \ , \tag{3.6}$$

where $\boldsymbol{x}$ is the inertial particle position, $\boldsymbol{v}$ is the particle velocity, $\tau_p = (2/9)\frac{\rho_p a^2}{\rho_f \nu}$ is the particle response time and $\boldsymbol{u}\left[\boldsymbol{x}(t)\right]$ denotes the fluid velocity at the inertial particle location. We have used $96,000$ particles for each of the Stokes numbers considered. These particles are introduced into the stationary flow field at random positions and with the fluid velocity at those locations. Particles are advanced in time according to (3.5) and (3.6) using an improved numerical scheme that was recently developed in our group (Ireland et al., 2012, 2013). This new algorithm,

Variable	DNS	FDNS
N	128	128
R_λ	95	-
$\kappa_{max}\eta$	1.508	-
k	1.178	1.080
ϵ	0.232	0.085
η	0.025	-
τ_η	0.139	-
L	1.490	-
Q	96,000	96,000

Table 3.1: Turbulence parameters for DNS and FDNS. N is the number of grid points in each of the 3 dimensions, R_λ is the Reynolds number based on the Taylor micro-scale, $k = \int_0^{\kappa_{max}} E(\kappa)\, d\kappa$ is the kinetic energy, $\epsilon = 2\nu \int_0^{\kappa_{max}} \kappa^2 E(\kappa)\, d\kappa$ is the dissipation rate, $\eta = \frac{\nu^{3/4}}{\epsilon^{1/4}}$ is the Kolmogorov length scale, $\tau_\eta = \sqrt{\frac{\nu}{\epsilon}}$ is the Kolmogorov time scale and $L = \frac{3\pi}{2k} \int_0^{\kappa_{max}} \frac{E(\kappa)}{\kappa}\, d\kappa$ is the integral length scale; For FDNS, k and ϵ are computed by replacing κ_{max} by the cut-off filter scale κ_c. Q is the total number of particles simulated for each St .

based on exponential integrators, is second-order accurate in time and can simulate particles with arbitrarily small St accurately. It allows us to use the fluid time-step (dictated by the CFL condition) to advance the inertial particles, irrespective of St, thereby significantly reducing the run times for low St particles. Fluid velocities at particle locations are obtained using eighth-order Lagrangian interpolation. We use the DNS velocity field to specify the fluid velocity seen by the particles in equations (3.5) and (3.6). This gives us an accurate description of the inertial particle positions and velocities. We allow sufficient time (four eddy turnover times) for the particles to equilibriate with the flow before taking statistics. Particle statistics are averaged over several eddy turnover times.

3.3.2 Filtering

We perform a low-pass filtering of the DNS velocity field in Fourier space so that all the Fourier modes of velocity beyond a preset cutoff wavenumber κ_c are removed from the flow and only the remaining 'large scales' are retained. Such a filtered DNS (FDNS) can be viewed as a 'perfect' LES velocity field, where the large scales are represented exactly, and not subject to any subgrid modeling errors. We apply a sharp spectral filter to the DNS velocity field at each time-step, that removes all wavenumbers above κ_c, yielding the following definition of the filtered velocity

$$\tilde{\hat{\boldsymbol{u}}}(\boldsymbol{\kappa},t) = \begin{cases} \hat{\boldsymbol{u}}(\boldsymbol{\kappa},t) & |\boldsymbol{\kappa}| \leq \kappa_c \\ \mathbf{0} & \text{otherwise} \end{cases} . \tag{3.7}$$

Here, $\tilde{\hat{\boldsymbol{u}}}(\boldsymbol{\kappa},t)$ and $\hat{\boldsymbol{u}}(\boldsymbol{\kappa},t)$ are the Fourier modes of the filtered and unfiltered velocity, respectively, and $\kappa_c\eta = 0.2$ is the cutoff wavenumber. Figure 3.1 shows the energy and dissipation spectra obtained from the DNS. Notice that the cutoff wavenumber (or filter scale) is chosen to lie within the inertial subrange. The turbulent kinetic energy and dissipation rate are computed for the filtered velocity field using the standard definitions shown in table 3.1, with κ_{max} replaced by κ_c. Inertial particles are advanced in the FDNS using the filtered velocity at particle locations in equations (3.5) and (3.6). As we will show in §3.5, the RDF and $\langle w_r \rangle^{(-)}$are not well-predicted by FDNS, which motivates the development of the KSSGM. It is worth noting that if we choose the cutoff wavenumber well into the dissipation subrange, the filtering has very little effect on clustering (Ray and Collins, 2011).

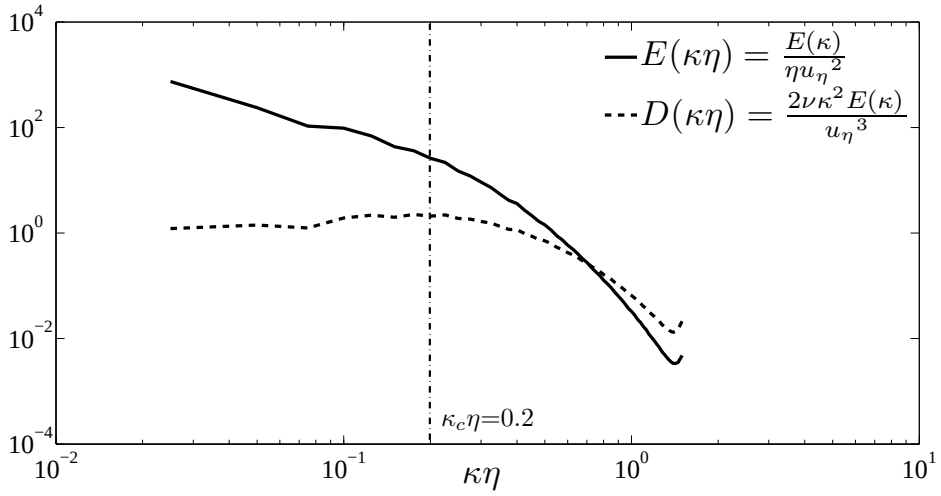

Figure 3.1: Filter cut-off scale ($\kappa_c\eta$=0.2) superimposed on the normalized energy ($E(\kappa)/\eta {u_\eta}^2$) and dissipation ($2\nu\kappa^2 E(\kappa)/{u_\eta}^3$) spectra. Notice that $\kappa_c\eta$ is within the inertial subrange.

3.4 Kinematic Simulation based SubGrid Model (KSSGM)

In this section, we describe the KSSGM. The model is based on a class of synthetic turbulence models known as kinematic simulations (KS) (Kraichnan, 1970; Fung et al., 1992). The standard form of the KSSGM velocity field is given by

$$\boldsymbol{u}_{\text{KSSGM}}(\boldsymbol{x},t) = \sum_{n=1}^{N_k}\sum_{m=1}^{M}\left\{\boldsymbol{a}_{nm}cos(\boldsymbol{\kappa}_{nm}\cdot\boldsymbol{x}+\omega_{nm}t) + \boldsymbol{b}_{nm}sin(\boldsymbol{\kappa}_{nm}\cdot\boldsymbol{x}+\omega_{nm}t)\right\}, \quad (3.8)$$

where $\boldsymbol{a}_{nm}$ and $\boldsymbol{b}_{nm}$ are real-valued, vector coefficients of the Fourier cosine and sine modes of velocity, respectively, $\boldsymbol{x}$ is the coordinate vector, t is the time, $\boldsymbol{\kappa}_{nm}$ is the wavevector, and ω_{nm} is the frequency. Note that vector quantities are written in boldface. The indices "nm" are not the standard Cartesian index notation. Instead we are using a spherical coordinate system, where the first index "n" denotes the wavenumber (i.e., magnitude of the wavevector, $\kappa_n = |\boldsymbol{\kappa}_{nm}|$), and the second index "m" is a counter of randomly oriented wavevectors of magnitude κ_n. We follow Flohr and Vassilicos (2000) and use a geometric distribution of wavenumbers

beyond the cut-off wavenumber $\boldsymbol{\kappa}_c$

$$\kappa_n = \kappa_c \left(\frac{\kappa_{max}}{\kappa_c} \right)^{\frac{n-1}{N_k - 1}} ,$$

where $n = 1, 2, \ldots, N_k$, and κ_{max} is the largest wavenumber considered. Flohr and Vassilicos (2000) investigated different distributions of the wavenumbers and determined that the above geometric distribution achieved the fastest convergence for fluid particle statistics. Orientation angles for the M wavevectors associated with each wavenumber n are chosen randomly so as to be uniformly (i.e., isotropically) distributed over the spherical shell of radius κ_n (see Appendix for details). For the present simulation, the periodic cubic domain imposes the additional restriction that $\boldsymbol{u}_{\text{KSSGM}}(\boldsymbol{x}, t)$ be periodic. We can ensure periodicity by only selecting wavevectors with integer components, which slightly degrades the isotropy of $\boldsymbol{\kappa}_{nm}$. Tests run with the periodic condition strictly enforced yielded no discernible effect on the results for the RDF and the statistics of w_r. We therefore chose to use the more generally applicable, isotropic distribution of $\boldsymbol{\kappa}_{nm}$ described in the Appendix.

A total of $N_k \times M$ wavevectors are used to construct $\boldsymbol{u}_{\text{KSSGM}}(\boldsymbol{x}, t)$. The number of wavevectors per shell, M, should be chosen large enough to achieve acceptable statistical convergence to the energy spectrum associated with that wavenumber. To ensure $\boldsymbol{u}_{\text{KSSGM}}(\boldsymbol{x}, t)$ is also incompressible, we define the coefficients $\boldsymbol{a}_{nm}$ and $\boldsymbol{b}_{nm}$ as

$$\boldsymbol{a}_{nm} = \boldsymbol{A}_{nm} \times \hat{\boldsymbol{\kappa}}_{nm} , \tag{3.9}$$

$$\boldsymbol{b}_{nm} = \boldsymbol{B}_{nm} \times \hat{\boldsymbol{\kappa}}_{nm} , \tag{3.10}$$

where $\hat{\boldsymbol{\kappa}}_{nm} \equiv \boldsymbol{\kappa}_{nm}/\kappa_n$ is a unit vector aligned with wavevector $\boldsymbol{\kappa}_{nm}$. $\boldsymbol{A}_{nm}$ and $\boldsymbol{B}_{nm}$ are random vectors with independent, normally-distributed components, each with zero mean and variance

$$\sigma_n^2 = \frac{1}{M} E(\kappa_n) \Delta\kappa_n . \tag{3.11}$$

Here, $E(\kappa)$ denotes the subgrid energy spectrum, which could be approximated by a known model spectrum (e.g., Pope (2000)); however, in this study we use the DNS spectrum, to minimize modeling errors in the KSSGM.

One of the key assumptions in arriving at the KS formulation (Eq. (3.8)) is the decoupling of the time and space dependence of the velocity modes. In a KS, the frequencies ω_{nm} are treated as independent variables that must be specified, and previous work (Osborne et al., 2005) has considered the effect of ω_{nm} on the Eulerian one-point two-time structure functions and Lagrangian velocity autocorrelations. However, as pointed out by Malik and Vassilicos (1999), and Flohr and Vassilicos (2000), the possible nontrivial specifications of ω_{nm} based on scaling arguments (e.g., $\omega_{nm} = \lambda\sqrt{\kappa_{nm}^3 E(\kappa_{nm})}$, or $\omega_{nm} = \lambda u_{rms}\kappa_{nm}$, where $0 < \lambda < 1$) have been shown to have little effect on the statistical properties of fluid particle pairs. Consistent with these earlier studies, we did not find any significant influence of the choice of ω_{nm} on the RDF and w_r. Therefore, as was done by Flohr and Vassilicos (2000), we set $\omega_{nm} = 0$ in the KSSGM. However, we note that the lack of realistic coupling between the spatial and temporal variations in the modes causes the KSSGM to be unable to capture the sweeping of small-scale structures by the large scales, which in turn leads to some of the errors in the predicted RDF. A complete discussion of this is given in §3.5.

By construction, $\boldsymbol{u}_{\mathrm{KSSGM}}(\boldsymbol{x}, t)$ is a real, incompressible model for the subgrid velocity field that is consistent with the subgrid energy spectrum specified by the user. The modeled velocity field at each particle position is then written as

$$\boldsymbol{u}_{\mathrm{MODEL}}(\boldsymbol{x}, t) = \boldsymbol{u}_{\mathrm{FDNS}}(\boldsymbol{x}, t) + \boldsymbol{u}_{\mathrm{KSSGM}}(\boldsymbol{x}, t) \ . \tag{3.12}$$

The particle equations (3.5) and (3.6) are evolved using $\boldsymbol{u}_{\mathrm{MODEL}}$ on the right hand side. This constitutes an *a priori* test of the model. Our cut-off wavenumber is

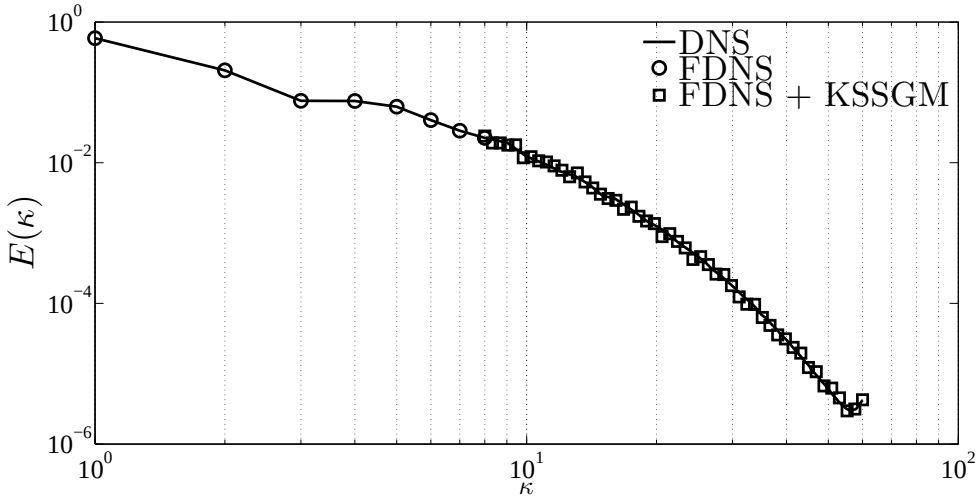

Figure 3.2: Comparison of the energy spectrum obtained from DNS, FDNS and KSSGM, with the cut-off wavenumber $\kappa_c = 8$ (corresponding to $\kappa_c\eta = 0.2$). The FDNS follows the DNS spectrum exactly uptill κ_c. Beyond κ_c, the KSSGM recovers the subgrid spectrum to a good approximation.

$\kappa_c = 8$, and the maximum wavenumber is $\kappa_{max} = 60$. We have found very little difference in our statistics, when we varied the total number of wavenumbers from 2500 ($N_k = 50,\ M = 50$) down to 400 ($N_k = 20,\ M = 20$). This makes the KSSGM a relatively inexpensive model when compared with the cost of performing a LES along with Lagrangian particle tracking. Figure 3.2 shows the energy spectrum in a DNS, FDNS and KSSGM. We ensure continuity in the spectrum by requiring $E(\kappa_c)|_{\text{KSSGM}} = E(\kappa_c)|_{\text{FDNS}}$. We can observe that the KSSGM recovers the subgrid energy spectrum quite accurately. Quantitatively, we find the *maximum* relative errors in predicting the total kinetic energy and dissipation rate using the KSSGM to be around 0.9% and 3.5% respectively.

Malik and Vassilicos (1999) have shown that as a Lagrangian model for particle dispersion in isotropic turbulence, KS performs better than existing Lagrangian stochastic models. They attribute this to the presence of well-defined eddying, straining, and streaming flow structures present in the KS (Fung et al., 1992). The

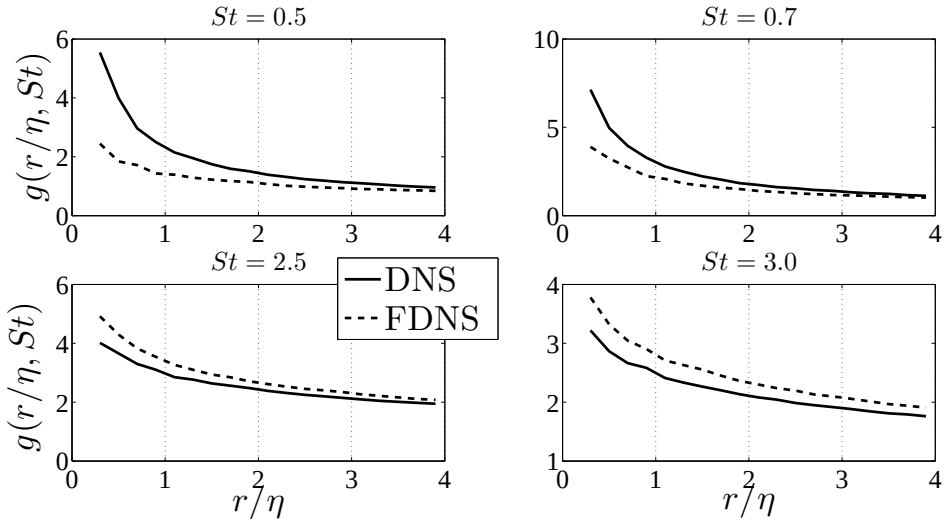

Figure 3.3: Effect of filtering on the variation of the RDF with r/η for Stokes numbers (St) of 0.5, 0.7, 2.5 and 3.0.

presence of small-scale structure, with specified Eulerian two-point correlations, makes the KSSGM an attractive choice for recovering particle clustering from a LES. We note here that LES subgrid models based on KS were introduced by Flohr and Vassilicos (2000) and have been used in a few studies since (Yao and He, 2009; Khan et al., 2010). However, such a model has never been applied to predict the RDF and w_r statistics of inertial particles.

3.5 Results and discussion

In this section, we compare predictions of the model velocity consisting of the FDNS plus the KSSGM velocity (hereafter referred to as 'FDNS + KSSGM') with DNS and FDNS.

Figure 3.3 shows the effect of filtering on the spatial variation of the RDF for 4 different St. We observe a strong effect of filtering on the RDF, especially at small separations. As observed previously (Fede and Simonin, 2006; Ray and Collins,

2011), filtering tends to reduce the RDF at low St and increase it at high St, with a crossover at approximately $St = 1.5$. This is due to the fact that at lower St, clustering is primarily driven by the centrifuging of the particles out of the vortical regions into the straining regions of the flow, and this process is strongest at the smallest scales of the flow; thus, removing the small-scales by filtering results in a weakening of the primary mechanism of clustering causing a reduction of the RDF predicted in FDNS with no subgrid model. At higher St, where the particle response times are larger than the Kolmogorov time-scale, the small-scales of the turbulence contribute less to the clustering and more to the random motion of the particles (i.e., dispersion) and hence their removal results in an enhanced clustering and an increased RDF.

Figure 3.4 shows the effect of introducing the KSSGM, on the spatial variation of the RDF. We can see that the model results are in excellent agreement with DNS for $St \geq 2.0$, whereas the agreement at $St < 2.0$ is not as good. It is also worth noting that although quantitatively inaccurate, the model predicts the correct qualitative trends at all Stokes numbers. In particular, the KSSGM contains sufficient physics of the subgrid scales to qualitatively capture the non-monotonic response of the RDF to filtering. This is likely a reflection of the fact that the KSSGM, by construction, yields the correct subgrid energy spectrum. However, it is quantitatively accurate only at higher Stokes numbers. Figure 3.5 verifies this by considering St up to 6.0, and shows that the KSSGM consistently yields an accurate RDF for $St \geq 2.0$.

Let us now consider the model performance for the statistics of w_r. We will consider the mean inward radial relative velocity $\langle w_r \rangle^{(-)}$, which appears in the formula for the collision kernel (3.2b). Figure 3.6 shows the effect of filtering on

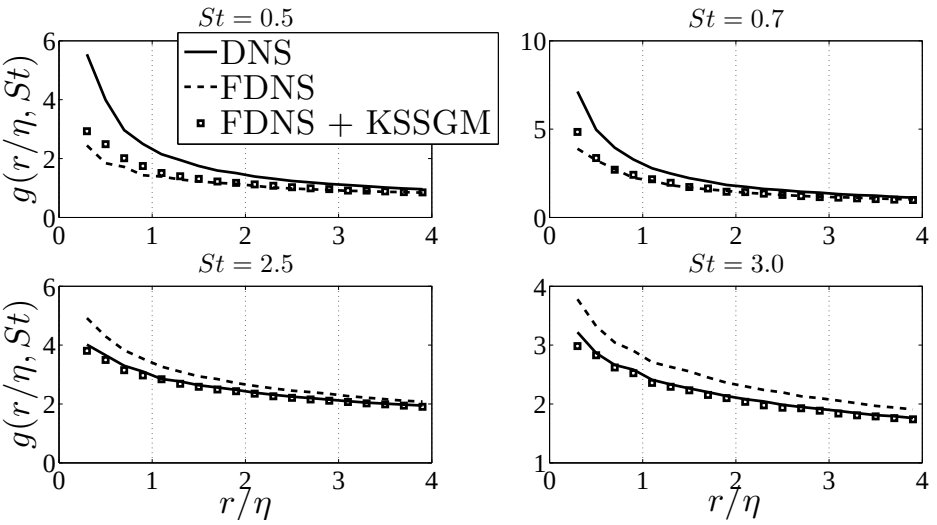

Figure 3.4: Results from *a priori* test of the KSSGM on the variation of the RDF with r/η for Stokes numbers (St) of 0.5, 0.7, 2.5 and 3.0.

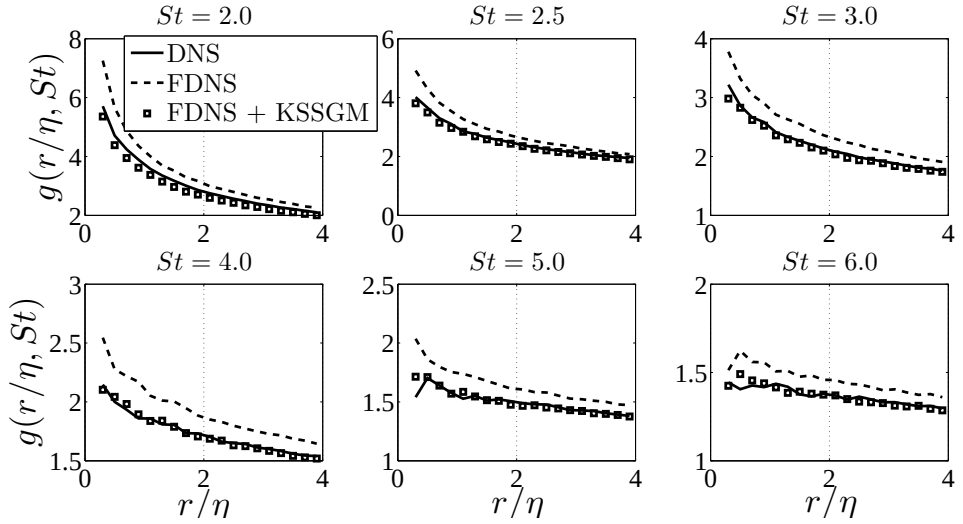

Figure 3.5: Results from *a priori* test of the KSSGM on the variation of the RDF with r/η for $St \geq 2.0$

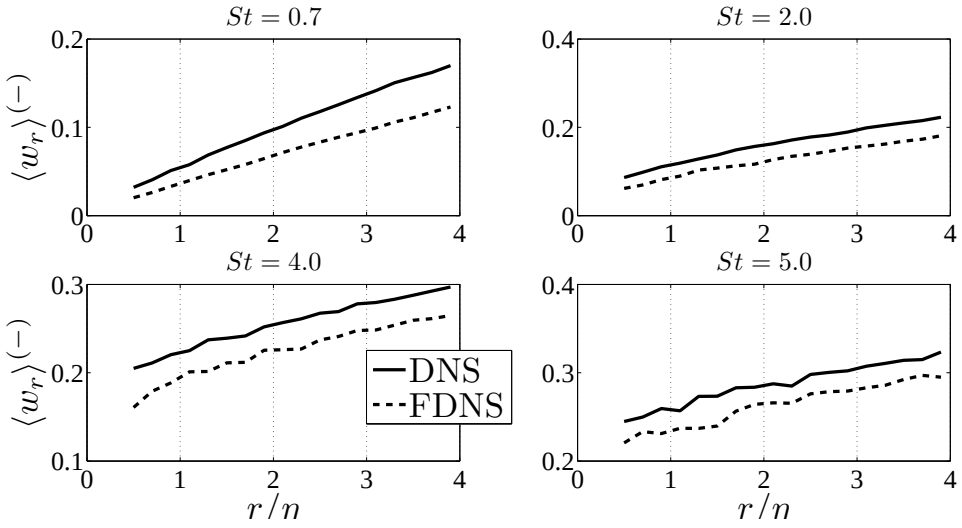

Figure 3.6: Effect of filtering on the variation of the mean inward radial relative velocity $\langle w_r \rangle^{(-)}$with r/η for Stokes numbers (St) of 0.7, 2.0, 4.0 and 5.0.

the spatial variation of $\langle w_r \rangle^{(-)}$for 4 different St . Unlike the RDF, the response of $\langle w_r \rangle^{(-)}$to filtering is qualitatively similar at all St . As noted by Ray and Collins (2011), the small-scale turbulent fluctuations give rise to large particle relative velocities and contribute to the tails of the PDF of w_r . Filtering out the small-scales reduces this effect and causes an attenuation of the tails of the PDF of w_r , thus reducing $\langle w_r \rangle^{(-)}$. Figures 3.7 and 3.8 show the result of introducing the KSSGM on $\langle w_r \rangle^{(-)}$. We find that the model is not only able to qualitatively recover the effect of filtering on $\langle w_r \rangle^{(-)}$for all St , but the quantitative agreement with DNS data at lower St is much better than that found for the RDF. We obtain similar results for the variance $\langle w_r^2 \rangle$, indicating that the first two moments of w_r are well captured by the KSSGM at all St. However, as with the RDF, we find that the KSSGM is only able to accurately predict the skewness (or the third-order moment) of w_r for $St \geq 2.0$. Ray and Collins (2011) had earlier showed that the skewness of w_r behaves qualitatively similarly to the RDF, and differently from the lower-order moments. The theoretical description of clustering in Zaichik and Alipchenkov (2009), and its analysis by Bragg and Collins (2013a) shows that the

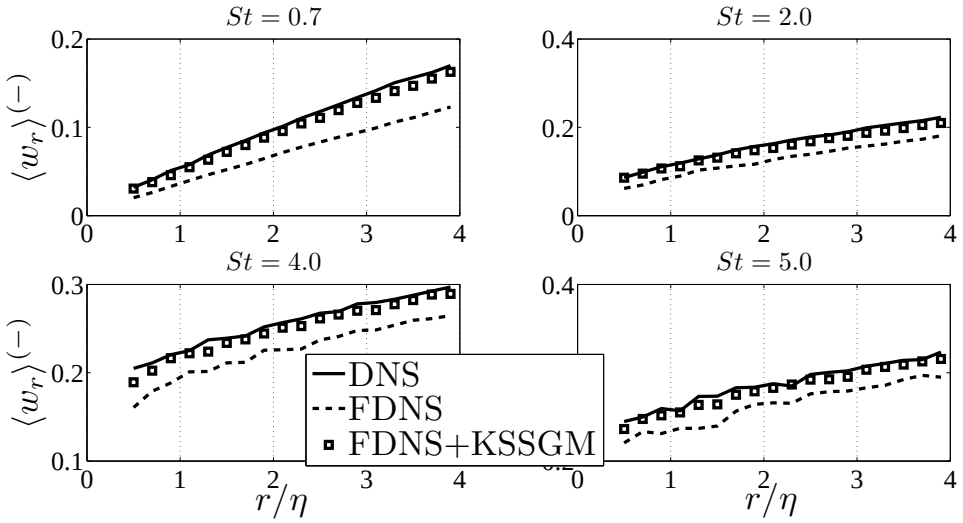

Figure 3.7: Results from *a priori* test of the KSSGM on the variation of the mean inward radial relative velocity $\langle w_r \rangle^{(-)}$with r/η for Stokes numbers (St) of 0.7, 2.0, 4.0 and 5.0.

mean inward drift responsible for clustering depends upon the divergence of the second-order particle structure function, which in turn is a function of the third-order particle structure function. Therefore, while the KSSGM can predict the moments of w_r up to order 2 for all St, its inability to predict the skewness of the relative velocity for $St < 2.0$ is strongly related to its analogous shortcomings with the RDF prediction.

Let us now explore why the KSSGM is not able to accurately predict the RDF (or the related skewness of the relative velocity) for $St < 2.0$. By construction, the KSSGM captures the subgrid energy and dissipation spectra, which are related to the Eulerian two-point correlations of the velocity and velocity gradient respectively. However, as noted earlier, it does not capture the sweeping of the small-scales by the large-scales, and it does not describe any of the coherent structures that are characteristic of small-scale turbulence. Since the earliest studies of preferential concentration in turbulence (Eaton and Fessler, 1994), it has been hypothesized that the small-scale coherent structures in the flow strongly influence

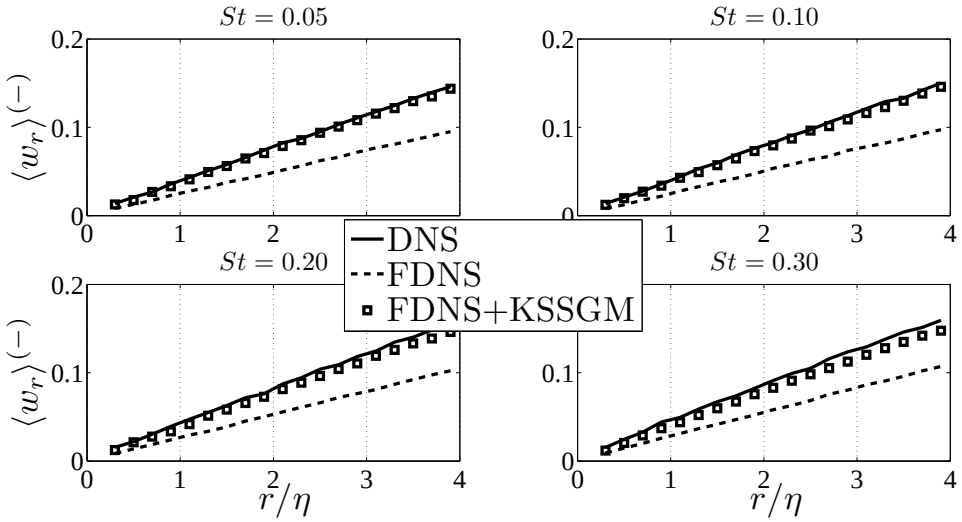

Figure 3.8: Results from *a priori* test of the KSSGM on the variation of the mean inward radial relative velocity $\langle w_r \rangle^{(-)}$with r/η for Stokes numbers (St) of 0.05, 0.10, 0.20 and 0.30.

particle clustering. A well-known signature of such coherent structures is the difference between the Lagrangian time-scales for the strain-rate and rotation-rate tensors, denoted by $\mathcal{T}_S^L$ and $\mathcal{T}_R^L$ respectively, and defined as

$$\mathcal{T}_S^L = \int_0^\infty \frac{\langle S_{ij}(t) S_{ij}(t+s) \rangle}{\langle S_{ij}(t)^2 \rangle} ds = \int_0^\infty \rho^S(s) ds \quad , i,j = 1 \ldots 3 \,, \tag{3.13a}$$

$$\mathcal{T}_R^L = \int_0^\infty \frac{\langle R_{ij}(t) R_{ij}(t+s) \rangle}{\langle R_{ij}(t)^2 \rangle} ds = \int_0^\infty \rho^R(s) ds \quad , i,j = 1 \ldots 3 \,. \tag{3.13b}$$

Here $S_{ij} = \frac{1}{2}\left(\frac{\partial u_i}{\partial x_j} + \frac{\partial u_j}{\partial x_i}\right)$ is the strain-rate tensor, $R_{ij} = \frac{1}{2}\left(\frac{\partial u_i}{\partial x_j} - \frac{\partial u_j}{\partial x_i}\right)$ is the rotation-rate tensor, and $\langle \cdot \rangle$ denotes an average over all particle trajectories. Theory (Zaichik and Alipchenkov, 2009; Bragg and Collins, 2013a) tells us that at small Stokes numbers, the inward drift velocity that is responsible for the clustering of inertial particles is related to $\mathcal{T}_S^L$ and $\mathcal{T}_R^L$. The presence of small-scale coherent vortices with finite life-times in an isotropic turbulent flow field results in $\mathcal{T}_R^L > \mathcal{T}_S^L$ for fluid particles. Figure 3.9 shows the average Lagrangian autocorrelations $\rho^S(s)$ and $\rho^R(s)$ obtained along fluid particle trajectories in a DNS, FDNS and FDNS + KSSGM. We find that the model underpredicts both $\mathcal{T}_S^L$ and $\mathcal{T}_R^L$ for fluid particles, where the relative error is 25% for $\mathcal{T}_S^L$, and 57% for $\mathcal{T}_R^L$ (refer to table 3.2). As

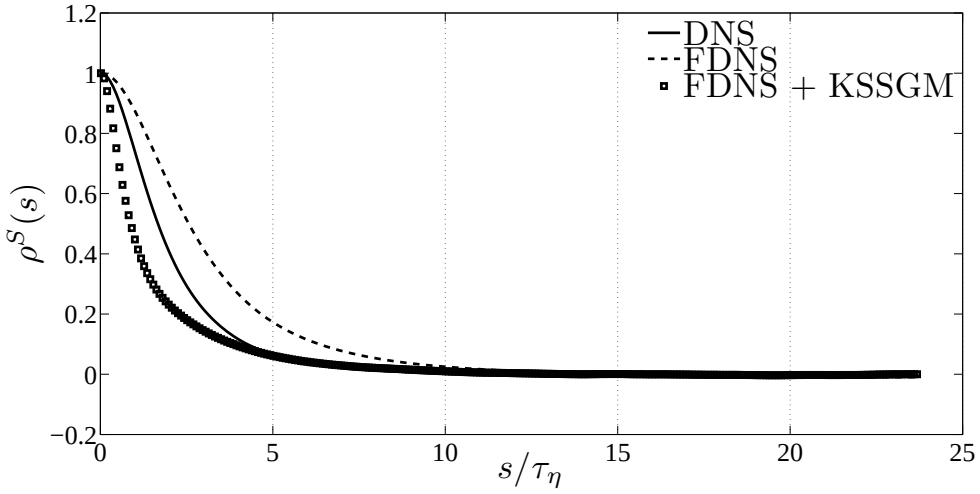

(a)

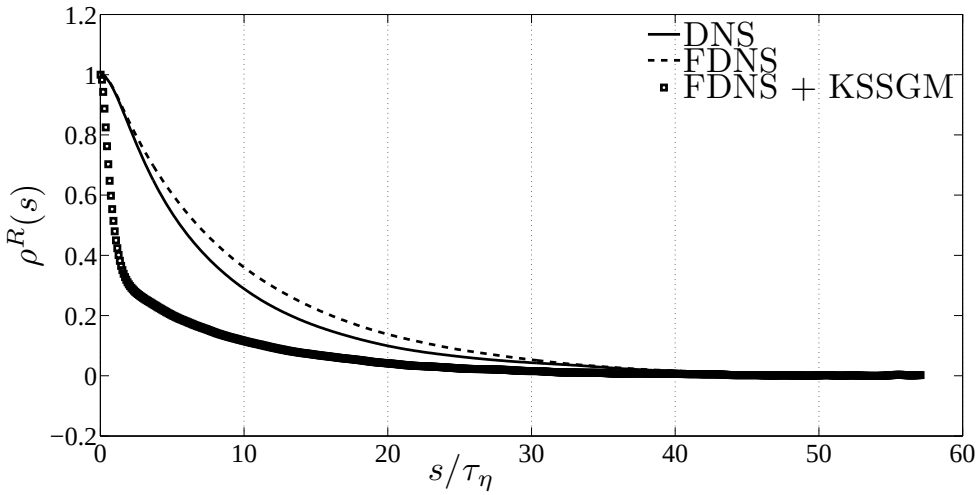

(b)

Figure 3.9: Comparison of the Lagrangian autocorrelations of (a) strain-rate ($\rho^S(s)$) and (b) rotation-rate ($\rho^R(s)$), obtained along fluid particle trajectories from DNS, FDNS and FDNS + KSSGM.

St	$\mathcal{T}_S^L/\tau_\eta$			$\mathcal{T}_R^L/\tau_\eta$		
	DNS	FDNS + KSSGM	DNS-SCR	DNS	FDNS + KSSGM	DNS-SCR
0.0	2.0921	1.5710	2.2678	8.7958	3.8392	6.0850
0.1	2.0694	1.5742	-	7.2539	3.4150	-
0.7	2.3221	1.7258	-	4.3340	2.2766	-
2.0	2.4401	1.9806	-	2.7526	1.9384	-
3.0	2.5888	2.0962	-	2.6722	1.8779	-

Table 3.2: Lagrangian time-scales of strain-rate ($\mathcal{T}_S^L$) and rotation-rate ($\mathcal{T}_R^L$) normalized by the Kolmogorov time-scale in DNS-SCR for fluid particles, and in DNS and FDNS + KSSGM for particles with Stokes numbers (St) of 0.0 (fluid particle), 0.1, 0.7, 2.0, and 3.0.

we shall explain below, such a severe underprediction of $\mathcal{T}_R^L$ by the KSSGM is due to the absence of both the correct sweeping of the small-scales by the large-scales, and the absence of small-scale coherent structures. To explore how the predictions for these time-scales vary with St, consider figures 3.10(a) and 3.10(b) where we plot $\mathcal{T}_S^L$ and $\mathcal{T}_R^L$ normalized by the Kolmogorov time-scale as a function of St. The numerical values are tabulated in table 3.2. We note that with increasing St, the KSSGM predictions approach the DNS values from below. Also, the discrepancy at small St is much larger for $\mathcal{T}_R^L$ than for $\mathcal{T}_S^L$. Due to the absence of small-scale coherent structures and the correct sweeping effect, the KSSGM is unable to distinguish between $\mathcal{T}_S^L$ and $\mathcal{T}_R^L$. For high St particles, these two time-scales approach each other, and hence the model is more accurate. However, the difference between $\mathcal{T}_S^L$ and $\mathcal{T}_R^L$ seems to play an important role in the clustering process at low St (as would be expected from the theoretical results of Zaichik and Alipchenkov (2009) and Bragg and Collins (2013a)), and the KSSGM cannot capture the effect.

Now that we have established the range of applicability of the KSSGM and the possible reasons for its errors at low St, we will now attempt to separate the errors due to the lack of sweeping from those due to the lack of coherent structures.

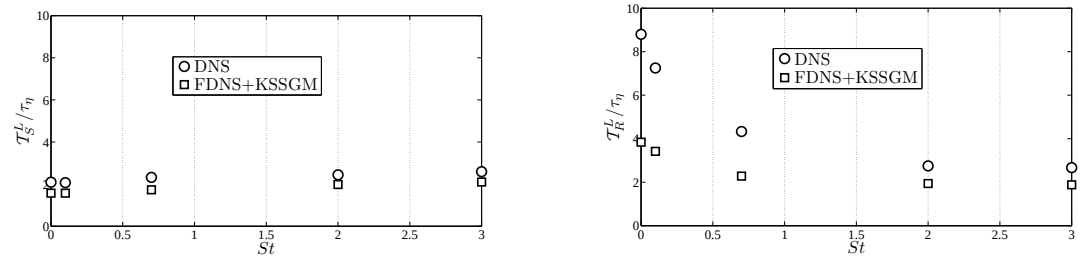

(a) (b)

Figure 3.10: Lagrangian time-scales for (a) strain-rate ($\mathcal{T}_S^L$) and (b) rotation-rate ($\mathcal{T}_R^L$), normalized by the Kolmogorov time-scale, in DNS and FDNS + KSSGM as a function of St.

This could guide the development of new models for capturing particle clustering at low St. To do this, we consider a DNS velocity field, in which we remove the coherent structures, but not the sweeping (except, of course, the sweeping associated with the coherent structures themselves). This can be achieved by scrambling the velocity modes beyond $\kappa = \kappa_c$ in order to destroy the coherent structures. Following Ulitsky and Collins (1997), we define the scrambled velocity field as

$$\hat{u}_{\mathrm{SCR},i}(\boldsymbol{\kappa}, t) = S(\boldsymbol{\kappa}, t)\hat{u}_i(\boldsymbol{\kappa}, t) \quad , \tag{3.14}$$

where the scrambling operator is defined as

$$S(\boldsymbol{\kappa}, t) = \begin{cases} 1 & |\boldsymbol{\kappa}| \leq \kappa_c \\ e^{2\pi i\theta(\boldsymbol{\kappa})} & \kappa_c < |\boldsymbol{\kappa}| \leq \kappa_{max} \end{cases}$$

Here, $\theta(\boldsymbol{\kappa})$ is a uniformly distributed random number in the interval $(0, 1]$ with the property $\theta(-\boldsymbol{\kappa}) = -\theta(\boldsymbol{\kappa})$. This ensures that all of the spectra involving velocity autocorrelations (like energy, helicity, dissipation, etc.), as well as the second-order velocity statistics like mean kinetic energy, mean vorticity, Kolmogorov scales, etc. are preserved in the scrambled velocity field (Ulitsky and Collins, 1997). The scrambling operator $S(\boldsymbol{\kappa})$ is chosen once at the beginning of the simulation and then is fixed throughout the simulation. This ensures that the scrambled velocity

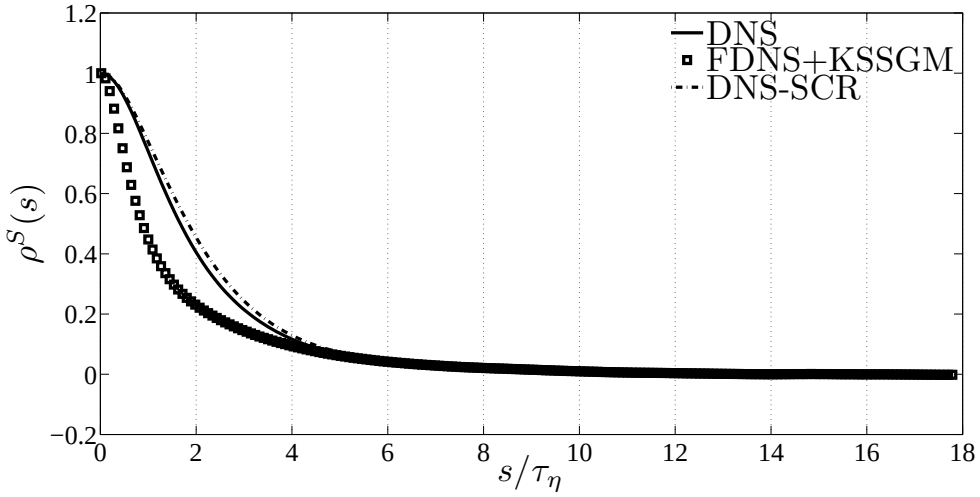

(a)

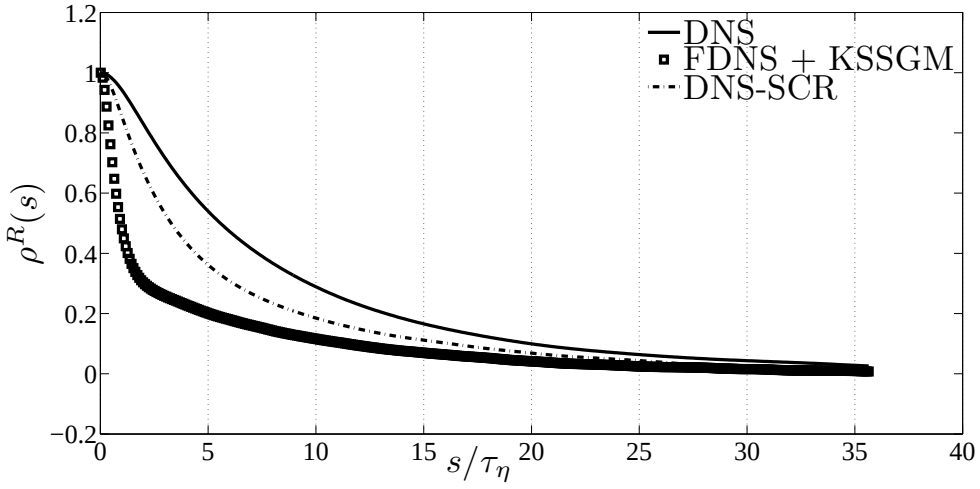

(b)

Figure 3.11: Comparison of the Lagrangian autocorrelations of (a) strain-rate ($\rho^S(s)$) and (b) rotation-rate ($\rho^R(s)$), obtained along fluid particle trajectories from DNS, FDNS + KSSGM and DNS-SCR

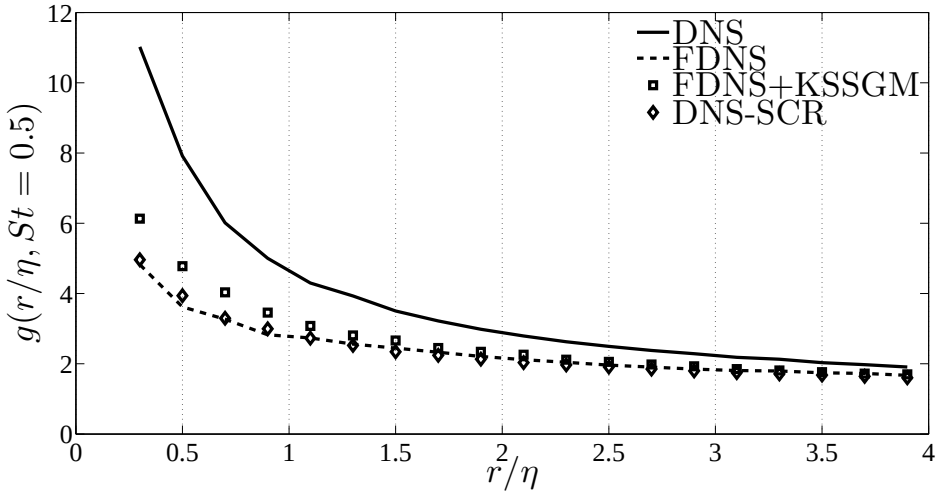

(a)

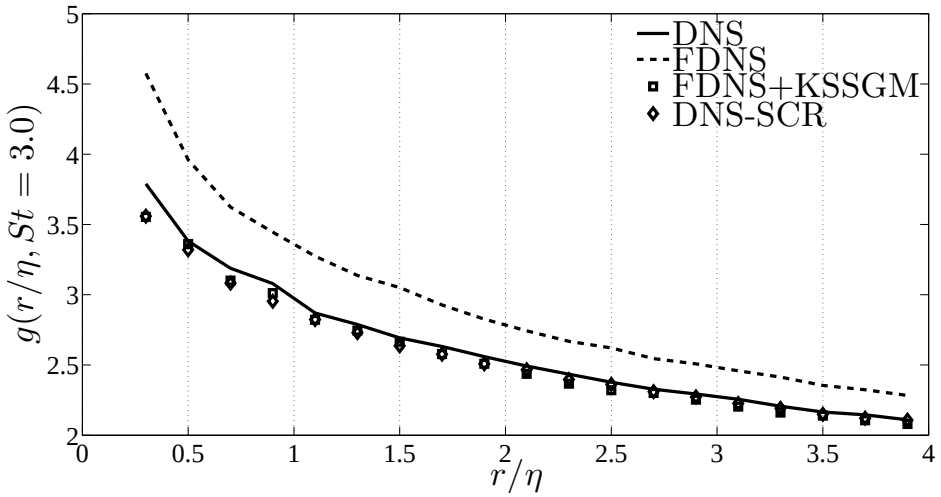

(b)

Figure 3.12: Variation of the RDF with r/η for Stokes numbers (St) of (a) 0.5, and (b) 3.0 in DNS, FDNS, FDNS + KSSGM and DNS-SCR.

field varies smoothly in time. Therefore, in the scrambled velocity field (referred to henceforth as DNS-SCR), we retain all the spectral modes from the DNS, preserving all of the Eulerian two-point correlations related to the velocity field. However, beyond $\kappa = \kappa_c$, the 'subgrid' velocity field is devoid of the strong small-scale coherent structures. Figure 3.11 shows $\rho^S(s)$ and $\rho^R(s)$ obtained along fluid particle trajectories in DNS-SCR. Referring to figure 3.11 and table 3.2, we find that the scrambled velocity field yields the correct Lagrangian time-scales for the strain-rate tensor, but significantly underpredicts the Lagrangian time-scales for the rotation-rate tensor indicating the strong dependence of $\mathcal{T}_R^L$ on the coherent structures. We also consider the predictions of the RDF at small and large St using DNS-SCR as shown in figure 3.12, and find that it gives results very similar to FDNS + KSSGM. It is noteworthy that the KSSGM seems to give slightly superior results for the RDF at $St = 0.5$ compared to DNS-SCR. This may be due to the frozen subgrid field of the KSSGM, which is known to overpredict the RDF. Both the DNS-SCR and the KSSGM are devoid of the small-scale coherent structures. However, a major difference between the DNS-SCR and a KSSGM (even with an infinite number of modes) is that the DNS-SCR, being derived from the solution to the Navier-Stokes equation, contains a more realistic description of the sweeping of the small scales by the large scales in comparison with the KSSGM, leading to a better prediction of $\mathcal{T}_R^L$. However, as is evident from figure 3.12, this is not sufficient to predict the RDF accurately at low St, underscoring the importance of the small-scale coherent structures in the clustering of particles at low Stokes numbers.

3.6 Conclusions

In this paper, we investigate the use of a properly tuned kinematic simulation as a subgrid model (the so-called KSSGM) to predict the RDF and the statistics of w_r in an *a priori* LES (filtered DNS) of isotropic turbulence. The KSSGM has the virtues of being an inexpensive model, that contains no arbitrarily adjustable parameters. The only inputs required to specify the model are the subgrid energy spectrum (a well-known quantity in isotropic turbulence), and the frequency distribution. In agreement with Flohr and Vassilicos (2000), we find very little sensitivity to the selection of the frequency distribution, and therefore set them to zero. We show that the KSSGM is able to quantitatively predict the RDF only for $St \geq 2.0$. Furthermore, the KSSGM can accurately predict the moments of w_r up to order 2 at all St, but can capture the skewness of w_r only for $St \geq 2.0$. Since the RDF is closely related to the skewness of w_r (Zaichik and Alipchenkov, 2009; Ray and Collins, 2011; Bragg and Collins, 2013a), the limitations with respect to the predictions of both statistics are related. One possible explanation for this is that the KSSGM is unable to properly capture the difference between $\mathcal{T}_S^L$ and $\mathcal{T}_R^L$, which at low St occurs due to the presence of small-scale coherent structures and the sweeping of the small-scales by the large-scales, both of which are not accounted for in the KSSGM. Since there is little difference between these time-scales for $St \geq 2.0$ ($\mathcal{T}_S^L \approx \mathcal{T}_R^L$), the KSSGM works well in that regime. By using a DNS field that is scrambled beyond $\kappa = \kappa_c$, we show that describing the small-scale coherent structures is essential to correct these time scales and accurately predict the RDF at low St. We hope that such understanding will assist in future developments of subgrid models aimed at predicting clustering for $St < 2.0$.

Finally we note an important advantage of the KSSGM is that it can been

adapted to inhomogeneous flows (Khan et al., 2010; Clark and Vassilicos, 2011). It is a natural extension of this work to evaluate the predictions from the KSSGM in these more complex flows.

3.7 Appendix A: Isotropic specification of $\boldsymbol{\kappa}$

In order to generate isotropic statistics with the KSSGM, we require an isotropic specification of the wavevectors $\boldsymbol{\kappa}_{nm}$ (Fung et al., 1992). The specification of $\boldsymbol{\kappa}_{nm}$ usually described in the literature (e.g., see Yao and He, 2009) is given by

$$\boldsymbol{\kappa}_{nm} = |\boldsymbol{\kappa}_{nm}|(sin\theta_{nm}cos\phi_{nm}, sin\theta_{nm}sin\phi_{nm}, cos\theta_{nm}) \tag{3.15}$$

where $\theta_{nm} \in [0, 2\pi]$ and $\phi_{nm} \in [0, \pi]$ are uniformly distributed random angles. We can show that this specification does not generate a truly isotropic distribution of $\boldsymbol{\kappa}$. For example, if we consider a sphere with a radius κ_{nm}, then for $m = 1, \ldots M$, equation (3.15) generates samples of vectors $\boldsymbol{\kappa}_{nm}$ that are clustered near the poles of the sphere (Weisstein, 2013), resulting in anisotropic flow statistics. For example, consider the velocity gradient tensor $\boldsymbol{\Gamma}$, which is a small-scale statistic likely to be influenced by the isotropy of the KSSGM flow field. If we consider the the lagrangian autocorrelations $\rho^{\Gamma}_{ij}(s) = \frac{\langle \Gamma_{ij}(t)\Gamma_{ij}(t+s)\rangle}{\langle \Gamma_{ij}(t)^2\rangle} \, \forall \, i, j = 1, 2, 3$ of each component of $\boldsymbol{\Gamma}$, isotropy implies that we will get two distinct set of curves, one for the diagonal terms $\rho^{\Gamma}_{ii}(s)$, $\forall \, i = 1, 2, 3$ and one for the off-diagonal terms $\rho^{\Gamma}_{ij}(s)$, $\forall \, i, j = 1, 2, 3 \, (i \neq j)$. Figure 3.13(a) shows this from DNS data, whereas figure 3.13(b) shows the same curves using FDNS + KSSGM with $\boldsymbol{\kappa}$ specified by equation (3.15). We find that the off-diagonal components of $\boldsymbol{\Gamma}$ generated by this method are not truly isotropic. A simple algorithm to generate an isotropic $\boldsymbol{\kappa}_{nm}$ uses equation (3.15) but with a different choice of the angles:

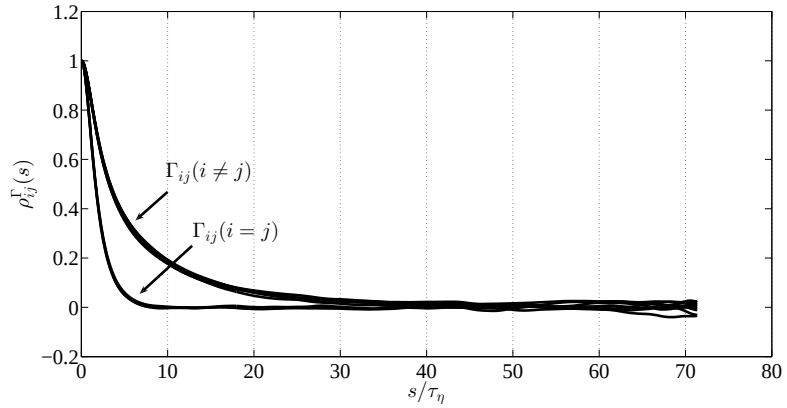

(a)

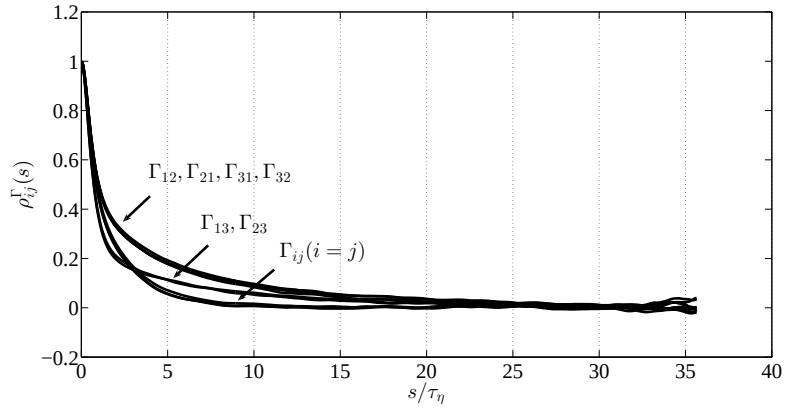

(b)

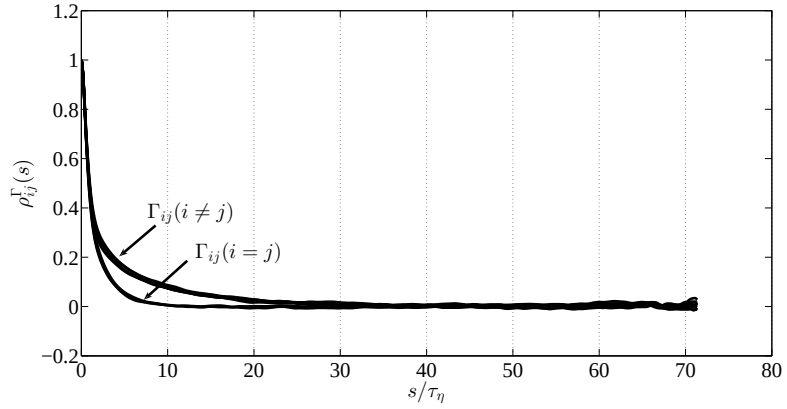

(c)

Figure 3.13: Lagrangian autocorrelations of the different components of the velocity gradient tensor along fluid particle trajectories obtained from (a) DNS, (b) FDNS + KSSGM with $\boldsymbol{\kappa}$ given by equation (3.15) and (c) FDNS + KSSGM with $\boldsymbol{\kappa}$ given by the improved isotropic specification.

1. Choose uniformly distributed random numbers $cos\theta_{nm} \in [-1, 1]$, $\phi_{nm} \in [0, 2\pi]$, and define $sin\theta_{nm} = \sqrt{1 - cos^2\theta_{nm}}$.

2. Generate isotropic distribution on a sphere of radius $|\boldsymbol{\kappa}_{nm}|$:

$$\boldsymbol{\kappa}_{nm} = |\boldsymbol{\kappa}_{nm}|(sin\theta_{nm}cos\phi_{nm}, sin\theta_{nm}sin\phi_{nm}, cos\theta_{nm}) \tag{3.16}$$

As shown in figure 3.13(c), such an isotropic specification of $\boldsymbol{\kappa}$ in the KSSGM generates isotropic statistics of $\boldsymbol{\Gamma}$. We would like to mention that we found negligible difference in the predictions for the RDF and the statistics of w_r using this improved specification. However, as figure 3.13 shows, the difference might be important depending upon the statistics of interest.

3.8 Acknowledgements

The authors gratefully acknowledge Andrew D Bragg for insightful inputs throughout the course of this work. This study was supported by the National Science Foundation under grant number CBET 0756510 and 0967349. The authors gratefully acknowledge the Texas Advanced Computing Center (TACC) at The University of Texas at Austin for providing HPC resources on Ranger and Stampede that have contributed to the research results reported within this paper. This work used the Extreme Science and Engineering Discovery Environment (XSEDE), which is supported by National Science Foundation grant number OCI-1053575.

CHAPTER 4

INVESTIGATION OF SUB-KOLMOGOROV INERTIAL PARTICLE PAIR DYNAMICS IN TURBULENCE USING NOVEL SATELLITE PARTICLE SIMULATIONS

4.1 Abstract

Clustering (or preferential concentration) of weakly inertial particles suspended in a homogeneous, isotropic turbulent flow is driven primarily by the smallest eddies at the so-called Kolmogorov scale. In particle-laden large-eddy simulations (LES), these small-scales are not resolved by the grid and hence their effect on both the resolved flow scales and the particle motion have to be modelled. In order to predict clustering in a particle-laden LES, it is crucial that the subgrid model for the particles captures the mechanism by which the subgrid scales affect the particle motion (Ray and Collins, 2011). In this paper, we describe novel satellite particle simulations (SPS), in which we study the clustering and relative velocity statistics of inertial particles at separation distances well below the Kolmogorov length scale. SPS is designed to isolate pairwise interactions of particles, and is therefore well-suited for developing two-particle models. We show that the power-law dependence of the radial distribution function (RDF), a statistical measure of clustering, is predicted by the SPS in excellent agreement with DNS for Stokes numbers up to 3, implying that no explicit information from the inertial range is required to accurately describe particle clustering. This result further explains our successful prediction of the RDF power using the drift-diffusion model of Chun et al. (2005) for $St \leq 0.4$. We also consider the second-order longitudinal relative velocity structure function for the particles, and show that the SPS is able to capture its

power-law exponent for $St \leq 0.5$ and attribute the disagreement at larger St to the effect of the larger scales of motion not captured by the SPS. Further, the SPS is able to capture the 'caustic activation' of the structure function at zero separation and predict the critical St and rate of activation in agreement with the DNS (Salazar and Collins, 2012). We show comparisons between filtered DNS and equivalently filtered SPS and the findings are similar to the unfiltered case. Overall, SPS is an efficient and accurate computational tool for investigating particle pair dynamics at small separations, as well as an interesting platform for developing LES subgrid models designed to accurately reproduce particle clustering.

4.2 Introduction

Inertial particles in turbulence have been shown to cluster outside of vortices, in the high-strain regions of the flow using both numerical simulations (Maxey, 1987; Squires and Eaton, 1991; Wang and Maxey, 1993; Eaton and Fessler, 1994; Sundaram and Collins, 1997) and experiments (Fessler et al., 1994; Salazar et al., 2008; Saw et al., 2008; Gibert et al., 2012). Such clustering can influence a broad range of aerosol processes, such as particle settling (e.g., Wang and Maxey, 1993), evaporation/condensation (e.g., Shaw et al., 1998) and interparticle collisions (e.g., Sundaram and Collins, 1997). It has been hypothesized that particle clustering plays a crucial role in the broadening of the droplet size distribution during both condensational growth and growth by collision and coalescence, in warm cumulus clouds (Pinsky and Khain, 1997; Shaw et al., 1998; Reade and Collins, 2000a,b; Falkovich et al., 2002; Shaw, 2003; Devenish et al., 2012; Grabowski and Wang, 2012).

The radial distribution function or RDF (McQuarrie, 1976) has been established as a measure of particle clustering in isotropic turbulence and is defined as the ratio of the average number of particle pairs per unit volume found at a given separation distance to the expected number if the particles were uniformly distributed. The RDF can be computed from a field of Q particles by binning the particles according to their separation distance and calculating

$$g(r) = \frac{Q_{p,r}/\Delta V_r}{Q_p/V} \ , \tag{4.1}$$

where $Q_{p,r}$ is the average number of particles found in an elemental shell volume ΔV_r at a distance $r = |\boldsymbol{r}|$ from a test particle, V is the total volume and $Q_p = Q(Q-1)/2$ is the total number of particle pairs in the flow. Sundaram and Collins (1997) showed that the RDF evaluated at particle contact precisely corrects the collision kernel for particle clustering. The average collision frequency for a monodisperse particulate system is given by

$$N_c = \frac{n^2}{2} K(\sigma) \ , \tag{4.2a}$$

where σ denotes the particle diameter, $n \equiv Q/V$ is the particle number density and $K(\sigma)$ is the collision kernel, defined for a statistically stationary suspension as

$$K(\sigma) = 4\pi\sigma^2 g(\sigma) \int_{-\infty}^{0} (-w_r) P(w_r|\sigma)\, dw_r \ . \tag{4.2b}$$

As can be seen from (4.2b), apart from the RDF, the other statistical input to the collision kernel is the probability density function (PDF) of the radial component of the relative velocity, w_r, defined as

$$w_r(\boldsymbol{r}) = [\boldsymbol{v}_2(\boldsymbol{x}+\boldsymbol{r}) - \boldsymbol{v}_1(\boldsymbol{x})] \cdot \frac{\boldsymbol{r}}{|\boldsymbol{r}|} \ , \tag{4.3}$$

where $\boldsymbol{v}_1(\boldsymbol{x})$ and $\boldsymbol{v}_2(\boldsymbol{x}+\boldsymbol{r})$ are the velocities of two particles located at $\boldsymbol{x}$ and $\boldsymbol{x}+\boldsymbol{r}$, respectively. The effect of inertia on the radial relative velocity statistics

has been investigated in the context of predicting the collision kernel (Wang et al., 2000; Ayala et al., 2008b,a; de Jong et al., 2010; Bec et al., 2010) and also for modeling the particle motion that leads to clustering (Chun et al., 2005; Zaichik and Alipchenkov, 2009; Pan and Padoan, 2010). Recently, it has been hypothesized that inertial particle relative velocities can be multi-valued in the limit of zero separation due to the formation of caustics (Falkovich et al., 2002; Wilkinson et al., 2006; Falkovich and Pumir, 2007; Salazar and Collins, 2012), which, if they exist, would tend to enhance the collision rate.

It is apparent from (4.2b) that the collision kernel for asymptotically small particles (i.e., $\sigma/\eta \ll 1$) will depend sensitively on the near-contact concentration and motion of particle pairs. DNS has proven effective for analyzing the behavior of these statistics as a function of the separation distance for small separations (i.e., $\Delta/\eta \ll 1$, where Δ is the smallest separation of interest); however, there are two fundamental challenges with DNS. Firstly, the number of particles required to achieve statistical convergence at a separation distance Δ scales like $Q \sim N^3(\eta/\Delta)^3$, where N is the number of grid points in each direction. This scaling is challenging, given the desire to simultaneously explore higher Reynolds numbers (i.e., larger N) and smaller separation distances (i.e., larger η/Δ). Secondly, the near contact motion of the particles will depend in some unknown way on the accuracy of the interpolation scheme used to obtain the fluid velocity at the particle center, particularly at these small separations. There has not been a systematic study of how errors in spatial interpolation (and even time stepping) manifest in the scaling of these near-contact statistics.

We present an alternative framework called 'satellite particle simulations' or SPS. With SPS, we simulate a cloud of satellite particles surrounding each pri-

mary particle assuming the satellites are sufficiently close to the primary particle that a locally linear flow assumption can be made. The relative velocity of the fluid is then defined completely in terms of the fluid velocity gradient along the inertial (primary) particle trajectory. This quantity is obtained from the DNS. The dynamics of the satellite particles are therefore the dynamics of particle pairs in the asymptotic limit $\Delta/\eta \to 0$, thus overcoming the first concern discussed above. The locally linear flow assumption also eliminates the interpolation errors, and so SPS can be considered the most accurate description of near-contact motion of particle pairs possible. However, SPS has limitations as well. Because SPS contains no information about the inertial subrange, it cannot predict the entire behaviour of the position and velocity statistics. For example, the RDF is known to behave as a power law in the dissipation range (Reade and Collins, 2000a; Kerstein and Krueger, 2006)—SPS predicts the power, but not the prefactor, which depends upon both the dissipation and inertial subranges. Secondly, we have no precise means for specifying the velocity of incoming satellites entering the fluid volume. As a first approximation, we assign these particles the corresponding fluid velocities at their spatial locations. This approximation is exact in the limit $St \to 0$, and is expected to become less accurate as the particle inertia increases. These simulations, therefore, allow us to test whether (and how) particle clustering in the dissipation range (across a wide range of St) is influenced by information from the larger scales of the flow. More details about the SPS can be found in §4.3.2 and §4.4.1.

In this paper, we compare DNS and SPS predictions of the RDF and the second-order velocity structure function. The velocity gradient required for the SPS was obtained from the same DNS, ensuring a fair comparison of the two methods. We make these comparisons over a wide range of particle Stokes numbers to quantify

the effect of the error associated with the arbitrary boundary condition in the SPS. The results also shed light on the theoretical framework of Chun et al. (2005), which is based on the same locally linear flow assumption.

The second goal of the paper is to consider the effect of filtering on sub-Kolmogorov clustering using the SPS. This is motivated by our previous work (Ray and Collins, 2011), where we used a filtered DNS (FDNS) as an *a priori* large-eddy simulation (LES) (Fede and Simonin, 2006) and established the effect of velocity filtering on the RDF and w_r across a wide range of St and r/η . In that paper, we concluded that in order to capture particle clustering in a LES, we need to model the mechanism by which particles cluster at the sub-grid scales. Recently, there has been considerable interest in particle-laden LES (Marchioli et al., 2008; Bini and Jones, 2008; Jin et al., 2010a; Ray and Collins, 2011) and various models have been put forth to capture the effect of the subgrid scales on particle motion. Shotorban and Mashayek (2005); Kuerten (2006) used the approximate deconvolution method to model the resolved scales exactly, while Shotorban and Mashayek (2006b,a) considered a generalized Langevin type model for fluid velocities 'seen' by inertial particles. But these studies focused primarily on one-particle statistics such as the root-mean-square velocity and displacement of the particles. In fact, attempts at predicting clustering via one-particle models (Pozorski and Apte, 2009) suggest that they contain insufficient physics to capture a phenomena that is essentially governed by two-particle dynamics. Our SPS provides a natural framework to investigate pair-wise interaction between particles. The feasibility of using the SPS as a test-bed for two-particle LES models is tested by using a filtered SPS (FSPS) and comparing it with results from FDNS. We will show that the SPS indeed provides a valid test-bed for *a priori* testing of LES models.

This paper is organized as follows. In §4.3.1 we describe the details of the numerical methods used to evolve the isotropic turbulent flow field and track a large number of inertial particles in it, spanning a wide range of St. Section 4.3.2 describes the concept and implementation of the SPS. Section 4.4 presents the results, beginning with the effect of the choice of R/η on the SPS in §4.4.1. Section 4.4.2 and 4.4.3 then compares the results of the RDF and the longitudinal relative velocity structure function for unfiltered and filtered DNS (and SPS) respectively. Section 4.5 provides some concluding remarks.

4.3 Numerical simulations

4.3.1 Direct Numerical Simulation

In this section, we present details of the DNS used to solve the three-dimensional, time-dependent Navier Stokes equations for the fluid phase with and without filtering, and the equations of motion for the inertial particles suspended in the fluid.

Fluid Phase

The governing equations for a three-dimensional incompressible flow are the continuity and the Navier Stokes equation. In rotational form, the equations are

$$\frac{\partial u_i}{\partial x_i} = 0 \quad , \tag{4.4}$$

$$\frac{\partial u_i}{\partial t} + \epsilon_{ijk}\omega_j u_k = -\frac{\partial (p/\rho + \frac{1}{2}u^2)}{\partial x_i} + \nu \frac{\partial^2 u_i}{\partial x_j \partial x_j} \quad , \tag{4.5}$$

where u_i is the velocity vector, $u \equiv \sqrt{u_i u_i}$ is the magnitude of the velocity vector, ρ is the fluid density, ν is the kinematic viscosity, ϵ_{ijk} is the alternating unit tensor, ω_i is the vorticity and p is the pressure. In order to maintain a statistically stationary isotropic turbulence, we use a time-dependent deterministic forcing function that injects energy into the first two wavenumbers in Fourier space (Witkowska et al., 1997). Equations (2.1) and (2.2) are solved using a pseudo-spectral algorithm with de-aliasing based on a combination of truncation and phase-shift (Patterson and Orszag, 1971; Johnson, 1998; Brucker et al., 2007) on a standard periodic cube of length 2π (in arbitrary units). We use 128 grid points in each direction, which yields $R_\lambda \approx 95$. This is smaller than earlier simulations (e.g., Ray and Collins, 2011), but this allows us to achieve excellent convergence in both SPS and DNS at very small separations. This is especially relevant for SPS, which has the more demanding memory requirements (as each primary particle has a cloud of several hundred satellite particles that are tracked). Fortunately, previous studies have shown that at small separations the RDF and the relative velocity structure function are only weak functions of R_λ (Wang et al., 2000; Hogan and Cuzzi, 2001; Collins and Keswani, 2004; Ray and Collins, 2011). Collins and Keswani (2004) analyzed this dependence in detail for $St \leq 1.5$ and found that the sensitivity increased slightly with increasing Stokes number. More recently Ray and Collins (2011) found a somewhat stronger dependence of the RDF on R_λ, but only for $St \geq 2.0$ (see figure 2(c) in that paper). We conclude that the present simulations at $R_\lambda = 95$ is sufficient for the purposes of comparing SPS and DNS at small separations. The time step for the fluid was chosen so that the CFL number is less than 0.5. We evolve the flow-field for about thirteen eddy turnover times to reach statistical stationarity. Additional details of simulation parameters and resolution are given in table 4.1.

Variable	DNS	FDNS	SPS (FSPS)
N	128	128	-
R_λ	95	-	95
$\kappa_{max}\eta$	1.508	-	1.508
k	1.178	1.080	1.178 (1.080)
ϵ	0.232	0.085	0.232 (0.085)
η	0.025	-	0.025
τ_η	0.139	-	0.139
L	1.490	-	1.490
N_p	6,000,000	6,000,000	1,152,000
$\langle N_s \rangle$	-	-	300
R	-	-	0.6η, 2η

Table 4.1: Turbulence parameters for DNS, FDNS and SPS. N is the number of grid points in each of the 3 dimensions, R_λ is the Reynolds number based on the Taylor micro-scale, $k = \int_0^{\kappa_{max}} E(\kappa)\, d\kappa$ is the kinetic energy, $\epsilon = 2\nu \int_0^{\kappa_{max}} \kappa^2 E(\kappa)\, d\kappa$ is the dissipation rate, $\eta = \frac{\nu^{3/4}}{\epsilon^{1/4}}$ is the Kolmogorov length scale, $\tau_\eta = \sqrt{\frac{\nu}{\epsilon}}$ is the Kolmogorov time scale and $L = \frac{3\pi}{2k} \int_0^{\kappa_{max}} \frac{E(\kappa)}{\kappa}\, d\kappa$ is the integral length scale; For FDNS, k and ϵ are computed by replacing κ_{max} by the cut-off filter scale κ_c. N_p is the total number of particles (primary particles in the case of SPS), $\langle N_s \rangle$ is the average number of satellite particles per primary particle and R is the chosen outer sphere radius bounding the SPS domain.

Filtering

We perform low-pass filtering of the DNS velocity field in Fourier space so that all the Fourier modes of velocity beyond a certain cutoff wavenumber κ_c are removed from the flow and only the remaining 'large scales' are retained. The filtering operation we perform is defined below. We apply a sharp spectral filter which removes all wavenumbers above a critical wavenumber κ_c, yielding the following definition of the filtered velocity

$$\tilde{\boldsymbol{u}}(\boldsymbol{k}, t) = \begin{cases} \boldsymbol{u}(\boldsymbol{k}, t) & \text{if } |\boldsymbol{k}| \leq \kappa_c \\ \boldsymbol{0} & \text{otherwise} \end{cases}, \tag{4.6}$$

where we use a cutoff wavenumber $\kappa_c\eta$=0.2. Figure 4.1 shows the energy and dissipation spectra obtained from our DNS as a function of wavenumber. Notice

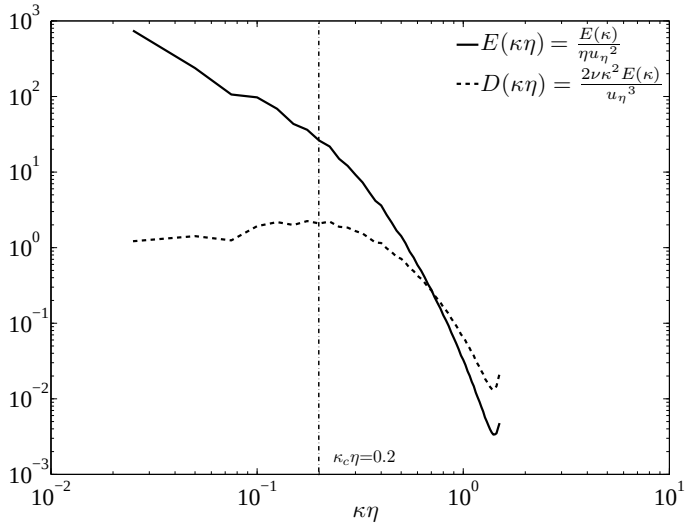

Figure 4.1: Filter cut-off scale ($\kappa_c\eta$=0.2) superimposed on the energy ($E(\kappa)/\eta {u_\eta}^2$) and dissipation ($2\nu\kappa^2 E(\kappa)/{u_\eta}^3$) spectra. Notice that $\kappa_c\eta$ is within the inertial subrange.

that the cutoff wavenumber (or filter scale) lies within the inertial subrange. The turbulent kinetic energy and dissipation rate are computed for the filtered velocity field using the standard definitions shown in table 4.1, with κ_{max} replaced by κ_c. In Ray and Collins (2011), we showed that the statistics of interest vary monotonically as a function of κ_c in the inertial range, and therefore any value in that range can be used to evaluate the effect of filtering. It is worth noting that if we choose the cutoff wavenumber in the dissipation subrange, the filtering has very little effect on clustering.

Inertial Particle Motion

We assume a dilute suspension of inertial particles which allows us to neglect the feedback of particle motion on the carrier fluid (Sundaram and Collins, 1999). We also consider particles whose radius a is much smaller than the Kolmogorov length scale η and simulate them as point-particles. Furthermore, we assume

that the particles are much denser than the surrounding fluid ($\rho_p/\rho_f \gg 1$), the particle Reynolds numbers are small, and collisions and gravitational settling are neglected. Under these assumptions, the equations of motion for the particles reduce to (Maxey and Riley, 1983)

$$\frac{d\boldsymbol{x}(t)}{dt} = \boldsymbol{v}(t) \ , \tag{4.7a}$$

$$\frac{d\boldsymbol{v}(t)}{dt} = \frac{\boldsymbol{u}\left[\boldsymbol{x}(t)\right] - \boldsymbol{v}(t)}{\tau_p} \ , \tag{4.7b}$$

where $\boldsymbol{x}$ is the inertial particle position, $\boldsymbol{v}$ is the particle velocity, $\tau_p = (2/9)\frac{\rho_p a^2}{\rho_f \nu}$ is the particle response time and $\boldsymbol{u}\left(\boldsymbol{x}\right)$ denotes the fluid velocity at the inertial particle location. We have used $1,152,000$ particles (as primary particles for SPS) divided equally into 12 different Stokes numbers. Since we need to compare the results from the SPS to those in the DNS at small separations, we have used $6,000,000$ particles divided into 12 different St for the DNS (and FDNS) to obtain reliable statistics at the sub-Kolmogorov scales. These particles are introduced into the stationary flow field at random positions and with the fluid velocity at those locations. Particles are advanced in time according to (4.7a) and (4.7b) using an improved numerical scheme that was recently developed in our group (Ireland et al., 2013). This new algorithm, based on exponential integrators, is second-order accurate in time and can simulate particles with arbitrarily small St accurately, allowing us to use the fluid time-step (dictated by the CFL condition) to advance the inertial particles, irrespective of St , thereby significantly reducing the run times for low St particles. Fluid velocities at particle locations are obtained using eighth-order Lagrangian interpolation. We allow sufficient time (four eddy turnover times) for the particles to equilibriate with the flow before taking statistics. Particle statistics are averaged over several eddy turnover times. In order to investigate the effect of filtering, the particles are similarly advanced using the filtered velocity field.

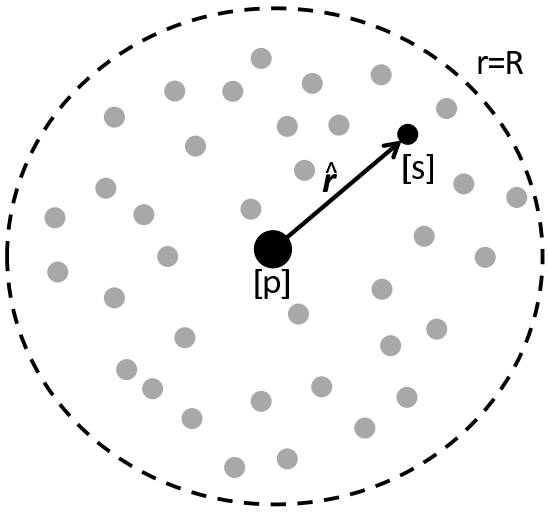

Figure 4.2: Illustration of the SPS: '[p]' denotes the primary particle, '[s]' denotes a satellite particle, $\hat{\boldsymbol{r}}$ is their separation vector and $r = R$ denotes the bounding sphere beyond which we no longer simulate the satellite particle motion.

4.3.2 Satellite particle simulation

We consider a reference frame moving with an inertial particle (henceforth referred to as a 'primary particle,' denoted by a superscript '[p]') and simulate the motion of a cloud of surrounding particles (henceforth referred to as 'satellite particles,' denoted by a superscript '[s]') with respect to the primary particle (see figure 4.2). Denoting the relative position and velocity of the satellite particles as $\hat{\boldsymbol{r}}$ and $\hat{\boldsymbol{w}}$, where $\hat{\boldsymbol{r}} = \boldsymbol{x}^{[s]} - \boldsymbol{x}^{[p]}$ and $\hat{\boldsymbol{w}} = \boldsymbol{v}^{[s]} - \boldsymbol{v}^{[p]}$, we use equations (4.7a) and (4.7b) to derive the equation of motion of a satellite particle as

$$\frac{d\hat{\boldsymbol{r}}(t)}{dt} = \hat{\boldsymbol{w}}(t) \ , \tag{4.8a}$$

$$\frac{d\hat{\boldsymbol{w}}(t)}{dt} = \frac{\Delta \boldsymbol{u}\left[\hat{\boldsymbol{r}}(t)\right] - \hat{\boldsymbol{w}}(t)}{\tau_p} \ , \tag{4.8b}$$

where $\Delta \boldsymbol{u}\left[\hat{\boldsymbol{r}}(t)\right] \equiv \boldsymbol{u}\left[\boldsymbol{x}^{[s]}\right] - \boldsymbol{u}\left[\boldsymbol{x}^{[p]}\right]$, and we have assumed the primary and satellite particles have the same response times (i.e., a monodisperse population of particles). Hereafter in this paper, we deliberately make a distinction between the phase-space variable $\boldsymbol{r}$ denoting the space of all possible values taken by the

separation vector between particle-pairs, and the lagrangian time-dependent separation vector $\hat{\boldsymbol{r}}(t)$ between a satellite particle and its primary particle. This will be relevant primarily in the discussion of the drift-diffusion model based on the theory of Chun et al. (2005) in §4.4.1.

The approach we take is to perform a traditional simulation of a population of primary particles using (4.7a) and (4.7b). Simultaneously we evolve the relative position and velocity of the satellite particles surrounding each primary particle according to (4.8a) and (4.8b). Such a solution requires the relative fluid velocity $\Delta\boldsymbol{u}[\hat{\boldsymbol{r}}(t)]$. In general, this is very difficult to specify in a turbulent flow; however, since we are interested in separation distances below the Kolmogorov length scale (i.e., $\hat{r}/\eta < 1$), we can approximate the relative fluid velocity based on a locally linear flow assumption, i.e.,

$$\Delta u_i[\hat{\boldsymbol{r}}(t)] = \Gamma_{ij}^{[p]}(t)\hat{r}_j \ , \tag{4.9}$$

where the Einstein summation convention is implied, and $\Gamma_{ij}^{[p]}(t) = \partial u_i^{[p]}(t)/\partial x_j$ is the velocity gradient at the primary particle location at time t. The task of specifying $\Delta\boldsymbol{u}$ now reduces to calculating $\Gamma_{ij}^{[p]}(t)$ along each *primary* particle trajectory in the DNS. We then have the information required to evolve (4.8a) and (4.8b). Note that $\Gamma_{ij}^{[p]}(t)$ could be obtained from a model such as the one by Chevillard and Meneveau (2006), which would eliminate the computational cost of performing the DNS, thereby drastically reducing the computational time for SPS.

We advance the particles following (4.8a) and (4.8b) using the second-order accurate exponential integrator defined in Ireland et al. (2013). However, this reduction in the phase space of the system generates another issue. Such a locally linear flow is applicable at small separations, but the satellite particles eventually diffuse beyond the satellite volume boundary at $r = R$ (see figure 4.2). To maintain

a statistically stationary sample of particles in the satellite volume, we must provide an equal source of particles diffusing into the satellite volume. This inward flux is generated by introducing new satellite particles at the boundary. There is no precise way of specifying the initial conditions for these particles, so we place them at random on the bounding surface corresponding to $\hat{r} = R$ and set the particle velocity to the underlying fluid velocity at that location (based on the locally linear flow approximation). In addition, we need to ensure that the velocity of the newly created particle points inward, i.e., $\hat{\boldsymbol{w}} \cdot \boldsymbol{n} < 0$ where $\hat{\boldsymbol{w}}$ is the velocity of the newly created particle relative to the primary particle and $\boldsymbol{n}$ is the outward normal to the surface of the sphere at the new particle location. We employ the following algorithm to create new (replacement) particles in a SPS (Ahluwalia, 2002; Chun et al., 2005). We define a probability of creating new particles in a particular trial as

$$P_{creation} = \frac{-\hat{\boldsymbol{w}} \cdot \boldsymbol{n}}{|\hat{\boldsymbol{w}} \cdot \boldsymbol{n}|_{max}} \quad , \tag{4.10}$$

where $|\hat{\boldsymbol{w}} \cdot \boldsymbol{n}|_{max} \approx 2R\langle\Gamma_{11}^2\rangle^{1/2} \approx \frac{2R}{\sqrt{15}\tau_\eta}$. Then, we generate a uniform random number $X \in [0, 1)$, and at each trial create a new particle only if $P_{creation} > 0$ and $P_{creation} > X$. We expect the number of satellite particles leaving the bounding sphere at any instant of time to differ for each primary particle, making it necessary to define an average number of satellite particles per primary particle. For example, primary particles lying in regions of high strain-rate would be likely to contain more satellite particles than those lying in regions of high rotation-rate. The above rule of thumb (4.10) generates $P_{creation} > 1$ for $2 - 3\%$ of the trials. In those cases, we create a particle and use the remaining probability $P_{creation} - 1$ to determine whether another particle should be created. By using the above algorithm, and selecting a fixed number of trials to create new particles (for each St), we can control the *average* number of satellite particles per primary particle.

The quantity $\langle N_s \rangle$ in table 4.1 denotes the average number of satellite particles per primary particle at stationary state. Clearly this boundary condition is artificial and so we will need to determine the impact this has on the accuracy of the SPS method. We expect the approximation to be accurate in the limit $St \to 0$, and to degrade with increasing Stokes number. Additional details on how to obtain statistics from our SPS are given below.

4.4 Results and discussion

We perform DNS and SPS in matched turbulent flows and with overlapping values of the particle Stokes numbers so that detailed comparisons can be made. In general, the RDF and the second-order longitudinal relative velocity structure function ($S_2 = \langle w_r^2 \rangle$) behave like power laws in the dissipation range, taking the form $g(r) \approx c_0(\eta/r)^{c_1}$ (e.g., Reade and Collins, 2000a) and $S_2 \approx a + b(r/\eta)^{\zeta_2}$ (Salazar and Collins, 2012). As noted earlier, the prefactors c_0 and a, b involve the inertial subrange as well and hence are not determined quantitatively in the SPS; therefore we focus the comparisons on the predicted powers c_1 and ζ_2, and on the qualitative behavior of $a(St)$, which is known as the 'caustic' contribution to S_2. In a SPS, we compute particle statistics by directly binning the position of the satellite particles (which denotes the relative two-particle separation $\boldsymbol{r}$) and then averaging this over all primary particles. For example, if the number of satellite particles lying within radii $r_{i+\frac{1}{2}}$ and $r_{i-\frac{1}{2}}$ from a primary particle is $N_{s,i}$ and the total number of satellite particles within its bounding sphere is $N_{s,T}$, then the RDF would be computed as $g(r_i) = \frac{\left\langle N_{s,i}/(r^3_{i+\frac{1}{2}} - r^3_{i-\frac{1}{2}}) \right\rangle}{\langle N_{s,T}/R^3 \rangle}$, where the average is over all the primary particles in the system (for a particular St). The results are further averaged over several Kolmogorov times, after achieving statistical stationarity.

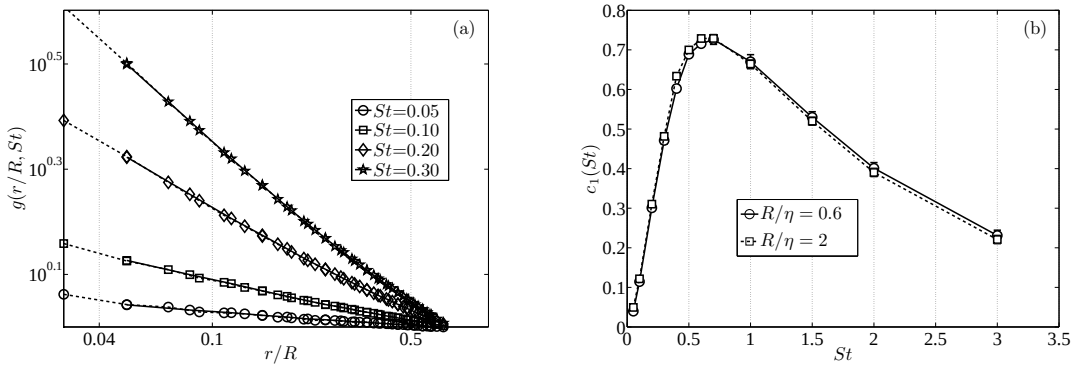

Figure 4.3: (a) Variation of the RDF predicted by the SPS as a function of r/R for four different St (0.05, 0.10, 0.20 and 0.30) and two different choices of R: solid line indicates $R = 0.6\eta$ and dashed line indicates $R = 2\eta$. (b) Variation of c_1 as a function of St for the two different choices of R. The errorbars correspond to 95% confidence intervals.

With SPS, the radius of the satellite shell volume, R, is arbitrary, introducing another parameter that we define as R/η. In addition to the significance of this parameter, which is discussed in §4.4.1, the bounding surface also introduces some arbitrariness in setting the boundary conditions for particles entering the satellite volume. We expect the imprecision of the boundary conditions to contaminate the particle statistics close to the boundary. Empirically we find that if we perform a least-squares fit of the RDF or relative velocity structure function, and limit the range of the fit to $r/R \leq 0.3$, the results are insensitive to the boundary conditions over the entire range of Stokes numbers in this study.

4.4.1 SPS: Effect of R/η

To analyze the effect of the satellite volume radius, we performed SPS using $R/\eta =$ 0.6 and 2.0. Figure 4.3(a) compares the RDFs plotted versus r/R for both values of R/η. Notice the two curves collapse on top of each other, indicating the choice of R/η has no effect on the RDF plotted in this coordinate system. This is verified

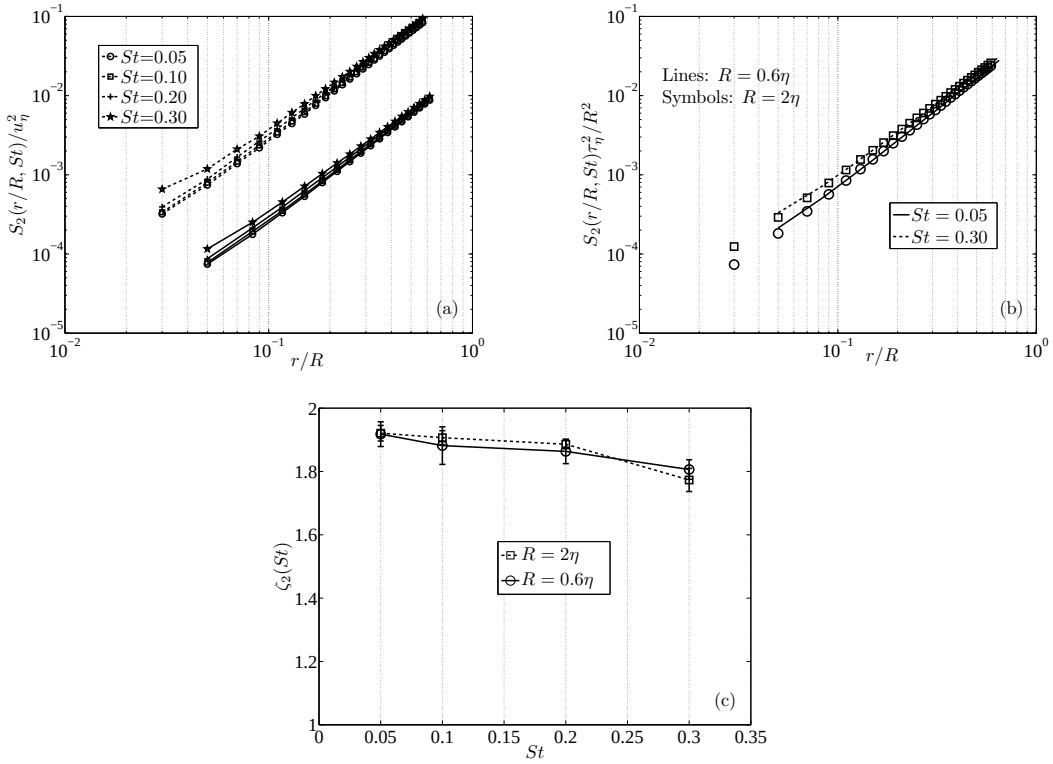

Figure 4.4: (a) The second-order longitudinal structure function S_2 as a function of r/R for $St = 0.05$, 0.10, 0.20 and 0.30 as indicated and for $R/\eta = 0.6$ (solid line) and 2.0 (dashed line). (b) Replotted S_2 normalized by $(R/\tau_\eta)^2$ as a function of r/R for $St = 0.05$ and 0.30 and for $R/\eta = 0.6$ (lines) and 2.0 (symbols). (c) Variation of ζ_2 as a function of St for the two values of R/η. Error bars correspond to 95% confidence intervals.

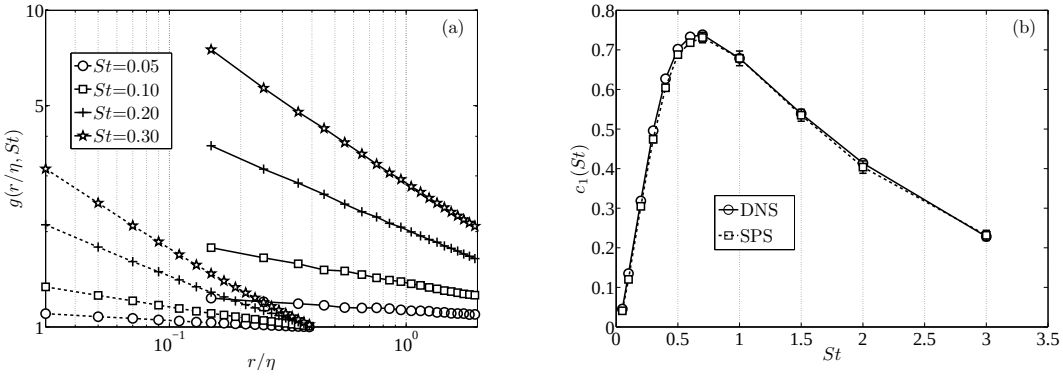

Figure 4.5: (a) Variation of the RDF as a function of r/η for four different St (0.05, 0.10, 0.20 and 0.30) in DNS and SPS: solid line indicates DNS and dashed line indicates SPS. (b) Variation of c_1 as a function of St in DNS and SPS. The errorbars correspond to 95% confidence intervals.

in figure 4.3(b) which shows that R/η has no effect on the power $c_1(St)$.

We also look at the effect of R/η on S_2 . Figure 4.4(a) shows the variation of S_2 normalized by u_η^2 as a function of r/R for same two R/η. In contrast to the RDF, the structure functions do not collapse in this coordinate. This is not surprising, as the magnitude of the velocity increases linearly with r and therefore the variance too should increase with increasing R/η. Taking this into consideration, figure 4.4(b) shows S_2 for $St = 0.05$ and 0.3 normalized by the factor $(R/\tau_\eta)^2$. The data for both R/η clearly collapse under this normalization. Furthermore, if we consider the exponent of the power law ζ_2, it is insensitive to R/η, as shown in figure 4.4(c).

We conclude that there are simple scalings that relate SPS with different R/η, and predictions of c_1 and ζ_2 are not affected by the choice of R/η.

4.4.2 DNS versus SPS: Unfiltered Turbulence

Now that we have established a basis for comparing DNS and SPS, we focus on comparisons for unfiltered turbulence. Before we begin, it is useful to review the theory of Chun et al. (2005) that, based on the same locally linear flow assumption as made in the SPS, derived the following closed differential equation for the RDF

$$\frac{\partial g(r,t)}{\partial t} = \frac{1}{r^2}\,\frac{\partial[A(St)r^3 g(r,t)]}{\partial r} + \frac{1}{r^2}\,\frac{\partial}{\partial r}\left[Br^4\frac{\partial g(r,t)}{\partial r}\right] \tag{4.11}$$

where $A(St)$ and B are the 'drift' and 'diffusion' coefficients respectively. The steady state solution of equation (4.11) takes the form $g(r/\eta) = c_0(r/\eta)^{-c_1}$, where $c_1 = A(St)/B$ and, as with SPS, c_0 is an undetermined parameter that depends on a boundary condition in the inertial subrange. The theory further predicts the mean inward drift velocity (in the absence of diffusion) to be

$$\langle \hat{w}_i(t) | \hat{r}_i(t) = r_i \rangle_p = -A(St) r_i \tag{4.12}$$

where the drift coefficient (same as in (5.1)) is given by

$$A(St) = \frac{St}{3}(\langle S^2 \rangle_p - \langle R^2 \rangle_p)\tau_\eta \ . \tag{4.13}$$

Note that $\hat{\boldsymbol{r}}(t)$ is a *lagrangian time-dependent* variable representing the separation vector between a satellite particle and its primary particle (distinguishable from the phase-space variable $\boldsymbol{r}$, as for example in equation (4.11)), $\langle\cdot\rangle_p$ denotes an average over all primary particle positions at time t, $\hat{w}_i(t)$ is the relative velocity of a satellite particle with respect to its primary particle and $S(t)^2 = S_{ij}(t)S_{ij}(t)$ and $R(t)^2 = R_{ij}(t)R_{ij}(t)$ are the second invariants of the rate of strain and rate of rotation tensors at the primary particle location, respectively. Under statistical stationarity, $A(St)$ is not a function of time. Based on this drift/diffusion argument, Chun et al. (2005) conclude that particle-pairs obeying the following relation

should cluster like inertial particles

$$\frac{d\hat{r}_i(t)}{dt} = -A(St)\hat{r}_i(t) + \Gamma_{ij}(t)\hat{r}_j(t) \ . \tag{4.14}$$

We will analyze this relation as well.

Figure 4.5(a) compares the variation of the RDF with r/η for the DNS and the SPS over a range of Stokes numbers. We can see that the qualitative behaviour is very similar. It should noted that the value of r/η in a SPS has no physical meaning when compared to DNS, unless the boundary condition specified at $r = R$ is exact. We show the comparison in figure 4.5(a) (and some of the figures to follow) as a function of r/η for illustration purposes only. It is meaningful, however, to compare the power c_1, as obtained from a non-linear least-square fit of the RDF data for DNS and SPS. Figure 4.5(b) shows that they are nearly identical, to within the 95% confidence intervals for the fits. This remarkable agreement suggests that the outer flow information coming from the inertial subrange and beyond has very little to do with the power-law scaling of the RDF within the dissipation range over the entire range of Stokes numbers considered in this study. This important result supports theories like those by Chun et al. (2005) and Zaichik and Alipchenkov (2007) that are based on a similar local assumption.

According to the model shown in (4.14), the satellite particles drift inward towards the primary particle with a velocity proportional to their separation, which is counteracted by a random diffusion term that is assumed to be given by the fluid velocity at the satellite particle position. We can test this model by advancing an ensemble of *fluid* particles as primary particles, each with a population of satellite particles obeying (4.14). In this model, all the information about particle inertia is embedded in the drift coefficient $A(St)$ defined in (4.13). The average values of the second invariants of the strain and rotation rates in $A(St)$ are required as inputs

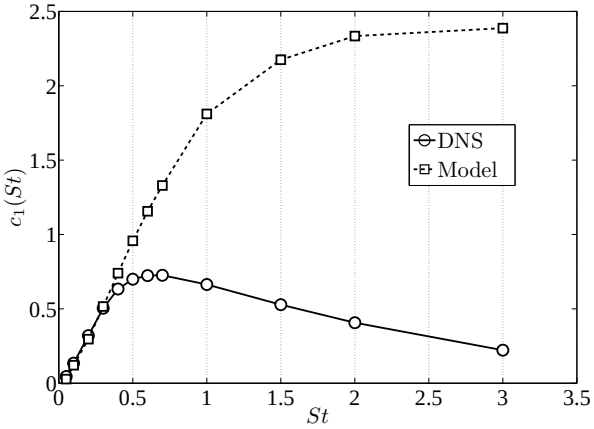

Figure 4.6: Variation of c_1 as a function of St predicted by the DNS and the model (4.14).

to the model and are computed from DNS. Figure 4.6 shows the comparison of c_1 obtained from the model and DNS. There is very good agreement for $St \leq 0.4$, supporting the low Stokes analysis in Chun et al. (2005). For $St > 0.4$, the model significantly overpredicts the values of c_1. This can be explained if we look at the drift term in (4.14) and how the drift coefficient $A(St)$ depends on St . As St increases beyond 0.4, $\langle S^2 \rangle_p - \langle R^2 \rangle_p$ continues to increase until $St = 0.6$, after which it decreases, but more slowly than the linear prefactor in (4.13) leading to an overall increase in $A(St)$ over the range of Stokes numbers considered. This is inconsistent with the DNS; indeed, the peak c_1 in the DNS occurs at $St \approx 0.7$ and then decreases thereafter. Apparently the drift/diffusion arguments in Chun et al. (2005) are valid for $St \leq 0.4$, but beyond that exaggerate the value of c_1 and hence the degree of clustering.

Next we consider the behavior of w_r in DNS and SPS. The SPS, by construction, is accurate in the limit of $St \to 0$, and we can test this by considering longitudinal structure functions of order p ($S_p(r/\eta, St = 0) = \langle w_r^p(r/\eta, St = 0) \rangle$) for fluid particles. Figure 4.7 shows structure functions of order $p = 2, 3, 4$ for fluid particles obtained from DNS and SPS. We find excellent quantitative agreement showing

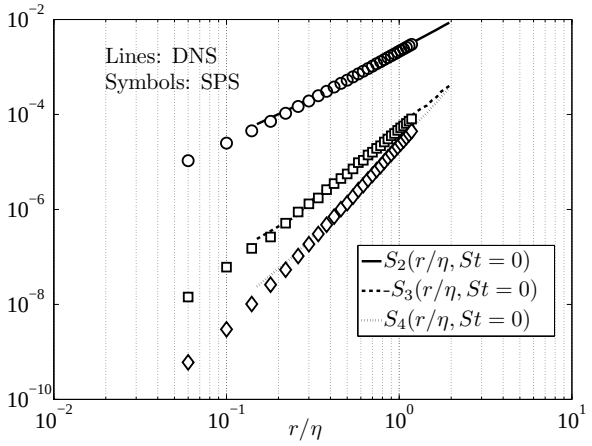

Figure 4.7: Comparison of longitudinal structure functions of order $p = 2, 3, 4$ for fluid particles in DNS (lines) and SPS (symbols).

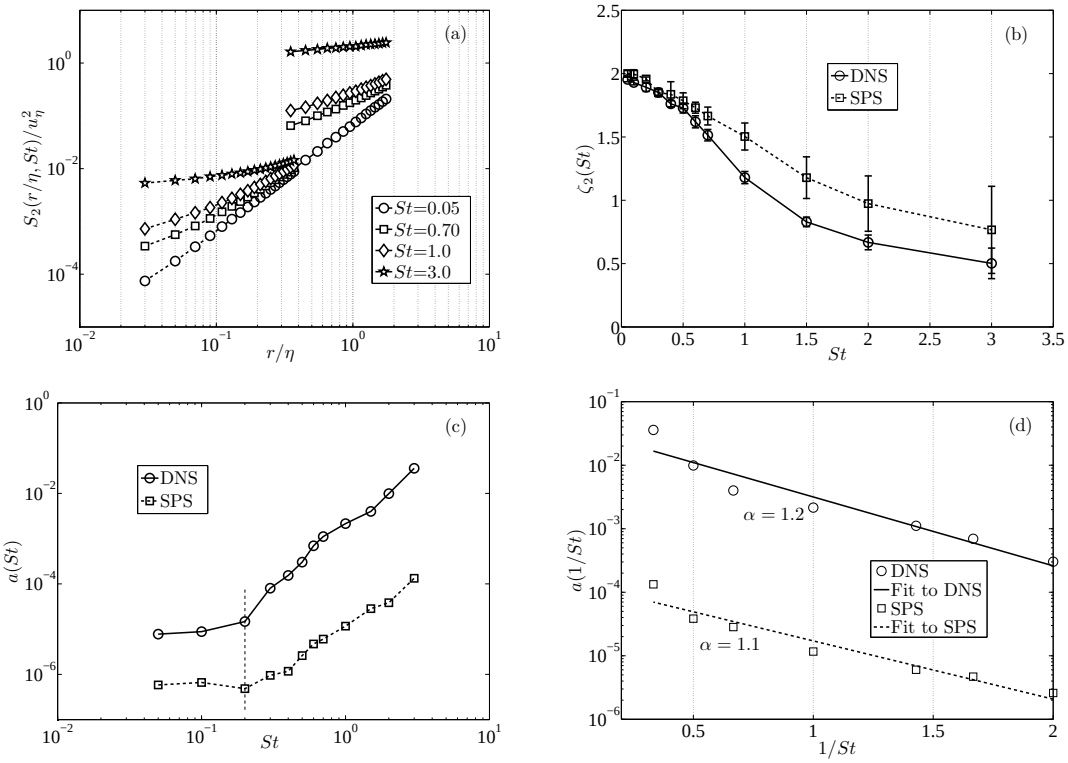

Figure 4.8: (a) Variation of S_2 normalized by u_η^2 as a function of r/η for four different St (0.05, 0.70, 1.00 and 3.00) for DNS and SPS: solid lines indicate DNS and dashed lines indicate SPS. (b) Variation of ζ_2 as a function of St for DNS and SPS. The errorbars correspond to 95% confidence intervals.(c) Variation of the $a(St) = S_2(r/\eta = 0, St)$ as a function of St, as obtained from a fit of the form (4.15). (d) Comparison of the values of a with the model $a(St) = \frac{1}{3}\beta^2 \exp(-2\alpha/St)$ for DNS and SPS.

that the SPS correctly captures the limit of $St = 0$. Let us now focus on the second-order structure function S_2 for inertial particles. Figure 4.8(a) shows this quantity for both the DNS and SPS plotted for four different St as a function of r/η . These St are chosen to span the entire range examined and illustrates the fact that although the qualitative behaviour is very similar, the magnitude of S_2 is not captured by the SPS, except for $St \to 0$. Let us now consider the following form

$$S_2(r/\eta, St) = a(St) + b(St)(r/\eta)^{\zeta_2} \quad , \tag{4.15}$$

where we allow $S_2(r = 0, St) = a(St)$ to be non-zero due to inertia induced caustics (Salazar and Collins, 2012). The rate of formation of caustics has been studied theoretically (Duncan et al., 2005; Wilkinson et al., 2006) and numerically (Falkovich and Pumir, 2007) and has been predicted to satisfy an Arrhenius type expression of the form $a(St) = \frac{1}{3}\beta^2 \exp(-2\alpha/St)$. Salazar and Collins (2012) found reasonably good agreement with this expression, however only for Stokes numbers above a critical value they defined as St_c.

We have used nonlinear least-squares to compute the coefficients a, b and ζ_2 in equation (4.15). Figure 4.8(c) shows the activated behavior of $a(St)$ in our DNS, where the threshold Stokes number St_c is in quantitative agreement with previous results (e.g. Salazar and Collins (2012)). More importantly, the SPS captures this activated behavior and predicts the correct St_c, further affirming that it can capture the physics of particle pair interactions at sub-Kolmogorov scales. However, the magnitude of $a(St)$ is not captured in our SPS, for the reasons discussed previously. In agreement with Salazar and Collins (2012), we find that the caustic activation occurs somewhere between St of 0.2 and 0.5, and we fit the data to the model using a linear least-square fit for $St \geq 0.5$. Figure 4.8(d) shows that both DNS and SPS data fit quite well to the model, with the predicted values

Run	α	β/u_η
DNS	1.2	1.9
SPS	1.1	0.1
FDNS	1.6	1.6
FSPS	1.4	0.1
Salazar and Collins (2012) ($R_\lambda = 60$)	1.5	2.8
Salazar and Collins (2012) ($R_\lambda = 120$)	1.2	2.2

Table 4.2: Results from the least-squares fit to $a(St) = \frac{1}{3}\beta^2 \exp(-2\alpha/St)$ for our DNS ($R_\lambda = 95$), SPS, FDNS and FSPS, together with values from Salazar and Collins (2012).

of α and β shown in table 4.2. We can see that the exponential decay law (α) is quite well-predicted by both DNS and SPS, in agreement with the values found by Salazar and Collins (2012). Unsurprisingly, the coefficient β representing the magnitude of $a(St)$ is not captured by the SPS. We could now consider the power-law exponent ζ_2. Figure 4.8(b) shows the comparison of ζ_2 obtained from the DNS and the SPS and we observe good agreement between the two up to $St \approx 0.5$. For larger St , we find that the SPS overpredicts the exponent. We attribute this disagreement to the boundary conditions at $r = R$, which are accurate only for $St \to 0$. This shows that the relative velocity statistics are more sensitive to the effect of the inertial range scales than the RDF.

4.4.3 DNS versus SPS: Filtered Turbulence

Next we consider the effect of filtering on both the DNS (referred to as FDNS) and SPS (referred to as FSPS). For the FDNS, the fluid velocity is advanced as in an unfiltered DNS and then filtered at every time-step for computing the fluid velocity that is used to advance the particle field. In this way, errors due to the filtering do not accumulate in the fluid velocity (we call this *a priori* LES). For the case of the FSPS, the primary inertial particles are advanced by the same algorithm as

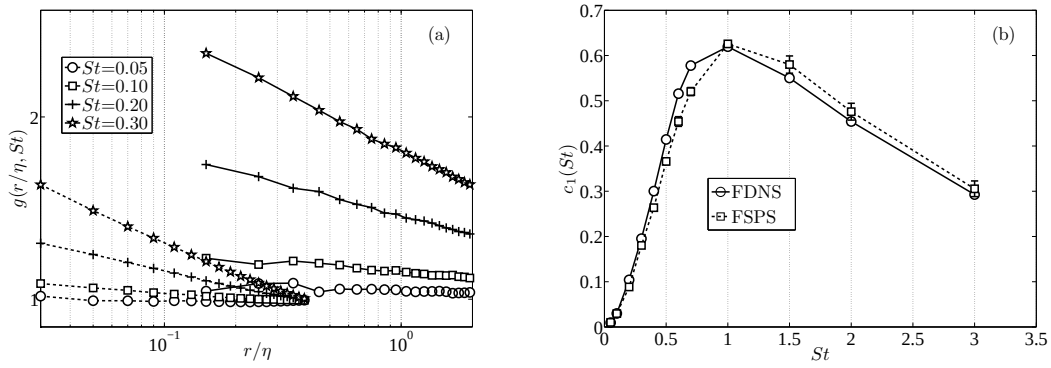

Figure 4.9: (a) Variation of the RDF as a function of r/η for four different St (0.05, 0.10, 0.20 and 0.30) in FDNS and FSPS: solid line indicates FDNS and dashed line indicates FSPS. (b) Variation of c_1 as a function of St in FDNS and FSPS. The errorbars correspond to 95% confidence intervals.

with the FDNS, and the filtered fluid velocity gradient $\tilde{\Gamma}_{ij}^{[p]}(t)$ is computed along the particle trajectory, and this gradient is used to advance the satellite particles. The results for the RDF are given in figure 4.9. Figure 4.9(b) compares c_1 for the two cases and we see there is excellent agreement for $St \leq 0.3$ and $St \geq 1.0$, with reasonable agreement in between (maximum relative error $\sim 15\%$). This shows that even though a filtered DNS is devoid of the small scales, statistics corresponding to those scales (in this case, the filtered velocity gradient following a primary particle) is sufficient to predict c_1 . Furthermore, this demonstrates the utility of the SPS framework for developing and *a priori* testing of LES subgrid models for inertial particles.

We compare the effect of filtering on S_2 in FDNS and FSPS in figure 4.10. Similar to the unfiltered case, we again observe in figure 4.10(a) that the magnitude of S_2 is not well predicted by the FSPS, except for $St \to 0$. Figure 4.10(c) compares the caustic contribution $a(St)$ (see equation (4.15)) for DNS, SPS, FDNS and FSPS. We find, quite interestingly, that the caustic activation appears to be delayed as a result of filtering up to $St = 0.4$ as compared to $St = 0.2$ in the DNS.

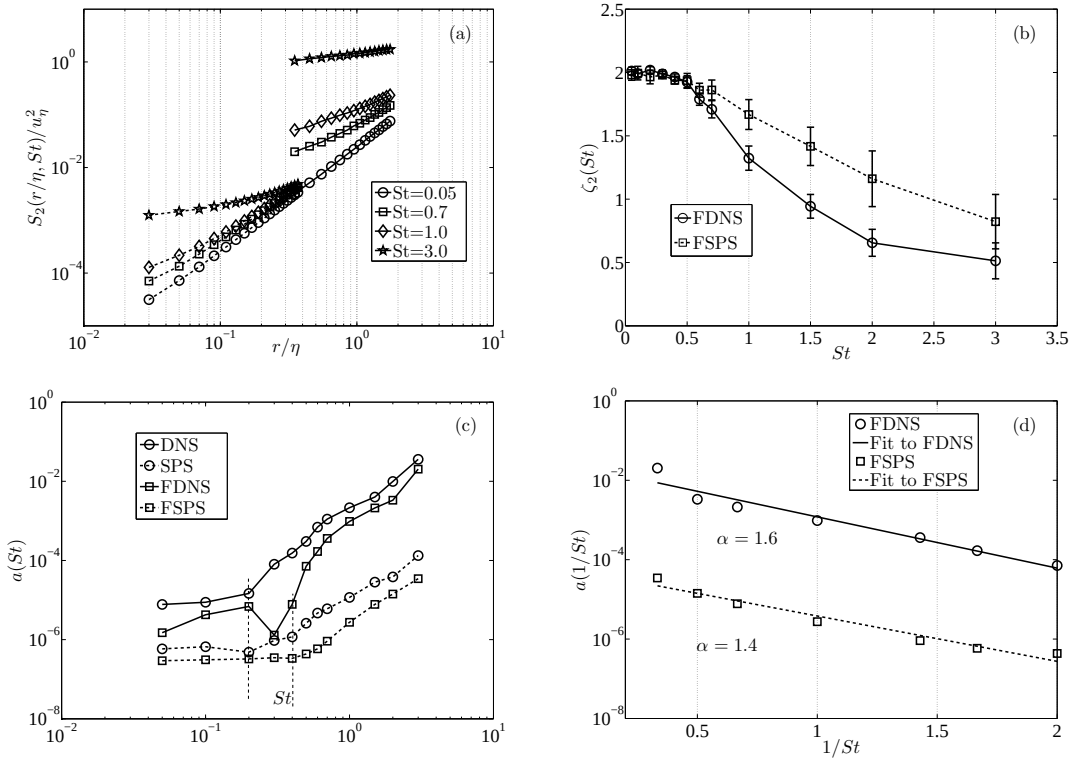

Figure 4.10: (a) Variation of S_2 normalized by u_η^2 as a function of r/η for four different St (0.05, 0.70, 1.00 and 3.00) for FDNS and FSPS: solid lines indicate FDNS and dashed lines indicate FSPS. (b) Variation of ζ_2 as a function of St for FDNS and FSPS. The errorbars correspond to 95% confidence intervals.(c) Variation of the $a(St) = S_2(r/\eta = 0, St)$ as a function of St , as obtained from a fit of the form (4.15) for DNS, SPS, FDNS and FSPS. (d) Comparison of the values of a with the model $a(St) = \frac{1}{3}\beta^2 \exp(-2\alpha/St)$ for FDNS and FSPS.

The caustic contribution to the relative velocity can be explained by the 'sling effect' argument of Falkovich and Pumir (2007), whereby energetic, uncorrelated vortices in the flow centrifuge out particles with a high velocity that, owing to their inertia, can eventually overlap in space with a finite difference in their velocities. Therefore, caustics are governed by the tails of the PDF of w_r , which are known to be attenuated as a result of filtering (Ray and Collins, 2011). Also, the filtered velocity field is devoid of the most intense vortices (vortex tubes having a core of characteristic length η) that are present in the unfiltered flow, leading to a weaker sling effect and a consequent delay in the caustic activation. Again, FSPS is able to capture this feature very well. As we did with the unfiltered case, we can compare $a(St)$ with the Arrhenius-type model $a(St) = \frac{1}{3}\beta^2 \exp(-2\alpha/St)$ and figure 4.10(d) shows that it fits the data well. Table 4.2 shows the fitted coefficients α and β, indicating that the decay-law α is quite well-predicted by FSPS. If we now look at the exponent ζ_2, shown in figure 4.10(b), we see good agreement between FDNS and FSPS for $St \leq 0.5$, beyond which the FDNS curve drops off more quickly with St . As mentioned previously, we attribute this discrepancy to the inability of the boundary conditions at $r = R$ in SPS to capture the effect of larger scales on the velocity of newly created satellite particles entering the solution domain.

4.5 Conclusions

In this paper, we have investigated the behavior of the radial distribution function (RDF) and the second-order longitudinal velocity structure function S_2 of inertial particles in homogeneous isotropic turbulence using novel satellite particle simulations (SPS). The SPS provides a natural framework for simulating pair-wise interaction of particles at the sub-Kolmogorov scales of turbulence, which are essen-

tial for predicting the particle collision rates, and very expensive in the framework of a DNS. We have described the concept and implementation of a SPS. We have considered the effect of varying the bounding sphere radius R and have shown that variations in R/η can be accounted for through simple scaling relations. The SPS, in its current implementation, does not contain any information regarding the larger scales of motion, and consequently cannot predict the magnitude of the RDF. However, it predicts the power-law c_1 of the RDF, in excellent agreement with DNS for St up to 3, indicating that c_1 is determined solely by the small-scales. SPS accurately predicts the statistics of w_r in the limit of $St \to 0$, but shows quantitative disagreements at moderate to high St . Specifically, the exponent ζ_2 of S_2 is predicted accurately for $St \leq 0.5$. We attribute the disagreement at larger St to the absence of information from the larger scales of motion on the newly created satellite particles entering the simulation domain. The SPS seems to be able to capture the qualitative behavior of $S_2(r/\eta = 0, St)$, which is known as the caustic contribution to the relative velocity and predicts the rate of 'caustic activation' accurately. We have also considered the effect of filtering and compared FDNS and FSPS, and the findings are very similar to the unfiltered case. We note that the 'caustic activation' seems to be delayed in the filtered velocity field, and attribute it to the attenuation of the tails of the PDF of w_r as a result of filtering. The FSPS predicts c_1 in agreement with FDNS, showing that the SPS can be used to test two-particle LES models for inertial particles designed to recover clustering.

4.6 Acknowledgments

This study was supported by the National Science Foundation under grant number CBET 0756510 and 0967349. The authors gratefully acknowledge the Texas

Advanced Computing Center (TACC) at The University of Texas at Austin for providing HPC resources on Ranger that have contributed to the research results reported within this paper. This work used the Extreme Science and Engineering Discovery Environment (XSEDE), which is supported by National Science Foundation grant number OCI-1053575.

CHAPTER 5

A NEW SUBGRID MODELING FRAMEWORK FOR INERTIAL PARTICLE CLUSTERING IN LARGE-EDDY SIMULATIONS OF TURBULENCE: LOW-INERTIA PARTICLES

5.1 Abstract

Preferential concentration or clustering of low-inertia particles suspended in an isotropic turbulent flow is primarily driven by the small-scales of the turbulence. By low-inertia particles, we mean particles that are much denser than the fluid, but whose response times (τ_p) are small compared to the Kolmogorov time-scale (τ_η), i.e., their Stokes number $St = \tau_p/\tau_\eta < 1$. In large-eddy simulations (LES) of turbulence, the small-scales are not captured on the grid and need to be modeled. Clustering of low-inertia particles is a sensitive function of the details of the small-scale turbulent structure; current LES subgrid models are unable to replicate the necessary statistical details of the subgrid scales to predict clustering accurately (Cernick, 2013; Ray and Collins, 2013b). For example, Ray and Collins (2013b) have shown that recovering the effect of the subgrid-scale coherent structures in the form of the Lagrangian time-scales of the rotation-rate tensor seen by the particles, is crucial to predict clustering. It is extremely challenging to predict such detailed subgrid scale statistics from a simple (computable) model for the subgrid velocity field. In this paper, we adopt an entirely different approach to subgrid modeling. In particular, we begin by deriving model equations governing particle motion from two existing theories of particle clustering, viz. the theory by Chun et al. (2005)(CT) and the theory by Zaichik and Alipchenkov (2009)(ZT). An essential feature of these theories (and hence of the model equations) is that

they are formulated in a relative reference frame i.e., in terms of the relative separations and velocities of the particles as opposed to their absolute positions and velocities. Therefore, we can use satellite particle simulations (SPS) (Ray and Collins, 2013a) as an efficient framework for the development and testing of these models. We call them Drift-Diffusion Models (DDMs) based on the forms of the underlying theories, which contain a deterministic 'drift' term and a stochastic 'diffusion' term. The model equation derived from the CT (i.e., DDM-CT) gives good agreement with DNS data for $St \leq 0.05$, whereas DDM-ZT is shown to give good agreement with DNS data for $St \leq 0.2$. Therefore, we propose the DDMs as viable LES models for inertial particles at low St. Finally, we discuss some conceptual and numerical issues related to implementing the DDM in a Lagrangian single-particle tracking framework.

5.2 Introduction

Inertial particles in turbulence have been shown to cluster outside of vortices, in the high-strain regions of the flow in both numerical simulations (Maxey, 1987; Squires and Eaton, 1991; Wang and Maxey, 1993; Eaton and Fessler, 1994; Sundaram and Collins, 1997) and experiments (Fessler et al., 1994; Salazar et al., 2008; Saw et al., 2008; Gibert et al., 2012; Bateson and Aliseda, 2012; Saw et al., 2012). Such clustering can influence a broad range of aerosol processes, such as particle settling (e.g., Wang and Maxey, 1993), evaporation/condensation (e.g., Shaw et al., 1998) and interparticle collisions (e.g., Sundaram and Collins, 1997). It has been hypothesized that particle clustering plays a crucial role in the broadening of the droplet size distribution in warm cumulus clouds, during both condensational growth and growth by collision and coalescence (Pinsky and Khain, 1997;

Shaw et al., 1998; Reade and Collins, 2000a,b; Falkovich et al., 2002; Shaw, 2003; Devenish et al., 2012; Grabowski and Wang, 2012).

The radial distribution function or RDF (McQuarrie, 1976) is an important measure of particle clustering in isotropic turbulence and is defined as the ratio of the average number of particle pairs per unit volume found at a given separation distance to the expected number if the particles were uniformly distributed. The RDF can be computed from a field of Q particles by binning the particles according to their separation distance and calculating

$$g(r) = \frac{Q_{p,r}/\Delta V_r}{Q_p/V} \ , \tag{5.1}$$

where $Q_{p,r}$ is the average number of particles found in an elemental shell volume ΔV_r at a distance $r = |\boldsymbol{r}|$ from a test particle, V is the total volume and $Q_p = Q(Q-1)/2$ is the total number of particle pairs in the flow. Sundaram and Collins (1997) showed that the RDF evaluated at particle contact precisely corrects the collision kernel for particle clustering. The average collision frequency for a monodisperse particulate system is given by

$$N_c = \frac{n^2}{2} K(\sigma) \ , \tag{5.2a}$$

where σ denotes the particle diameter, $n \equiv Q/V$ is the particle number density and $K(\sigma)$ is the collision kernel, defined for a statistically stationary suspension as

$$K(\sigma) = 4\pi\sigma^2 g(\sigma) \int_{-\infty}^{0} (-w_r) P(w_r|\sigma)\, dw_r \ . \tag{5.2b}$$

As can be seen from (5.2b), apart from the RDF, the other statistical input to the collision kernel is the probability density function (PDF) of w_r, where w_r is the relative velocity of a particle pair along their line of centers. The effect of inertia on the radial relative velocity statistics has been investigated in the context of predicting the collision kernel (Wang et al., 2000; Ayala et al., 2008b,a; de Jong

et al., 2010; Bec et al., 2010) and also for modeling the particle motion that leads to clustering (Chun et al., 2005; Zaichik and Alipchenkov, 2009; Pan and Padoan, 2010). Ray and Collins (2013b) showed that their model can accurately predict the relative velocity component of the collision kernel for all St, but can only predict the RDF for $St \geq 2.0$. In this paper, we will focus solely on models designed to recover the RDF at low St.

Since particle clustering is strongly influenced by the details of the small-scale turbulent fluctuations, RANS based turbulence models are unable to capture it. Direct numerical simulations (DNS) resolve all of the turbulent scales and hence provide an accurate prediction of particle clustering, but are limited to modest Reynolds numbers due to the computational cost. Large-eddy simulations (LES) provide a compromise by accurately simulating the largest scales of the turbulent fluctuations, while modeling the scales that are below the grid spacing (subgrid scales). With increasing computing power, LES appears to be an attractive choice for performing practical turbulent flow calculations more accurately than RANS-based methods. Consequently, particle-laden LES has emerged as a viable tool for computing particle statistics in turbulence, and has received considerable attention recently (Wang and Squires, 1996b,a; Armenio et al., 1999; Boivin et al., 2000; Fede and Simonin, 2006; Marchioli et al., 2008; Pozorski and Apte, 2009). However, subgrid models that work well for flow statistics are not easily translated to describing inertial particle statistics. There have been attempts to develop models specifically aimed towards recovering inertial particle statistics. Shotorban and Mashayek (2005), and Kuerten (2006) used the approximate deconvolution method (ADM) to recover the scales of the turbulence represented on the grid in a LES. But, as has been shown previously (Jin et al., 2010a; Ray and Collins, 2011, 2013a), an exact representation of the larger turbulent fluctuations in a LES

does not necessarily yield the correct particle clustering. Shotorban and Mashayek (2006b,a), Fede et al. (2006), and Pozorski and Apte (2009) constructed stochastic Langevin-type models to recover the subgrid fluctuations seen by inertial particles. Pozorski and Apte (2009) were able to match the RDF approximately for $St = 2.0$ with their model, but only after choosing an appropriate but arbitrary value of their model constant. In fact, Cernick (2013) compared the ADM, and the subgrid models of Fukagata et al. (2004), Shotorban and Mashayek (2006b), and Berrouk et al. (2007) and showed that they contain insufficient physics to recover the correct levels of particle clustering.

Ray and Collins (2013b) developed a subgrid model based on the kinematic simulation of turbulence (so-called KSSGM), that sought to predict some information about the subgrid flow structure by approximating the correct subgrid energy (and dissipation) spectrum. In isotropic turbulence, this means that we capture the Eulerian two-point correlations of the subgrid fluid velocity (and velocity gradient) seen by the inertial particles. They showed that the KSSGM can accurately predict the moments of w_r up to order 2 for all St, but can only capture the RDF for $St \geq 2.0$. Their results indicate that the small-scale statistical information necessary to predict the RDF for $St < 2.0$ is extremely difficult to reproduce in a model for the unresolved velocity fluctuations.

In this work, we present a new framework for modeling particle clustering in a LES for low St. The central idea of our approach is to consider the existing statistical mechanical theories of inertial particle clustering, and derive usable models from them. We consider the theories of Chun et al. (2005) (CT) and Zaichik and Alipchenkov (2009) (ZT) in this paper, although our approach could be adapted to any similar theory or advancement to an existing theory. A key feature of the

CT and the ZT is that they are formulated in a relative reference frame ($\boldsymbol{r}$ and $\boldsymbol{w}$) as opposed to an absolute reference frame ($\boldsymbol{x}$ and $\boldsymbol{v}$). Therefore, the models we derive are also formulated in a ($\boldsymbol{r}$,$\boldsymbol{w}$) space. For development and testing of these models, we have utilized the satellite particle simulation (SPS) framework (Ray and Collins, 2013a), which provides an efficient way to simulate particle-pair interactions in turbulence at small separations (i.e., for $r < \mathcal{O}(\eta)$). The approach we take constitutes an entirely new way of formulating LES subgrid models for inertial particles. We call them Drift-Diffusion Models (DDMs), since they contain a deterministic 'drift' term and a stochastic 'diffusion' term.

In §5.3, we describe a general method to derive DDMs starting from a statistical mechanical description of the particulate system. Based on the particular closures for different terms in the theory, the terms in the model are determined. Our results show that the DDM-CT performs well up to $St = 0.05$, whereas the DDM-ZT performs well for $St \leq 0.2$. We consider the DDMs to be a viable basis for a LES subgrid model for $St \leq 0.2$. We discuss improvements that could be (or need to be) made to the DDM-ZT. Finally, we consider some issues related to implementing the DDMs in a Lagrangian single-particle tracking framework.

5.3 Derivation of the Drift-Diffusion Model (DDM)

In this section, we consider the derivation of DDMs from the theories of particle clustering. Throughout this paper, we shall be interested in predicting inertial particle clustering in the dissipation range, which is the separation distance of importance in predicting the collision kernel. We will illustrate our method of deriving the DDMs using the ZT as an example. We could also analyze the CT

following Chun et al. (2005); Bragg and Collins (2013a) to arrive at a similar model. But, we have chosen to focus on the ZT in this paper because of two major reasons: (i) the ZT is the more general formulation in that it accounts for particles of all St and separation distances depending upon the specific closure models employed, and hence it is amenable to improvements in these closures from other theories or models; and (ii) the DDM derived from the ZT can be shown to recover the correct drift term from a filtered velocity field.

As in the ZT, we begin by considering the Lagrangian PDF $p(\boldsymbol{r},\boldsymbol{w},t) = \langle P(\boldsymbol{r},\boldsymbol{w},t)\rangle = \langle \delta(\boldsymbol{r}^p(t)-\boldsymbol{r})\delta(\boldsymbol{w}^p(t)-\boldsymbol{w})\rangle$ in the $(\boldsymbol{r},\boldsymbol{w})$ space, where $\boldsymbol{r}$ and $\boldsymbol{w}$ denote the phase space variables for the particle-pair separation and particle relative velocities, and $P(\boldsymbol{r},\boldsymbol{w},t)$ denotes the so-called *fine-grained* PDF (Pope, 2000). The superscript 'p' on a quantity indicates a Lagrangian time-dependent variable, and $\langle\cdot\rangle$ denotes the ensemble average over all initial conditions of the particle-pairs and all realizations of the flow field. The nomenclature used in this paper is similar to the ones in the analysis of the ZT by Bragg and Collins (2013a). With this nomenclature, the evolution equation of the *fine-grained* PDF is given by

$$\frac{\partial P}{\partial t} = -\frac{\partial}{\partial r_i}\left[\frac{dr_i^p(t)}{dt}P\right] - \frac{\partial}{\partial w_i}\left[\frac{dw_i^p(t)}{dt}P\right]. \tag{5.3a}$$

Using the *sifting* property of delta functions (Pope, 2000) and the equation of motion of particle-pairs (see equation (5.11) and (5.12) in §3.1.3) $\frac{d\boldsymbol{w}^p(t)}{dt} = \frac{\Delta\boldsymbol{u}^p(t)-\boldsymbol{w}^p(t)}{St\tau_\eta}$ in equation (5.3a), and averaging, we get

$$\frac{\partial p}{\partial t} = -\frac{\partial}{\partial r_i}\left[w_i p\right] + (St\tau_\eta)^{-1}\frac{\partial}{\partial w_i}\left[w_i p\right] - (St\tau_\eta)^{-1}\frac{\partial}{\partial w_i}\left\langle \Delta u_i^p P\right\rangle. \tag{5.3b}$$

In the ZT, the term $\langle\Delta\boldsymbol{u}^p P\rangle$ on the right-hand side is unclosed, and is modeled in order to complete the description in equation (5.3b). However, it is not necessary to close this term *a priori* for the purposes of the DDM. Multiplying equation (5.3b) by w_j and integrating over $\boldsymbol{w}$, we can construct the transport equation for the

normalized RDF ρ where $\rho(\boldsymbol{r},t) = \int_{\boldsymbol{w}} p(\boldsymbol{r},\boldsymbol{w},t)d\boldsymbol{w} = \langle \delta(\boldsymbol{r}^p(t)-\boldsymbol{r})\rangle$ as

$$St\,\tau_\eta \frac{\partial}{\partial t}\left[\left\langle w_j^p\right\rangle_{\boldsymbol{r}}\rho\right] = -St\,\tau_\eta \frac{\partial}{\partial r_i}\left[\rho\left\langle w_i^p w_j^p\right\rangle_{\boldsymbol{r}}\right] - \left\langle w_j^p\right\rangle_{\boldsymbol{r}}\rho + \rho\left\langle \Delta u_j(\boldsymbol{r}^p(t),t)\right\rangle_{\boldsymbol{r}} . \quad (5.4)$$

Here, $\langle\cdot\rangle_{\boldsymbol{r}}$ denotes the ensemble average conditioned on a particle-pair arriving at separation $\boldsymbol{r}$ at time t, i.e., $\boldsymbol{r}^p(t) = \boldsymbol{r}$. We now decompose the particle relative velocity into a mean and a fluctuating part, $\boldsymbol{w}^p = \langle \boldsymbol{w}^p\rangle_{\boldsymbol{r}} + \boldsymbol{w}'^p$ and define the second-order structure function of particle velocity as $S^p_{2ij} = \left\langle w_i'^p w_j'^p\right\rangle_{\boldsymbol{r}}$. Dividing (5.4) by ρ yields

$$\begin{aligned} St\,\tau_\eta \tfrac{1}{\rho}\tfrac{\partial}{\partial t}\left[\left\langle w_j^p\right\rangle_{\boldsymbol{r}}\rho\right] + \left\langle w_j^p\right\rangle_{\boldsymbol{r}} &= \left\langle \Delta u_j^p\right\rangle_{\boldsymbol{r}} - \tfrac{1}{\rho} St\,\tau_\eta \tfrac{\partial}{\partial r_i}\left[\rho\left\langle w_i^p w_j^p\right\rangle_{\boldsymbol{r}}\right] \\ &= \left\langle \Delta u_j^p\right\rangle_{\boldsymbol{r}} - St\,\tau_\eta \left\langle w_i^p w_j^p\right\rangle_{\boldsymbol{r}} \tfrac{1}{\rho}\tfrac{\partial \rho}{\partial r_i} - St\,\tau_\eta(\partial/\partial r_i)S^p_{2ij} \\ &\quad - St\,\tau_\eta \tfrac{\partial}{\partial r_i}\left[\langle w_i^p\rangle_{\boldsymbol{r}}\left\langle w_j^p\right\rangle_{\boldsymbol{r}}\right] \\ &\approx \left\langle \Delta u_j^p\right\rangle_{\boldsymbol{r}} + (St\,\tau_\eta\, c_1/r^2)\left\langle w_i^p w_j^p\right\rangle_{\boldsymbol{r}} r_i^p \\ &\quad - St\,\tau_\eta(\partial/\partial r_i)S^p_{2ij} - St\,\tau_\eta \tfrac{\partial}{\partial r_i}\left[\langle w_i^p\rangle_{\boldsymbol{r}}\left\langle w_j^p\right\rangle_{\boldsymbol{r}}\right] . \end{aligned} \quad (5.5)$$

In arriving at the last line of equation (5.5), we have used a power-law expression $\rho(\boldsymbol{r}) \approx \bar{c}_0 r^{-c_1}$ based on the knowledge that in the dissipation range of isotropic turbulence, the RDF behaves as a power-law (Reade and Collins, 2000a). Note that the normalization of the RDF (i.e., the difference between the RDF defined by equation (5.1) and ρ) is reflected in the pre-factor $\bar{c}_0$, which does not appear in equation (5.5). We are interested in the statistically stationary state, where equation (5.5) reduces to

$$\left\langle w_j^p\right\rangle_{\boldsymbol{r}} = -St\,\tau_\eta(\partial/\partial r_i)S^p_{2ij} + \left\langle \Delta u_j^p\right\rangle_{\boldsymbol{r}} + (St\,\tau_\eta\, c_1/r^2)\left\langle w_i^p w_j^p\right\rangle_{\boldsymbol{r}} r_i^p . \quad (5.6)$$

Equation (5.6) is essentially a balance equation for the mean relative velocity of inertial particles. The right hand side of equation (5.6) contains 3 terms. The first term has a negative sign in front, and represents the inward drift velocity that causes clustering. The last two terms represent the diffusion that counteracts

the drift so that at stationary state $\langle \boldsymbol{w}^p(t) \rangle_{\boldsymbol{r}} = \mathbf{0}$. A detailed physical explanation of the drift and diffusion terms can be found in Bragg and Collins (2013a). Equation (5.6) forms the basis of our DDM. We design the DDM to reproduce the average behavior of particle relative velocities at stationary state following equation (5.6). We obtain our DDM by removing the averages in equation (5.6) except on the drift term, yielding

$$\begin{aligned} \frac{dr_j^p}{dt} &= -St\,\tau_\eta(\partial/\partial r_i)S_{2ij}^p + \Delta u_j^p + (St\,\tau_\eta\,c_1/(r^p)^2)w_i^p w_j^p r_i^p \\ &= -A(\boldsymbol{r}^p)r_j^p + \Delta u_j^p + (St\,\tau_\eta\,c_1/(r^p)^2)w_i^p w_j^p r_i^p\,, \end{aligned} \tag{5.7}$$

where $A(\boldsymbol{r}^p)$ is called the drift coefficient. Note that we have embedded averaged terms into the instantaneous equation (5.7). As a consequence, the DDM does not capture any correlations between the drift and the diffusion terms. We cannot, in general, write an appropriate form of the instantaneous drift velocity because it involves the divergence operator acting on the particle relative velocity $\boldsymbol{w}^p$, which is not a *field* in $\boldsymbol{r}$ space. Therefore, we have chosen to use the averaged drift in our model, in the hope that it will still recover the correct RDF at stationary state.

In order to use equation (5.7), we require the divergence of the particle structure function $\boldsymbol{S}_2^p$ at stationary state. Note that thus far, the derivation has not introduced any of the specific closures in the ZT. However, in order to complete the expression for the drift term, we need a model for the divergence of the structure function. We now appeal to the ZT, which provides a model for $\boldsymbol{S}_2^p$ by introducing a closure for $\langle \Delta \boldsymbol{u}^p P \rangle$, and by assuming that the fourth-order structure function $\boldsymbol{S}_4^p$ behaves similar to the fourth moment of a Gaussian distribution. Using such a model, we can derive an analytical expression for the drift coefficient, in the limit of low inertia ($St \ll 1$). Some details of the derivation are given in Appendix A. The result of this low St analysis is the following model equation for the evolution

of the particle relative velocity:

$$\frac{dr_j^p}{dt} = -A\, r_j^p + \Delta u_j^p + (St\,\tau_\eta\, c_1/(r^p)^2) w_i^p w_j^p r_i^p\,, \tag{5.8a}$$

where the drift coefficient A in the present analysis is given by

$$A = A_1 + A_2\,, \tag{5.8b}$$

with

$$\begin{aligned} A_1 &= \tfrac{St^2}{6}\left[\tfrac{1}{N_S} - \tfrac{1}{N_R}\right]\,, \\ A_2 &= \tfrac{St^4}{6}\left[\tfrac{\mathcal{T}_S^L}{N_S^2}\left\{\tfrac{7}{60}+\tfrac{1}{6}\right\} - \tfrac{\mathcal{T}_S^L+\mathcal{T}_R^L}{12 N_S N_R} + \tfrac{\mathcal{T}_R^L}{N_R^2}\left\{\tfrac{1}{4}+\tfrac{1}{6}\right\}\right]\,, \end{aligned} \tag{5.8c}$$

and

$$\begin{aligned} N_S &= St\tau_\eta\left(1+\tfrac{St\tau_\eta}{\mathcal{T}_S^L}\right)\,, \\ N_R &= St\tau_\eta\left(1+\tfrac{St\tau_\eta}{\mathcal{T}_R^L}\right)\,. \end{aligned} \tag{5.8d}$$

Note that in this low St analysis of the ZT, the drift coefficient A is not a function of the particle-pair separation $\boldsymbol{r}$, and requires only the Kolmogorov time-scale τ_η and the Lagrangian time-scales of strain-rate ($\mathcal{T}_S^L$) and rotation-rate($\mathcal{T}_R^L$) of fluid particles for specification. The dependence of the drift coefficient A on $\boldsymbol{r}$ is related to the departure from r^2 scaling of the particle longitudinal (S_{ll}^p) and transverse (S_{nn}^p) structure functions (note that isotropy implies $S_{2ij}^p(\boldsymbol{r}) = S_{nn}^p\delta_{ij} + (S_{ll}^p - S_{nn}^p)\frac{r_i r_j}{r^2}$). At low St, the ZT predicts an approximately r^2 scaling for S_{ll}^p and S_{nn}^p which is related to the fact that it predicts the onset of caustics (see Falkovich et al., 2002; Wilkinson et al., 2006; Salazar and Collins, 2012) at a St larger than what is observed in DNS (Bragg and Collins, 2013b). We will analyze the effect of this deficiency by using DNS data for $\boldsymbol{S}_2^p$ in §5.5. We emphasize here that once we choose our phase space as ($\boldsymbol{r}$,$\boldsymbol{w}$), the general expression (5.7) does not use any modeling (as long as we are in the dissipation range). The only modeling necessary is for the divergence of $\boldsymbol{S}_2^p$ in the drift term. If more accurate models for $\boldsymbol{S}_2^p$ become available, we could easily introduce them into the DDM.

5.4 Numerical simulations

5.4.1 Direct Numerical Simulation (DNS)

Fluid Phase

The governing equations for a three-dimensional incompressible flow are the continuity and the Navier Stokes equation. In rotational form, the equations are

$$\frac{\partial u_i}{\partial x_i} = 0 \quad , \tag{5.9a}$$

$$\frac{\partial u_i}{\partial t} + \epsilon_{ijk}\omega_j u_k = -\frac{\partial (p'/\rho + \frac{1}{2}u^2)}{\partial x_i} + \nu \frac{\partial^2 u_i}{\partial x_j \partial x_j} \quad , \tag{5.9b}$$

where u_i is the velocity vector, $u \equiv \sqrt{u_i u_i}$ is the magnitude of the velocity vector, ρ is the fluid density, ν is the kinematic viscosity, ϵ_{ijk} is the alternating unit symbol, ω_i is the vorticity and p' is the pressure. In order to maintain a statistically stationary isotropic turbulence, we use a time-dependent deterministic forcing function that injects energy into the first two wavenumbers in Fourier space (Witkowska et al., 1997). Equations (5.9) are solved using a pseudo-spectral algorithm with de-aliasing based on a combination of truncation and phase-shift (Patterson and Orszag, 1971; Johnson, 1998; Brucker et al., 2007) on a standard periodic cube of length 2π (in arbitrary units). We use 128 grid points in each direction, which yields $R_\lambda \approx 95$. The time step for the fluid was chosen so that the CFL number is less than 0.5. We evolve the flow-field for about thirteen eddy turnover times to reach statistical stationarity. Additional details of simulation parameters and resolution are given in table 5.1.

Filtering

We perform low-pass filtering of the DNS velocity field in Fourier space so that all the Fourier modes of velocity beyond a certain cutoff wavenumber κ_c are removed from the flow and only the remaining 'large scales' are retained. We apply a sharp spectral filter which removes all wavenumbers above a critical wavenumber κ_c, yielding the following definition of the filtered velocity

$$\tilde{u_i}(\mathbf{k},t) = \begin{cases} u_i(\mathbf{k},t) & \text{if } |\mathbf{k}| \leq \kappa_c \\ 0 & \text{otherwise} \end{cases} , \tag{5.10}$$

where we use a cutoff wavenumber $\kappa_c\eta$=0.2. Such a filtered DNS (FDNS) field can be thought of as a 'perfect' LES field in the sense that the large scales are represented exactly, without any subgrid modelling errors. We will use the results from the FDNS to evaluate model performance in a LES. Figure 5.1 shows the energy and dissipation spectra obtained from the DNS. Notice that the cutoff wavenumber (or filter scale) lies within the inertial subrange. The turbulent kinetic energy and dissipation rate are computed for the filtered velocity field using the standard definitions shown in table 5.1, with κ_{max} replaced by κ_c. Ray and Collins (2011) showed that the statistics of interest vary monotonically as a function of κ_c in the inertial range, and therefore any value in that range can be used to evaluate the effect of filtering. It is worth noting that if we choose the cutoff wavenumber in the dissipation subrange, the filtering has very little effect on clustering.

Inertial Particle Motion

We assume a dilute suspension of inertial particles, which allows us to neglect the feedback of particle motion on the carrier fluid (Sundaram and Collins, 1999). We also consider particles whose radius a is much smaller than the Kolmogorov

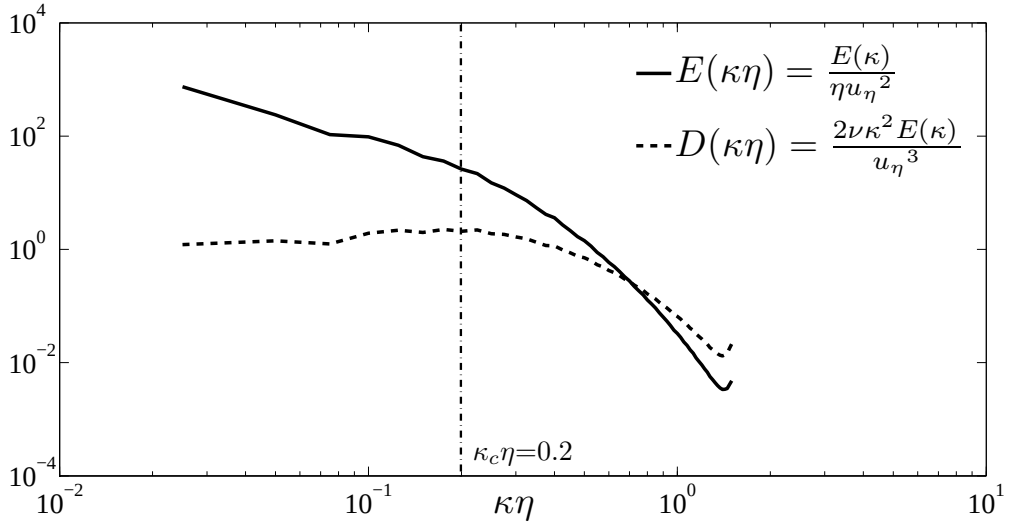

Figure 5.1: Filter cut-off scale ($\kappa_c\eta$=0.2) superimposed on the energy ($E(\kappa)/\eta {u_\eta}^2$) and dissipation ($2\nu\kappa^2 E(\kappa)/{u_\eta}^3$) spectra. Notice that $\kappa_c\eta$ is within the inertial subrange.

length scale η and simulate them as point-particles. Furthermore, we assume that the particles are much denser than the surrounding fluid ($\rho_p/\rho_f \gg 1$), the particle Reynolds numbers are small, and collisions and gravitational settling are neglected. Under these assumptions, the equations of motion for the particles reduce to (Maxey and Riley, 1983)

$$\frac{dx_i^p(t)}{dt} = v_i^p(t) \ , \tag{5.11}$$

$$\frac{dv_i^p(t)}{dt} = \frac{u_i\left[\boldsymbol{x}^p(t)\right] - v_i^p(t)}{\tau_p} \ , \tag{5.12}$$

where $\boldsymbol{x}^p$ is the inertial particle position, $\boldsymbol{v}^p$ is the particle velocity, $\tau_p = (2/9)\frac{\rho_p a^2}{\rho_f \nu}$ is the particle response time and $\boldsymbol{u}\left(\boldsymbol{x}^p\right)$ denotes the fluid velocity at the inertial particle location. Since we are interested in testing the DDM predictions with DNS at small separations, we have used $500,000$ particles for each St in order to obtain reliable statistics at the sub-Kolmogorov scales. These particles are introduced into the stationary flow field at random positions and with the fluid velocity at those locations. Particles are advanced in time according to (5.11) and (5.12) using an

Variable	DNS	FDNS	SPS
N	128	128	-
R_λ	95	-	95
$\kappa_{max}\eta$	1.508	-	1.508
k	1.178	1.080	1.178
ϵ	0.232	0.085	0.232
η	0.025	-	0.025
τ_η	0.139	-	0.139
L	1.490	-	1.490
Q	500,000	500,000	96,000

Table 5.1: Turbulence parameters for DNS, FDNS and SPS. N is the number of grid points in each of the 3 dimensions, R_λ is the Reynolds number based on the Taylor micro-scale, $k = \int_0^{\kappa_{max}} E(\kappa)\, d\kappa$ is the kinetic energy, $\epsilon = 2\nu \int_0^{\kappa_{max}} \kappa^2 E(\kappa)\, d\kappa$ is the dissipation rate, $\eta = \frac{\nu^{3/4}}{\epsilon^{1/4}}$ is the Kolmogorov length scale, $\tau_\eta = \sqrt{\frac{\nu}{\epsilon}}$ is the Kolmogorov time scale and $L = \frac{3\pi}{2k} \int_0^{\kappa_{max}} \frac{E(\kappa)}{\kappa}\, d\kappa$ is the integral length scale; For FDNS, k and ϵ are computed by replacing κ_{max} by the cut-off filter scale κ_c. Q is the number of particles (primary particles in the case of SPS) used for each St.

improved numerical scheme that was recently developed (Ireland et al., 2012, 2013). This new algorithm, based on exponential integrators, is second-order accurate in time and can simulate particles with arbitrarily small St accurately, allowing us to use the fluid time-step (dictated by the CFL condition) to advance the inertial particles, irrespective of St, thereby significantly reducing the run times for low St particles. Fluid velocities at particle locations are obtained using eighth-order Lagrangian interpolation. We allow sufficient time (four eddy turnover times) for the particles to equilibriate with the flow before taking statistics. Particle statistics are averaged over several eddy turnover times. In order to investigate the effect of filtering, the particles are similarly advanced using the filtered velocity field.

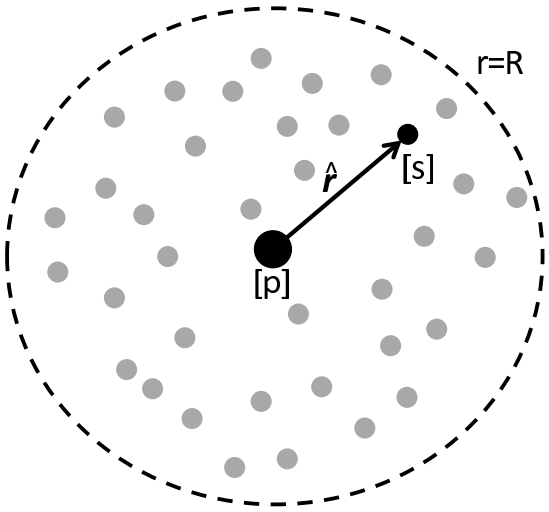

Figure 5.2: Illustration of the SPS: '[p]' denotes the primary particle, '[s]' denotes a satellite particle, $\hat{\boldsymbol{r}}$ is their separation vector and $r = R$ denotes the bounding sphere beyond which we no longer simulate the satellite particle motion.

5.4.2 Satellite Particle Simulation (SPS) for DDM

We will use SPS to test our DDMs. Ray and Collins (2013a) had earlier described the SPS in detail, and showed that it is a valid test-bed for *a priori* testing of LES models designed to recover particle clustering. In this subsection, we describe how we use the SPS framework to develop and test our DDM.

With SPS, we consider a reference frame moving with an inertial particle (henceforth referred to as a 'primary particle' and denoted by a superscript '[p]', not to be confused with the superscript 'p' without brackets used to denote Lagrangian time-dependent particle-pair quantities) and simulate the motion of a cloud of surrounding particles (henceforth referred to as 'satellite particles,' denoted by a superscript '[s]') with respect to the primary particle (see figure 5.2). Denoting the relative position and velocity of the satellite particles as $\hat{\boldsymbol{r}}$ and $\hat{\boldsymbol{w}}$, where $\hat{\boldsymbol{r}} = \boldsymbol{x}^{[s]} - \boldsymbol{x}^{[p]}$ and $\hat{\boldsymbol{w}} = \boldsymbol{v}^{[s]} - \boldsymbol{v}^{[p]}$, we can use equations (5.7) to write the equation

of motion of a satellite particle as

$$\frac{d\hat{r}_i(t)}{dt} = \hat{w}_i(t) \ , \tag{5.13a}$$

$$\hat{w}_i(t) = -A\left[\hat{\boldsymbol{r}}(t)\right]\hat{r}_i(t) + w_{\mathrm{D},i} \, , \tag{5.13b}$$

where we have used $\boldsymbol{w}_{\mathrm{D}}$ to denote the diffusion velocity in equation (5.7).

As with the traditional SPS, we evolve a population of primary particles and simultaneously evolve the relative position and velocity of the satellite particles surrounding each primary particle according to equations (5.13). We have used $96,000$ primary particles for each Stokes number and approximately 400 satellite particles for each primary particle. Such a solution requires the relative fluid velocity $\Delta\boldsymbol{u}[\hat{\boldsymbol{r}}(t)]$ as part of $\boldsymbol{w}_{\mathrm{D}}$. Since we are interested in separation distances in the dissipation range (i.e., $\hat{r} < \mathcal{O}(\eta)$), we can approximate the relative fluid velocity based on a locally linear flow assumption, i.e.,

$$\Delta u_i[\hat{\boldsymbol{r}}(t)] = \Gamma_{ij}^{[p]}(t)\hat{r}_j \ , \tag{5.14}$$

where the Einstein summation convention is implied, and $\Gamma_{ij}^{[p]}(t) = \partial u_i^{[p]}(t)/\partial x_j$ is the velocity gradient at the primary particle location at time t. Therefore, $\boldsymbol{\Gamma}^{[p]}(t)$ along each *primary* particle trajectory is all the information we need to evolve equations (5.13) in a SPS. For testing DDMs, we do not know *a priori* how the particles would sample the flow field. Therefore, we have decided to represent the primary particles as fluid particles in all of the results shown in §5.5. We have also used inertial particles evolved by equations (5.11) and (5.12) as primary particles, and found no difference in the results for clustering. This indicates a certain insensitivity of the two-particle statistics to the primary particle evolution, as long as it reproduces the correct turbulent fluctuations in $\boldsymbol{\Gamma}^{[p]}(t)$. Note that $\boldsymbol{\Gamma}^{[p]}(t)$ could be obtained from a model (Girimaji and Pope, 1990; Chevillard and Meneveau, 2006),

which would eliminate the computational cost of performing the DNS, thereby drastically reducing the computational time for SPS. We introduce a bounding sphere of radius R around each primary particle, beyond which we no longer evolve the satellite particles. To attain a stationary satellite particle population, we replenish the satellites leaving the bounding sphere with new satellites that are located on the bounding sphere with the corresponding fluid velocity assigned to them (Brunk et al., 1998; Chun et al., 2005; Ray and Collins, 2013a). Note that since we are only simulating the dissipation range in a SPS, we can only hope to capture the slope of the RDF, and not its magnitude. This means that in the power-law form of the RDF ($g(r/\eta) = c_0(r/\eta)^{-c_1}$), we can predict c_1 using the SPS, but not c_0, since c_0 depends on how the locally linear flow transitions into the inertial range. We will compare c_1 obtained from the DDM (with $\mathbf{\Gamma}^{[p]}$ specified from DNS) against c_1 obtained from DNS LPT data, to evaluate its accuracy. Our results for c_1 are independent of R, which acts only as a scaling factor in the magnitude of the RDF. Additional details on the numerical implementation of the SPS, and guidelines on computing the RDF from it, can be found in Ray and Collins (2013a).

Since our goal in this work is to arrive at a LES model for particles, we will also test the DDM in a filtered velocity field. This means that along primary particle trajectories, we will use $\mathbf{\Gamma}^{[p]}$ obtained from FDNS along with a subgrid model to account for the unresolved scales. In this paper, we use the KSSGM (Ray and Collins, 2013a) as a subgrid model to recover the fluid velocity (and velocity gradient) fluctuations. The results for c_1 can then be compared to the DDM with unfiltered $\Gamma_{ij}^{[p]}$, indicating how the model would perform in a LES. This essentially allows us to test whether the DDM can be adequately specified from a filtered velocity field, thereby evaluating its suitability as a LES model.

5.5 Results and discussion

In this section, we present the results from the DDMs implemented in the SPS framework. Let us begin by considering the DDM obtained from the CT, which has previously been considered in Chun et al. (2005), and Ray and Collins (2013a). The form of DDM-CT is

$$\begin{aligned} \frac{dr_i^p}{dt} &= -A\, r_i^p + \Delta u_i^p \\ &= -\frac{St\,\tau_\eta}{3}\left\langle S^2 - R^2 \right\rangle_p r_i^p + \Delta u_i^p \\ &\approx -\frac{St^2\tau_\eta^3}{12\nu^2}\left[\langle \epsilon'^2\rangle T_{\epsilon\epsilon} + \langle \zeta'^2\rangle T_{\zeta\zeta} - \langle \epsilon'\zeta'\rangle\{T_{\epsilon\zeta} + T_{\zeta\epsilon}\}\right] r_i^p + \Delta u_i^p\,, \end{aligned} \tag{5.15}$$

where S^2 and R^2 denote the second invariants of the strain-rate and rotation-rate tensors, the averages $\langle\cdot\rangle_p$ and $\langle\cdot\rangle$ are over all inertial particle positions and fluid particle positions respectively, $\epsilon = \langle\epsilon\rangle + \epsilon' = 2\nu S^2$ is the dissipation rate, $\zeta = \langle\zeta\rangle + \zeta' = 2\nu R^2$ is the enstrophy, and the time-scales are defined as $T_{XY} = \frac{1}{\tau_\eta}\frac{\int_{-\infty}^{0}\langle X'(0)Y'(t)\rangle dt}{\sqrt{\langle X'(0)^2\rangle\langle Y'(t)^2\rangle}}$. The last line of equation (5.15) is derived in Chun et al. (2005) in the limit of $St \ll 1$, and consists of only fluid particle statistics. As mentioned earlier, we use the SPS to test the model, where we move the primary particles as fluid particles and evolve the satellite particles following equation (5.15). We use $R = 0.6\eta$ in the SPS, but the results shown here are independent of R (Ray and Collins, 2013a). Since we are in the dissipation range in a SPS, we always consider $\Delta\boldsymbol{u}^p = \boldsymbol{\Gamma}^{[p]}\cdot\boldsymbol{r}^p$, where $\boldsymbol{\Gamma}^{[p]}$ is the velocity gradient tensor at the primary particle location. As mentioned earlier, we will compare the power-law c_1 of the RDF obtained from our model with DNS data. Figure 5.3 shows this comparison indicating that beyond $St = 0.05$, the model overpredicts c_1 substantially. Ray and Collins (2013a) considered equation (5.15) but used DNS data to specify $\langle S^2 - R^2\rangle_p$, and found the predictions for c_1 to be accurate up to $St = 0.4$. This indicates the $St \ll 1$ assumption in the CT model for $\langle S^2 - R^2\rangle_p$ breaks down beyond $St = 0.05$.

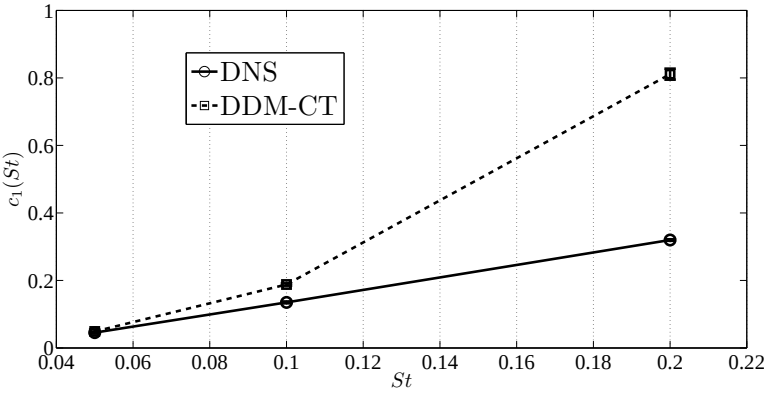

Figure 5.3: Comparison of c_1 obtained from DDM-CT (equation (5.15)) with DNS data showing disagreement beyond $St = 0.05$.

For the rest of this section, our focus will be on the ZT and the DDM obtained from it. Before considering the DDM-ZT, we will assess the accuracy with which the ZT predicts inertial particle clustering. To do that, we will numerically solve the ZT model equations (ZT-NUMSOL) using the closures described in Zaichik and Alipchenkov (2009). Following Bragg and Collins (2013a), the only additional modification we introduce is to use the non-local value of the diffusion coefficient (Chun et al., 2005) instead of the local value used in the ZT. This modification is based on arguments put forward in the CT, and significantly improves the results in the ZT. We mention here that the *value* of the non-local diffusion coefficient that we found (using the results of DDM-CT) is $B_{nl} = 0.056$, which differs from the value ($B_{nl} = 0.093$) given in Chun et al. (2005). This would also explain the discrepancy found when comparing the CT with the experimental data of Lu et al. (2010). We solve the ZT equations in the dissipation range of the turbulence. Therefore, the theory can only give predictions for c_1 and not c_0. We compare the ZT-NUMSOL predictions of c_1 with DNS in figure 5.4, showing very good agreement for $St \leq 0.2$. This shows that the ZT is an accurate theory for particle clustering for low St, and lends credibility to models derived from the ZT in that regime. Let us now consider the DDM-ZT, in the form derived in equation (5.7). First, let us neglect the

second diffusion term so that the form of the DDM becomes

$$\frac{dr_i^p}{dt} = -A(\boldsymbol{r}^p) r_i^p + \Delta u_i^p \,. \tag{5.16}$$

We will refer to this form as DDM-ZT1. The significance of this model will become clearer later when we discuss issues related to implementation in a LPT (or single-particle tracking) framework. Consider the drift coefficient A obtained from the low St analysis of the ZT, as expressed in equation (5.8) and derived in Appendix A. Figure 5.4 shows the comparison of c_1 obtained using this drift coefficient in equation (5.16) with DNS. We see reasonable agreement for $St \leq 0.2$. We should mention here that beyond $St = 0.2$, the RDF keeps increasing with time and does not seem to converge even if we run for a very long time, perhaps indicating that the low St approximation of the drift coefficient in ZT breaks down for $St > 0.2$. We have included the data for $St = 0.3$ in our plots just to illustrate how the DDM-ZT with constant A overpredicts the RDF (and c_1) beyond $St = 0.2$. Although the agreement in figure 5.4 is reasonable, we see some underprediction at low St and some overprediction at $St = 0.2$. This can be improved by including the second diffusion term in equation (5.7), which should be zero in the limit of $St \to 0$, but should give a positive contribution to diffusion at finite St. Let us now add this to our model, which is written as

$$\frac{dr_i^p}{dt} = -A(\boldsymbol{r}^p) r_i^p + \Delta u_i^p + (St\, \tau_\eta\, c_1/(r^p)^2)(w_j^p r_j^p) w_i^p \,. \tag{5.17}$$

We will call this form DDM-ZT2. The results for c_1 with this added diffusion term (but still with constant A) is also shown in figure 5.4. We find that, as expected, it makes negligible difference to the results for St up to 0.1, but reduces the clustering for $St = 0.2$ resulting in a better agreement with DNS.

So far, we have been using DNS values for $\Gamma_{ij}^{[p]}$ to evaluate the model performance. Since we are ultimately interested in using these DDMs in a LES, we

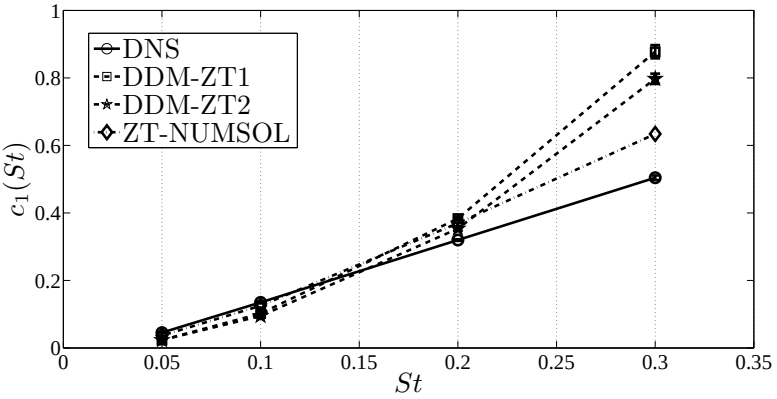

Figure 5.4: Comparison of c_1 obtained from DDM-ZT1 and DDM-ZT2 (equation (5.16) and (5.17)), and from ZT-NUMSOL with DNS data.

can test the models by using $\Gamma_{ij}^{[p]}$ specified from a FDNS. In that case, we use a KSSGM (Ray and Collins, 2013b) to recover the subgrid fluctuations in $\Gamma_{ij}^{[p]}$, and assume that the Kolmogorov time-scales can be accurately estimated from the filtered velocity field (since the KSSGM recovers the dissipation rate ϵ quite accurately). We also assume known values of the Lagrangian time-scales $\mathcal{T}_S^L$ and $\mathcal{T}_R^L$ from DNS data, which means that the drift coefficient is completely specified. The diffusion velocity involves the use of the KSSGM to account for the subgrid fluctuations of $\Gamma_{ij}^{[p]}$. We can now compare the DDMs computed from such a 'LES' field against the results shown in figure 5.4. Consider the DDM-ZT1 with $\Gamma_{ij}^{[p]}$ specified by FDNS+KSSGM for illustration (we refer to this as DDM-ZT1F). Figure 5.5 shows that recovering the correct subgrid fluctuations in $\Delta \boldsymbol{u}^p = \boldsymbol{\Gamma}^{[p]} \cdot \boldsymbol{r}^p$ via the KSSGM is sufficient to recover c_1 for the DDM-ZT1. A similar result can be obtained using DDM-ZT2. This attests to the suitability of the DDM-ZT as a LES model for particle clustering.

We have thus far used the ZT to specify the drift coefficient in DDM-ZT. Bragg and Collins (2013a) have shown that the ZT describes the RDF very accurately, whereas there is more significant error in the closure model for the particle relative

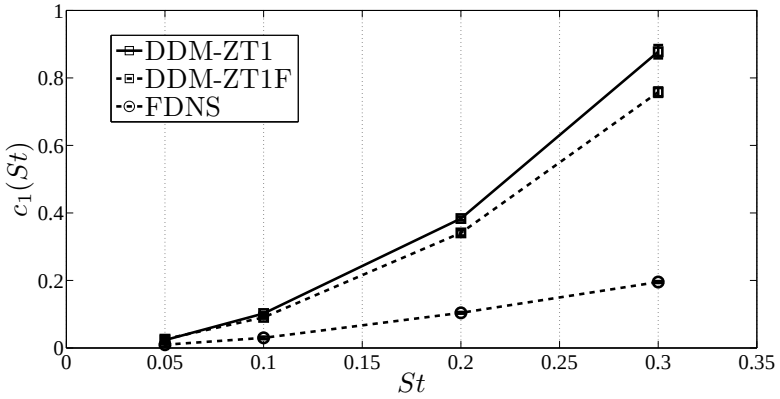

Figure 5.5: Comparison of c_1 obtained from DDM-ZT1F (equation (5.16) using FDNS + KSSGM to specify $\Gamma_{ij}^{[p]}$), with the result from DDM-ZT1 using DNS data to specify $\Gamma_{ij}^{[p]}$. c_1 obtained in a FDNS is also shown as a reference.

velocity statistics, especially at low to moderate St. In the RDF equation derived by the ZT (and also the DDM-ZT), particle relative velocity statistics enter through the divergence of the structure function, and hence any error in the description of the structure function will affect the drift coefficient in the DDM and hence the prediction of the RDF. For example, the disagreement in c_1 obtained from ZT-NUMSOL with DNS data for $St \geq 0.2$ (refer to figure 5.4) can be attributed to the inaccuracy of the model for S_{2ij}^p in the ZT. Therefore, to reduce the errors in the specification of S_{2ij}^p, we can use DNS data. The only errors then arise from the way the divergence is computed from the data. We have used piecewise polynomial fits to our DNS data, and computed the divergence from the fit. The results from using such a specification is shown in figure 5.6. We can see that the predictions are improved for all St up to 0.2, showing very good agreement with DNS. From a practical standpoint, this implies that if we use a more accurate model for S_{2ij}^p than the ZT, in the DDM-ZT, we would have an improved model for clustering. In the literature, we have found the theory by Pan and Padoan (2010) to provide such an improved usable model for S_{2ij}^p (Bragg and Collins, 2013b). Once again, we emphasize that the DDM-ZT has no 'adjustable parameters', and can

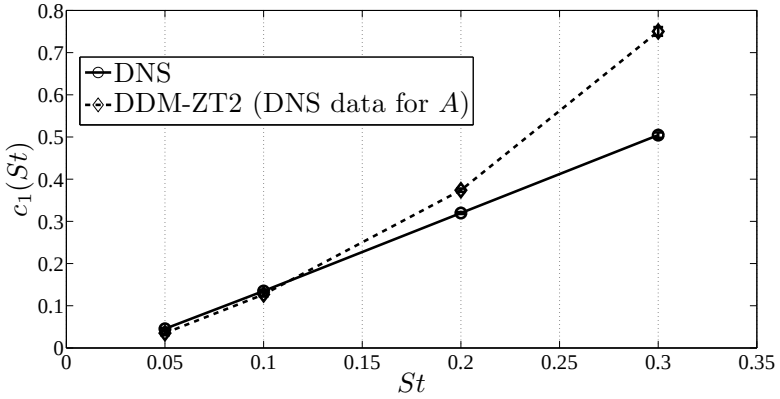

Figure 5.6: Comparison of DNS data for c_1 with c_1 obtained from DDM-ZT2 (equation (5.15)) using a piecewise polynomial fit to DNS data to compute the divergence of S^p_{2ij} in the drift coefficient A.

be specified by quantities which are readily available from the LES flow-field and known data. This makes the DDM-ZT an attractive subgrid model for predicting inertial particle clustering in a LES.

Now that we have established a framework to derive DDMs from existing theories of clustering and test them against DNS data, we can look at the issue of using them in actual calculations. One scenario in which we would like to use these models is in LES with Lagrangian particle tracking (LPT). In LPT, we track the position and velocity of individual (or single) particles through the flow field. To use the DDM in a LPT framework requires conversion from a two-particle framework to a single-particle framework. A simple way to consider this transformation is given below. Consider a system of M particles, where a particle-pair $(1,2)$ governed by the DDM follows

$$\frac{dr_i^{(1,2)}}{dt} = G_i(\boldsymbol{r}^{(1,2)})\,, \tag{5.18}$$

where $\boldsymbol{r}^{(1,2)} = \boldsymbol{x}^{(2)} - \boldsymbol{x}^{(1)}$. The equation for the absolute position of particle 1 is then given by

$$\frac{dx_i^{(1)}}{dt} = \frac{dx_i^{(2)}}{dt} - G_i(\boldsymbol{r}^{(1,2)})\,. \tag{5.19}$$

One can imagine that particle 1 can be paired with every other particle in the system, and we can seek the condition under which one would obtain an unique evolution equation for $x_i^{(1)}$ irrespective of the particle it pairs with (of course, we will only consider particles lying within the dissipation range around particle 1). We can show that this is the case only when $G_i(\boldsymbol{r})$ is a linear function of $\boldsymbol{r}$ i.e., $G_i(\boldsymbol{r}^{(1,2)}) + G_i(\boldsymbol{r}^{(2,3)}) = G_i(\boldsymbol{r}^{(1,3)})$ and so on. Looking at equation (5.7), this means that we cannot use the second diffusion term, and that the drift coefficient A has to be a constant. Therefore, under this construction, the form of the DDM admissible for use in LPT is given by

$$\frac{dr_i^p}{dt} = -A\, r_i^p + \Delta u_i(\boldsymbol{r}^p) = G_i(\boldsymbol{r}^p)\,. \tag{5.20}$$

Admittedly, this reduces the accuracy of the DDM-ZT, since the best results are obtained with A being a function of $\boldsymbol{r}$ and using the second diffusion term. For the purposes of a preliminary discussion, let us accept this deficiency and consider equation (5.20) to be the DDM we want to use. Then, we can identify the following issues related to using the DDM in a single-particle framework:

- Consider equation (5.18) for all possible *unique* particle-pairs. Casting it as a linear system with M unknowns and $M(M-1)/2$ equations, we can show that we only have a solution under the condition of linearity of $\boldsymbol{G}(\boldsymbol{r})$. Also, we can only get unique solutions for $M-1$ particles, depending on how we evolve 1 of the particles in the system. We need to evaluate how the evolution equation for this 1 particle affects the entire system. The results of the DDM using the SPS framework seems to indicate an insensitivity of the two-particle statistics to the details of the single-particle evolution, but this needs to be tested.
- Searching for pairs by brute force method is a $\mathcal{O}(M^2)$ process. Instead, since

we are interested only in particle-pairs within a certain separation, we can use the cell-index method (Allen and Tildesley, 1987) which reduces the cost to $\mathcal{O}(M^2/n_c^3)$, where we divide our simulation box into n_c^3 cells. This method is suitable for parallelization, and searching for particle-pairs that lie across processors is possible. However, since we are interested in finding unique pairs, using this method in parallel only allows us to use a one-sided neighborhood search that restricts our search to half of the neighboring cells (the concept is described, in a different context, in Sundaram and Collins, 1996). Searching over all of the neighboring cells for unique pairs would require performing the search one processor at a time with additional communication between processors, slowing down the calculation considerably.

- As with the SPS framework, our results should be independent of the threshold distance R within which we search for pairs, as long as it is within the dissipation range. Now, the DDM has been tested using a locally linear flow assumption. Even with $R < \mathcal{O}(\eta)$, the approximation of a locally linear flow is not exact, and with reduction in R, the approximation gets better. It is necessary to consider if the departure from locally linear flow affects the results from the DDM.

- The model results for the RDF should converge irrespective of the number of particles, as long as we have enough particles to sample the flow adequately and obtain good statistics. A related issue is the sensitivity of the results to particles that do not find a pair. For a given R, at each time-step, there is likely to be a number of particles for which we do not find a unique pair. This depends on the total number of particles simulated and the value of R, but for practical particle populations, this seems unavoidable. Therefore, we require a way to evolve these 'loner' particles at each time-step. We have to

check whether our results are sensitive to how we deal with loner particles. This issue is necessarily coupled with the issue of convergence with R, since for a fixed population, reducing R is likely to increase the number of loner particles.

5.6 Conclusions

In this paper, we have presented a new framework for modeling the effect of subgrid scales on inertial particle clustering in a LES. In this new approach, instead of modeling the unresolved velocity field seen by inertial particles, we derive model equations governing inertial particle motion from existing statistical mechanical theories of particle clustering. We consider two theories (CT and ZT) and call the models Drift-Diffusion Models (DDMs) based on their form. A key feature of these models is that they are formulated in a relative reference frame, and the one's considered in this paper are valid in the dissipation range of the turbulence. Therefore, we use the SPS framework to develop and test these models against DNS data. We show that the DDM-CT cannot predict c_1 accurately beyond $St = 0.05$, whereas DDM-ZT works for $St \leq 0.2$. We show that the drift in DDM-ZT requires the specification of $\boldsymbol{\nabla} \cdot \boldsymbol{S}_2^p$, and derive an analytical form for the same in the limit of $St \ll 1$. Finally, we provide a preliminary assessment of some issues related to implementing the DDMs in a LPT framework.

5.7 Appendix A: Analytical expression for the drift coefficient from the ZT

Let us begin with the expression for the drift velocity in the ZT

$$\begin{aligned} d_i &= -St\,\tau_\eta\,\tfrac{\partial}{\partial r_j} S^p_{2ij} \\ &= -St\,\tau_\eta\,\tfrac{\partial}{\partial r_j}\left[St\,\tau_\eta\,\mathcal{M}_{ij} - \tfrac{St\,\tau_\eta}{2}\tfrac{\partial}{\partial r_k} S^p_{3ijk}\right] \\ &= d_i^{(1)} + d_i^{(2)}\,. \end{aligned} \tag{5.21}$$

Here the tensor $\boldsymbol{\mathcal{M}}$ is given by

$$\mathcal{M}_{ji}(\boldsymbol{r}) = \frac{r_m r_n}{N_S}\left\langle S_{jm} S_{in}\right\rangle + \frac{r_m r_n}{N_R}\left\langle R_{jm} R_{in}\right\rangle\,, \tag{5.22}$$

where N_R and N_S are defined in equation (5.8), and the ZT predictions for S^p_{2ij} (at statistically stationary state in homogeneous isotropic turbulence, for low St) is given by

$$S^p_{2ij} = St\,\tau_\eta\,\mathcal{M}_{ij} - \frac{St\,\tau_\eta}{2}\frac{\partial}{\partial r_k} S^p_{3ijk}\,. \tag{5.23}$$

In equation (5.21), $d_i^{(1)} = -St\,\tau_\eta\,\frac{\partial}{\partial r_j}\left[St\,\tau_\eta\,\mathcal{M}_{ij}\right]$ denotes the 'local' contribution to the drift velocity, whereas $d_i^{(2)} = St\,\tau_\eta\,\frac{\partial}{\partial r_j}\left[\frac{St\,\tau_\eta}{2}\frac{\partial}{\partial r_k} S^p_{3ijk}\right]$ is the 'non-local' contribution. For more details, the reader is referred to the excellent physical explanation of the drift in the ZT given in Bragg and Collins (2013a). In essence, the 'non-local' contribution $d_i^{(2)}$ in the ZT arises due to the ability of a particle-pair to retain the memory of the scales that it had encountered before arriving at their present separation. As we shall see, this 'non-local' drift velocity is the major contributor to the total drift velocity and entirely responsible for a *negative* drift velocity that leads to clustering. Let us first analyze the local drift velocity. Since we are focussed on the dissipation range of isotropic turbulence in this work, we consider

the following definitions of the strain-rate and rotation-rate structure functions.

$$\begin{aligned}\Sigma_{ij}(\boldsymbol{r}) &= \langle S_{ik}r_k S_{jn}r_n\rangle = \tfrac{\epsilon}{20\nu}\left(r^2\delta_{ij}+\tfrac{r_i r_j}{3}\right), \\ \Omega_{ij}(\boldsymbol{r}) &= \langle R_{ik}r_k R_{jn}r_n\rangle = \tfrac{\epsilon}{12\nu}\left(r^2\delta_{ij}-r_i r_j\right).\end{aligned} \tag{5.24}$$

Here, ϵ denotes the energy dissipation rate. Then, we have

$$\begin{aligned}d_i^{(1)} &= -(St\,\tau_\eta)^2\tfrac{\partial}{\partial r_j}\mathcal{M}_{ij} \\ &= -(St\,\tau_\eta)^2\tfrac{\partial}{\partial r_j}\left[\tfrac{\Sigma_{ij}}{N_S}+\tfrac{\Omega_{ij}}{N_R}\right] \\ &= -\tfrac{(St\,\tau_\eta)^2}{6\tau_\eta^2}\left[\tfrac{1}{N_S}-\tfrac{1}{N_R}\right]r_i\,.\end{aligned} \tag{5.25}$$

If we consider our DNS values for the Lagrangian time-scales $\mathcal{T}_S^L \approx 2.1\tau_\eta$ and $\mathcal{T}_R^L \approx 8.8\tau_\eta$, we find that $N_S > N_R$, implying $d_i^{(1)} > 0$. This means that the local contribution to the drift velocity is always positive. The negative drift velocity leading to clustering must, therefore, be entirely due to the non-local drift velocity $d_i^{(2)}$. To derive an usable expression for $d_i^{(2)}$, let us begin with the ZT closure for the third-order particle velocity structure function $\boldsymbol{S}_3^p$.

$$S_{3ijk}^p(\boldsymbol{r}) = -\frac{St\,\tau_\eta}{3}\left[\left(S_{2in}^p+\mathcal{L}_{in}\right)\frac{\partial}{\partial r_n}S_{2jk}^p+\left(S_{2jn}^p+\mathcal{L}_{jn}\right)\frac{\partial}{\partial r_n}S_{2ik}^p+\left(S_{2kn}^p+\mathcal{L}_{kn}\right)\frac{\partial}{\partial r_n}S_{2ij}^p\right], \tag{5.26}$$

where the tensor $\boldsymbol{\mathcal{L}}$ is given by

$$\mathcal{L}_{ji}(\boldsymbol{r}) = \frac{r_m r_n \mathcal{T}_S^L}{N_S}\langle S_{jm}S_{in}\rangle + \frac{r_m r_n \mathcal{T}_R^L}{N_R}\langle R_{jm}R_{in}\rangle\,. \tag{5.27}$$

In the ZT, equation (5.26) is arrived at by assuming that $\boldsymbol{S}_4^p$ behaves similar to the fourth order moments of a Gaussian distribution, thereby closing the hierarchy of moment equations and relating $\boldsymbol{S}_4^p$ with $\boldsymbol{S}_2^p$ (Bragg and Collins, 2013a). In order to make equation (5.26) analytically tractable, we neglect the $\boldsymbol{S}_2^p$ terms pre-mulitplying the gradients of $\boldsymbol{S}_2^p$. Bragg and Collins (2013a) have shown that in the limit of $St \ll 1$, the dynamics of particle relative velocities are strongly coupled to the underlying flow-field $\Delta\boldsymbol{u}$, implying $\boldsymbol{\mathcal{L}} \gg \boldsymbol{S}_2^p$. Hence this assumption is valid as long as we are in the low St regime. To compute the gradients of $\boldsymbol{S}_2^p$ in the

expression for $\boldsymbol{S}_3^p$, we further assume that $S_{2ij}^p \approx St\,\tau_\eta\,\mathcal{M}_{ij}$. We then end up with the following expression for the non-local drift velocity

$$d_i^{(2)} = -\frac{(St\,\tau_\eta)^4}{6}\frac{\partial^2}{\partial r_j \partial r_k}\left[\mathcal{L}_{in}\frac{\partial}{\partial r_n}\mathcal{M}_{jk} + \mathcal{L}_{jn}\frac{\partial}{\partial r_n}\mathcal{M}_{ik} + \mathcal{L}_{kn}\frac{\partial}{\partial r_n}\mathcal{M}_{ij}\right], \qquad (5.28)$$

where the tensors $\boldsymbol{\mathcal{M}}$ and $\boldsymbol{\mathcal{L}}$ are given by equations (5.22) and (5.27) respectively. We can simplify the above equation using equations (5.22), (5.27) and (5.24) to obtain

$$d_i^{(2)} = -\frac{(St\,\tau_\eta)^4}{6}\left[\frac{\mathcal{T}_S^L}{N_S^2}\left\{\frac{7}{60}+\frac{1}{6}\right\} - \frac{\mathcal{T}_S^L+\mathcal{T}_R^L}{12N_SN_R} + \frac{\mathcal{T}_R^L}{N_R^2}\left\{\frac{1}{4}+\frac{1}{6}\right\}\right] r_i\,. \qquad (5.29)$$

Hence, combining equations (5.25) and (5.29), we get the total drift velocity to be

$$\begin{aligned} d_i &= d_i^{(1)} + d_i^{(2)} \\ &= -\tfrac{(St\,\tau_\eta)^2}{6\tau_\eta^2}\left[\tfrac{1}{N_S}-\tfrac{1}{N_R}\right] r_i - \tfrac{(St\,\tau_\eta)^4}{6}\left[\tfrac{\mathcal{T}_S^L}{N_S^2}\left\{\tfrac{7}{60}+\tfrac{1}{6}\right\} - \tfrac{\mathcal{T}_S^L+\mathcal{T}_R^L}{12N_SN_R} + \tfrac{\mathcal{T}_R^L}{N_R^2}\left\{\tfrac{1}{4}+\tfrac{1}{6}\right\}\right] r_i \\ &= -A\,r_i\,, \end{aligned} \qquad (5.30)$$

where A is the drift coefficient shown in equation (5.8).

5.8 Acknowledgments

We thank Andrew D Bragg for assisting in the derivation of the DDMs from the theories. This study was supported by the National Science Foundation under grant number CBET 0756510 and 0967349. The authors gratefully acknowledge the Texas Advanced Computing Center (TACC) at The University of Texas at Austin for providing HPC resources on Ranger that have contributed to the research results reported within this paper. This work used the Extreme Science and Engineering Discovery Environment (XSEDE), which is supported by National Science Foundation grant number OCI-1053575.

CHAPTER 6

CONCLUSIONS

6.1 Summary and contribution

1. In chapter 2 (Ray and Collins, 2011), we have shown the effect of velocity filtering on the RDF and relative velocity statistics of inertial particles, for the first time across the entire range of particle Stokes numbers and particle separation distances.

   (a) We show the non-monotonic response of the RDF to filtering, both visually and statistically. This can be explained by noting that at low St, the small-scales drive the clustering and hence, removing the small-scales via filtering reduces the RDF. However, at high St, the small-scales act to randomize the motion of the particles and therefore, their absence causes the RDF to increase.

   (b) In contrast to the RDF, the statistics of w_r vary monotonically with filtering. This is because the tails of the PDF of w_r are attenuated in the filtered velocity field at all St, due to the absence of small-scale fluctuations.

   (c) We find a hitherto unexplored relationship between the skewness of the PDF of w_r and the RDF, establishing a way in which the relative velocity distribution of the particles influence their spatial distribution.

   (d) We consider a simple model to account for the subgrid scales, based on a scale-shifted Stokes number defined with respect to the time-scale of the filtered velocity field, and show that it does not recover the correct RDF

and relative velocity statistics. This suggests that we need to model the *mechanism* by which the subgrid scales affect particle clustering.

(e) We consider the effect of filter-scale and find a linear response for both the RDF and the statistics of w_r, when the filter-scale lies in the inertial range.

(f) We confirm previous findings on the Reynolds number dependence of the RDF and the PDF of w_r over a larger range of R_λ.

2. In chapter 3 (Ray and Collins, 2013b), we consider a Kinematic Simulation based SubGrid Model (KSSGM) and for the first time, apply it to compute the RDF and $\langle w_r \rangle^{(-)}$from a FDNS flow field.

(a) We show that the KSSGM is an inexpensive LES subgrid model with no arbitrarily adjustable constants.

(b) The KSSGM is able to capture the effect of filtering on $\langle w_r \rangle^{(-)}$, both qualitatively and quantitatively at all St.

(c) The KSSGM is able to capture the non-monotonic effect of filtering on the RDF, with quantitative agreement with DNS only for $St \geq 2.0$.

(d) We show that the reason the KSSGM fails to capture the RDF at $St < 2.0$ is related to its inability to capture the difference between the Lagrangian time-scales of the rotation-rate at small and large St. This means that it is unable to predict the effect of the small-scale coherent structures on inertial particles, which is critical to predicting clustering for $St < 2.0$.

3. In chapter 4 (Ray and Collins, 2013a), we develop a novel satellite particle simulation (SPS) methodology for investigating pair-wise interactions of inertial particles in the dissipation range of turbulence.

(a) We show that the power c_1 in the power-law form of the RDF is determined *solely* by the dissipation range dynamics of the turbulence irrespective of the St, whereas the pre-factor c_0 is determined by the larger scales.

(b) c_1 obtained from FSPS agrees with FDNS for all St, indicating that the SPS can be used for *a priori* testing of LES models formulated in the two-particle framework.

(c) We also consider the structure functions of inertial particles, and show that their exponents are captured by the SPS up to $St \approx 0.5$. The SPS is also able to capture the correct St at which the caustics (or the 'sling effect') start affecting the relative velocity statistics, and captures the correct rate of caustic activation.

4. In chapter 5 (Ray et al., 2013), we develop a new subgrid modeling framework to capture clustering of low-inertia particles.

(a) We consider two-particle models (referred to as Drift-Diffusion Models (DDMs)) that are based on existing theories of clustering (the theories by Chun et al. (2005) (CT) and Zaichik and Alipchenkov (2009) (ZT)).

(b) We show the derivation of a DDM starting from a general statistical mechanical framework, and use the SPS to test the DDMs.

(c) The DDM-CT gives good agreement with DNS results for $St \leq 0.05$, whereas the DDM-ZT works well for $St \leq 0.2$.

(d) We show that the DDM-ZT can be improved by improving the model for the divergence of the particle structure function ($\boldsymbol{\nabla} \cdot \boldsymbol{S}_2^p$), which is the only statistical input it requires.

(e) We also discuss some issues related to implementing the DDMs in a single-particle tracking framework for use with LES+LPT.

Therefore, in this work, we have advanced the understanding of the how the subgrid scales in a LES affect the RDF and relative velocity statistics of inertial particles, and hence their collision kernel. To the best of our knowledge, we have shown the first application of the KSSGM for collision-related statistics of inertial particles. The KSSGM allowed us to identify that describing the small-scale coherent structures of turbulence may be the key to predicting clustering, especially at $St < 2.0$. We recognize the difficulty in obtaining such statistics from a modeled subgrid velocity field at a particle location, and shift our attention to a two-particle modeling framework. We develop a novel satellite particle simulation (SPS) methodology that allows us to efficiently simulate particle-pair interactions at small separations. The SPS allows us to determine that the power-law c_1 of the RDF is determined *solely* by the small-scales of the turbulence, whereas the pre-factor c_0 depends on the outer scales. We then derive new models, that we refer to as Drift-Diffusion Models (DDMs) from two existing theories of clustering (Chun et al. (2005) (CT), and Zaichik and Alipchenkov (2009) (ZT)). A key feature of these models (and the theories) is that they are formulated in a reference frame consisting of particle relative separations and relative velocities, as opposed to their absolute positions and velocities. The DDMs constitute an entirely new way of modeling the motion of inertial particles to capture their clustering. We use the SPS framework to test the DDMs. We show that the DDM-CT works for $St \leq 0.05$, while the DDM-ZT gives good agreement with DNS for $St \leq 0.2$. Overall, the DDMs appear promising as the first LES models that can capture the clustering of low St particles in turbulence.

6.2 Future directions

One of the major findings from the study of the KSSGM has been understanding the importance of correctly describing the small-scale coherent structures in a subgrid model for predicting the RDF at $St < 2.0$. Progress in this area could be focused designing subgrid models that can correctly predict the Lagrangian time-scales of rotation-rate seen by inertial particles. The KSSGM has the added advantage that it can be adapted to inhomogeneous flows (Khan et al., 2010; Clark and Vassilicos, 2011), and has been shown to provide improved predictions of the particle deposition in LES of turbulent channel flows (Khan et al., 2010). Studies of inertial particle clustering in highly anisotropic flows have begun only recently. Nicolai et al. (2011) explored clustering in homogeneous turbulent shear flow, and found that in contrast to isotropic flows, the particles orient themselves preferentially along a direction dependent on the direction of mean shear. However, they also found discrepancies in their experimental and numerical results for whether the particle distribution 'returns to isotropy' at small-scales. Therefore, a better understanding of small-scale clustering in highly anisotropic flows is necessary before an appraisal of LES subgrid models can be done.

An important consideration in LES subgrid models is the dependence of model performance on the filter-scale. The KSSGM does not explicitly depend on the filter-scale, but implicitly through the approximation of the energy spectrum. Since the effect of turbulence on the collision kernel is dependent on dissipation range dynamics, we do not expect the performance of the KSSGM to change with filter-scale. We find that simple linear relations exist when looking at both the RDF and statistics of w_r in a FDNS, as a function of filter-scale in the inertial range (Ray and Collins, 2011). However, for quantities that are governed by dynamics in the

inertial range and beyond, the effect of filter-scale needs to studied carefully.

We have considered an alternative to the conventional single-particle modeling approach, by constructing two-particle models, and demonstrated their promise in the low St regime. This approach has the important advantage of being supported by existing theories. Therefore, we can expect improvements in two-particle models to go hand-in-hand with advancements in the theoretical understanding of turbulence-induced collisions and clustering. A major step in the viability of the two-particle models (such as DDMs) is the ability to use them in a single-particle tracking framework. Once this is accomplished, these models can be used for tracking low St particles in a LES to predict their clustering.

In a typical cloud, the rain drops have a certain size distribution (i.e., a polydisperse droplet distribution) and gravity plays an important role. Incorporating these in the formulations of both the KSSGM and the DDMs is trivial. However, the models need to be tested for the additional physics and parametric dependencies that are introduced by gravity and polydispersity. In an actual cloud-resolving LES calculation (e.g., see Stevens et al., 2005) containing thermodynamic effects, etc. that have been ignored in this work, our interest is to provide the correct parameterization of the microphysical transformations arising from droplet collisions. For details on the microphysical models used in LES of clouds, refer to Savic-Jovcic and Stevens (2008), and references therein. Our models can be used to compute the collision kernel from a simplified LES and improve this parameterization. An important consideration with such an approach is the huge gap in Reynolds numbers ($R_\lambda \sim 10^4$ in clouds (Warhaft, 2009)) and domain sizes (Wang et al., 2011) in an actual cloud, with what can be achieved in DNS, and even in a well-resolved LES. Fortunately, in the low St regime that is of importance to clouds, both the

RDF and the PDF of w_r seem to be relatively insensitive to R_λ (again in the limited range achieved by DNS).

Finally, we have performed *a priori* tests of the subgrid models, in order to identify their merits and shortcomings. However, the ultimate test of a subgrid model is *a posteriori*, when it is used in an actual calculation. Typically, the models described in this work will be used for the particles, in conjunction with other models used to close the filtered Navier-Stokes equation. These closure models will affect the accuracy of the represented scales in the LES, and the effect of such errors on the particle statistics need to be studied.

BIBLIOGRAPHY

Ahluwalia, A. (2002). Preferential concentration of finite Stokes number particles in homogeneous isotropic turbulent flow. Master's thesis, The Pennsylvania State University.

Aliseda, A., Cartellier, A., Hainaux, F., and Lasheras, J. C. (2002). Effect of preferential concentration on the settling velocity of heavy particles in homogeneous isotropic turbulence. *J. Fluid Mech.*, 468:77–105.

Allen, M. P. and Tildesley, D. J. (1987). *Computer simulation of liquids*. Oxford University Press, Oxford.

Armenio, V., Piomelli, U., and Fiorotto, V. (1999). Effect of the subgrid scales on particle motion. *Phys. Fluids*, 11:3030–3042.

Ayala, O., Rosa, B., and Wang, L. P. (2008a). Effects of turbulence on the geometric collision rate of sedimenting droplets. part 2. theory and parameterization. *New J. Phys.*, 10 075016.

Ayala, O., Rosa, B., Wang, L. P., and Grabowski, W. W. (2008b). Effects of turbulence on the geometric collision rate of sedimenting droplets. part 1. results from direct numerical simulation. *New J. Phys.*, 10 075015.

Bateson, C. P. and Aliseda, A. (2012). Wind tunnel measurements of the preferential concentration of inertial droplets in homogeneous isotropic turbulence. *Exp. Fluids*, 52(6):1373–1387.

Bec, J., Biferale, L., Cencini, M., Lanotte, A. S., and Toschi, F. (2010). Intermittency in the velocity distribution of heavy particles in turbulence. *J. Fluid Mech.*, 646:527–536.

Bec, J., Celani, A., Cencini, M., and Musacchio, S. (2005). Clustering and collisions of heavy particles in random smooth flows. *Phys. Fluids*, 17:073301.

Berrouk, A. S., Laurence, D., Riley, J. J., and Stock, D. E. (2007). Stochastic modelling of inertial particle dispersion by subgrid motion for les of high reynolds number pipe flow. *J. Turb.*, 8(50):1–20.

Berrut, J. P. and Trefethen, L. N. (2004). Barycentric Lagrange interpolation. *Siam Rev.*, 46:501–517.

Bini, M. and Jones, W. P. (2007). Particle acceleration in turbulent flows: A class of nonlinear stochastic models for intermittency. *Phys. Fluids*, 19(3):035104.

Bini, M. and Jones, W. P. (2008). Large-eddy simulation of particle-laden turbulent flows. *J. Fluid Mech.*, 614:207–252.

Boivin, M., Simonin, O., and Squires, K. D. (2000). On the prediction of gas-solid flows with two-way coupling using large eddy simulation. *Phys. Fluids*, 12:2080–2090.

Bragg, A. D. and Collins, L. R. (2013a). New insights from comparing statistical theories for inertial particles in turbulence. Part I. Spatial distribution of particles. *New J. Phys. (In review).*

Bragg, A. D. and Collins, L. R. (2013b). New insights from comparing statistical theories for inertial particles in turbulence. Part II. Relative velocities of particles. *New J. Phys. (In review).*

Brucker, K. A., Isaza, J. C., Vaithianathan, T., and Collins, L. R. (2007). Efficient algorithm for simulating homogeneous turbulent shear flow without remeshing. *J. Comp. Phys.*, 225:20–32.

Brunk, B. K., Koch, D. L., and Lion, L. W. (1998). Turbulent coagulation of colloidal particles. *J. Fluid Mech.*, 364:81–113.

Caraeni, D., Bergström, C., and Fuchs, L. (2000). Modeling of liquid fuel injection, evaporation and mixing in a gas turbine burner using large eddy simulations. *Flow Turb. Combust.*, 65(2):223–244.

Cernick, M. J. (2013). Particle subgrid scale modeling in large-eddy simulation of particle-laden turbulence. Master's thesis, McMaster University. Open Access Dissertations and Theses. Paper 7664.

Chevillard, L. and Meneveau, C. (2006). Lagrangian dynamics and statistical geometric structure of turbulence. *Phys. Rev. Lett.*, 97:174501.

Chun, J., Koch, D. L., Rani, S., Ahluwalia, A., and Collins, L. R. (2005). Clustering of aerosol particles in isotropic turbulence. *J. Fluid Mech.*, 536:219–251.

Clark, N. and Vassilicos, J. (2011). Kinematic simulation of fully developed turbulent channel flow. *Flow, Turb. Combust.*, 86:263–293.

Collins, L. R. and Keswani, A. (2004). Reynolds number scaling of particle clustering in turbulent aerosols. *New J. Phys.*, 6:119.

Crowe, C. T., editor (2005). *Multiphase Flow Handbook*. Mechanical and Aerospace Engineering Series. CRC Press.

Crowe, C. T., Sommerfeld, M., and Tsuji, Y. (1998). *Multiphase Flows with Droplets and Particles*. CRC Press.

de Jong, J., Salazar, J. P. L. C., Cao, L., Woodward, S. H., Collins, L. R., and Meng, H. (2010). Measurement of inertial particle clustering and relative velocity

statistics in isotropic turbulence using holographic imaging. *Int. J. Multiphase Flow*, 36:324–332.

Devenish, B. J., Bartello, P., Brenguier, J.-L., Collins, L. R., Grabowski, W. W., IJzermans, R. H. A., Malinowski, S. P., Reeks, M. W., Vassilicos, J. C., Wang, L.-P., and Warhaft, Z. (2012). Droplet growth in warm turbulent clouds. *Quart. J. Royal Meteor. Soc.*, 138(667):1401–1429.

Duncan, K., Mehlig, B., Östlund, S., and Wilkinson, M. (2005). Clustering by mixing flows. *Phys. Rev. Lett.*, 95:240602.

Eaton, J. K. and Fessler, J. R. (1994). Preferential concentration of particles by turbulence. *Int. J. Multiphase Flow*, 20:169–209.

Falkovich, G., Fouxon, A., and Stepanov, M. G. (2002). Acceleration of rain initiation by cloud turbulence. *Nature*, 419:151–154.

Falkovich, G. and Pumir, A. (2007). Sling effect in collisions of water droplets in turbulent clouds. *J. Atm. Sci.*, 64:4497.

Fede, P. and Simonin, O. (2006). Numerical study of the subgrid fluid turbulence effects on the statistics of heavy colliding particles. *Phys. Fluids*, 18:045103.

Fede, P., Simonin, O., P.Villedieu, and Squires, K. D. (2006). Stochastic modeling of turbulent subgrid fluid velocity along inertia particle trajectories. In *Proceedings of the 2006 CTR Summer Program (Center for Turbulence Research, Stanford, CA)*, pages 247–258.

Fessler, J. R., Kulick, J. D., and Eaton, J. K. (1994). Preferential concentration of heavy particles in a turbulent channel flow. *Phys. Fluids*, 6:3742–3749.

Flohr, P. and Vassilicos, J. C. (2000). A scalar subgrid model with flow structure for large-eddy simulations of scalar variances. *J. Fluid Mech.*, 407:315–349.

Fukagata, K., Zahrai, S., and Bark, F. (2004). Dynamics of brownian particles in a turbulent channel flow. *Heat and Mass Transfer*, 40(9):715–726.

Fung, J. C. H., Hunt, J. C. R., Malik, N. A., and Perkins, R. J. (1992). Kinematic simulation of homogeneous turbulence by unsteady random fourier modes. *J. Fluid Mech.*, 236:281–318.

Germano, M., Piomelli, U., Moin, P., and Cabot, W. H. (1991). A dynamic subgrid-scale eddy viscosity model. *Phys. Fluids A*, 3:1760–1765.

Gibert, M., Xu, H., and Bodenschatz, E. (2012). Where do small, weakly inertial particles go in a turbulent flow? *J. Fluid Mech.*, 698:160–167.

Girimaji, S. S. and Pope, S. B. (1990). A diffusion model for velocity gradients in turbulence. *Phys. Fluids A*, 2:242–256.

Grabowski, W. W. and Wang, L.-P. (2012). Growth of cloud droplets in a turbulent environment. *Ann. Rev. Fluid Mech.* Submitted.

Grabowski, W. W. and Wang, L.-P. (2013). Growth of cloud droplets in a turbulent environment. *Ann. Rev. Fluid Mech.*, 45:293–324.

Hogan, R. C. and Cuzzi, J. N. (2001). Stokes and Reynolds number dependence of preferential particle concentration in simulated three-dimensional turbulence. *Phys. Fluids*, 13:2938–2945.

Ireland, P. J., Vaithianathan, T., and Collins, L. R. (2012). Massively parallel simulations of inertial particles in high-reynolds-number turbulence. In *Proceed-*

ings of ICCFD 7 - the Seventh International Conference on Computational Fluid Dynamics, July 09 - 13, 2012. Hawaii, USA.

Ireland, P. J., Vaithianathan, T., Sukheswalla, P. S., Ray, B., and Collins, L. R. (2013). Highly parallel particle-laden flow solver for turbulence research. *Computers & Fluids*, 76:170 –177.

Jin, G., He, G.-W., and Wang, L.-P. (2010a). Large-eddy simulation of turbulent collision of heavy particles in isotropic turbulence. *Phys. Fluids*, 22:055106.

Jin, G., He, G.-W., Wang, L.-P., and Zhang, J. (2010b). Subgrid scale fluid velocity timescales seen by inertial particles in large-eddy simulation of particle-laden turbulence. *Int. J. Multiphase Flow*, 36:432–437, Brief Communication.

Johansen, A., Oishi, J. S., Low, M.-M. M., Klahr, H., Henning, T., and Youdin, A. (2007). Rapid planetesimal formation in turbulent circumstellar disks. *Nature*, 448:1022–1025.

Johnson, R. W., editor (1998). *The Handbook of Fluid Dynamics*, chapter Mathematics of Fluid Mechanics. CRC Press.

Kerstein, A. R. and Krueger, S. K. (2006). Clustering of randomly advected low-inertia particles: A solvable model. *Phys. Rev. E*, 73:025302.

Khan, M. A. I., Luo, X. Y., Nicolleau, F. C. G. A., Tucker, P. G., and Lo Iacono, G. (2010). Effects of les sub-grid flow structure on particle deposition in a plane channel with a ribbed wall. *Int. J. Num. Meth. Biomedical Eng.*, 26(8):999–1015.

Kim, W.-W., Menon, S., and Mongia, H. C. (1999). Large-eddy simulation of a gas turbine combustor flow. *Combust. Sci. Tech.*, 143(1-6):25–62.

Kraichnan, R. H. (1970). Diffusion by a random velocity field. *Phys. Fluids*, 13:22–31.

Kuerten, J. G. M. (2006). Subgrid modeling in particle-laden channel flow. *Phys. Fluids*, 18(2):025108.

Kuerten, J. G. M. (2008). *Quality and Reliability of Large-Eddy Simulations*, chapter Large-Eddy Simulation of Particle-Laden Channel Flow, pages 367–378. Springer Netherlands.

Li, W.-I., Perzl, M., Heyder, J., Langer, R., Brain, J. D., Englmeier, K.-H., Niven, R. W., and Edwards, D. A. (1996). Aerodynamics and aerosol particle deaggregation phenomena in model oral-pharyngeal cavities. *J. Aerosol Sci.*, 27(8):1269 – 1286.

Lu, J., Nordsiek, H., and Shaw, R. A. (2010). Clustering of settling charged particles in turbulence: theory and experiments. *New J. Phys.*, 12(12):123030.

Malik, N. A. and Vassilicos, J. C. (1999). A lagrangian model for turbulent dispersion with turbulent-like flow structure: Comparison with direct numerical simulation for two-particle statistics. *Phys. Fluids*, 11(6):1572–1580.

Marchioli, C., Salvetti, M. V., and Soldati, A. (2008). Some issues concerning large-eddy simulation of inertial particle dispersion in turbulent bounded flows. *Phys. Fluids*, 20:040603.

Mason, P. J. (1994). Large-eddy simulation: A critical review of the technique. *Quart. J. Royal Meteor. Soc.*, 120(515):1–26.

Maxey, M. R. (1987). The gravitational settling of aerosol particles in homogeneous turbulence and random flow fields. *J. Fluid Mech.*, 174:441–465.

Maxey, M. R. and Riley, J. J. (1983). Equation of motion for a small rigid sphere in a nonuniform flow. *Phys. Fluids*, 26:883–889.

McQuarrie, D. A. (1976). *Statistical Mechanics*. Harper & Row, New York.

Metais, O. and Lesieur, M. (1992). Spectral large-eddy simulation of isotropic and stably stratified turbulence. *J. Fluid Mech.*, 239:157–194.

Monchaux, R., Bourgoin, M., and Cartellier, A. (2010). Preferential concentration of heavy particles: A vorono[i-umlaut] analysis. *Phys. Fluids*, 22(10):103304.

Moody, E. G. and Collins, L. R. (2003). Effect of mixing on nucleation and growth of titania particles. *Aerosol Sci. Tech.*, 37:403–424.

Nicolai, C., Jacob, B., Gualtieri, P., and Piva, R. (2011). Inertial particles in homogeneous shear turbulence. *J. Phys.: Conf. Ser.*, 318(5):052009.

Osborne, D. R., Vassilicos, J. C., and Haigh, J. D. (2005). One-particle two-time diffusion in three-dimensional homogeneous isotropic turbulence. *Phys. Fluids*, 17(3):035104.

Pan, L. and Padoan, P. (2010). Relative velocity of inertial particles in turbulent flows. *J. Fluid Mech.*, 661:73–107.

Pan, L., Padoan, P., Scalo, J., Kritsuk, A. G., and Norman, M. L. (2011). Turbulent clustering of protoplanetary dust and planetesimal formation. *The Astrophys. J.*, 740(1):6.

Patterson, G. S. and Orszag, S. A. (1971). Spectral calculation of isotropic turbulence: efficient removal of aliasing interactions. *Phys. Fluids*, 14:2538–2541.

Pinsky, M. B. and Khain, A. P. (1997). Turbulence effects on droplet growth and size distribution in clouds—a review. *J. Aerosol Sci.*, 28:1177–1214.

Poinsot, T. (2010). Large eddy simulation of real combustors. In Sengupta, T. and Poinsot, T., editors, *Instabilities of Flows: With and Without Heat Transfer and Chemical Reaction*, volume 517 of *CISM International Centre for Mechanical Sciences*, pages 251–266. Springer Vienna.

Pope, S. B. (2000). *Turbulent Flows*. Cambridge University Press, New York.

Pope, S. B. (2004). Ten questions concerning the large-eddy simulation of turbulent flows. *New J. Phys.*, 6(1):35.

Pozorski, J. and Apte, S. V. (2009). Filtered particle tracking in isotropic turbulence and stochastic modeling of subgrid-scale dispersion. *Int. J. Multiphase Flow*, 35:118–128.

Ray, B., Bragg, A. D., and Collins, L. R. (2013). A new subgrid modelling framework for inertial particle clustering in large-eddy simulations of turbulence: Low-inertia particles. *J. Fluid Mech. (In preparation)*.

Ray, B. and Collins, L. R. (2011). Preferential concentration and relative velocity statistics of inertial particles in Navier-Stokes turbulence with and without filtering. *J. Fluid Mech.*, 680:488–510.

Ray, B. and Collins, L. R. (2013a). Investigation of sub-kolmogorov inertial particle pair dynamics in turbulence using novel satellite particle simulations. *J. Fluid Mech.*, 720:192–211.

Ray, B. and Collins, L. R. (2013b). A subgrid model for clustering of high-inertia particles in large-eddy simulations of turbulence. *J. Turb. (Submitted)*.

Reade, W. C. and Collins, L. R. (2000a). Effect of preferential concentration on turbulent collision rates. *Phys. Fluids*, 12:2530–2540.

Reade, W. C. and Collins, L. R. (2000b). A numerical study of the particle size distribution of an aerosol undergoing turbulent coagulation. *J. Fluid Mech.*, 415:45–64.

Saffman, P. G. and Turner, J. S. (1956). On the collision of drops in turbulent clouds. *J. Fluid Mech.*, 1:16–30.

Salazar, J. P. L. C. and Collins, L. R. (2012). Inertial particle relative velocity statistics in homogeneous isotropic turbulence. *J. Fluid Mech.*, 696:45–66.

Salazar, J. P. L. C., de Jong, J., Cao, L., Woodward, S., Meng, H., and Collins, L. R. (2008). Experimental and numerical investigation of inertial particle clustering in isotropic turbulence. *J. Fluid Mech.*, 600:245–256.

Savic-Jovcic, V. and Stevens, B. (2008). The structure and mesoscale organization of precipitating stratocumulus. *J. Atmos. Sci.*, 65:1587 – 1605.

Saw, E. W., Shaw, R. A., Ayyalasomayajula, S., Chuang, P. Y., and Gylfason, A. (2008). Inertial clustering of particles in high-Reynolds-number turbulence. *Phys. Rev. Lett.*, 100:214501.

Saw, E.-W., Shaw, R. A., Salazar, J. P. L. C., and Collins, L. R. (2012). Spatial clustering of polydisperse inertial particles in turbulence: Ii. comparing simulation with experiment. *New J. Phys.*, 14(10):105031.

Shaw, R. A. (2003). Particle-turbulence interactions in atmospheric clouds. *Annu. Rev. Fluid Mech.*, 35:183–227.

Shaw, R. A., Kostinski, A. B., and Larsen, M. L. (2002). Towards quantifying droplet clustering in clouds. *Quart. J. Royal Meteor. Soc.*, 128(582):1043–1057.

Shaw, R. A., Reade, W. C., Collins, L. R., and Verlinde, J. (1998). Preferential concentration of cloud droplets by turbulence: effects on the early evolution of cumulus cloud droplet spectra. *J. Atmos. Sci.*, 55:1965–1976.

Shotorban, B. and Mashayek, F. (2005). Modeling subgrid-scale effects on particles by approximate deconvolution. *Phys. Fluids*, 17:081701.

Shotorban, B. and Mashayek, F. (2006a). On stochastic modeling of heavy particle dispersion in large-eddy simulation of two-phase turbulent flow. In *IUTAM Symposium on Computational Multiphase Flow*, pages 373–380. Springer, Netherlands.

Shotorban, B. and Mashayek, F. (2006b). A stochastic model for particle motion in large-eddy simulation. *J. Turb.*, 7 N11.

Smagorinsky, J. (1963). General circulation experiments with the primitive equations. *Mon. Wea. Rev.*, 91:99–164.

Squires, K. D. and Eaton, J. K. (1991). Preferential concentration of particles by turbulence. *Phys. Fluids A*, 3:1169–1178.

Stevens, B., Moeng, C.-H., Ackerman, A. S., Bretherton, C. S., Chlond, A., de Roode, S., Edwards, J., Golaz, J.-C., Jiang, H., Khairoutdinov, M., Kirkpatrick, M. P., Lewellen, D. C., Lock, A., MÃijller, F., Stevens, D. E., Whelan, E., and Zhu, P. (2005). Evaluation of large-eddy simulations via observations of nocturnal marine stratocumulus. *Mon. Wea. Rev.*, 133:1443 – 1462.

Sundaram, S. and Collins, L. R. (1996). Numerical considerations in simulating a turbulent suspension of finite-volume particles. *J. Comput. Phys.*, 124:337–350.

Sundaram, S. and Collins, L. R. (1997). Collision statistics in an isotropic, particle-laden turbulent suspension. Part I. direct numerical simulations. *J. Fluid Mech.*, 335:75–109.

Sundaram, S. and Collins, L. R. (1999). A numerical study of the modulation of isotropic turbulence by suspended particles. *J. Fluid Mech.*, 379:105–143.

Taghipour, F., Ellis, N., and Wong, C. (2005). Experimental and computational study of gasâĂŞsolid fluidized bed hydrodynamics. *Chem. Eng. Sci.*, 60(24):6857 – 6867.

Ulitsky, M. and Collins, L. R. (1997). Relative importance of coherent structures vs background turbulence in the propagation of a premixed flame. *Combust. Flame*, 111:257–275.

Vaillancourt, P. A. and Yau, M. K. (2000). Review of particle-turbulence interactions and consequences for cloud physics. *Bull. Am. Meteor. Soc.*, 81:285–298.

Wang, L.-P., Ayala, O., Parishani, H., Grabowski, W. W., Wyszogrodzki, A. A., Piotrowski, Z., Gao, G. R., Kambhamettu, C., Li, X., Rossi, L., Orozco, D., and Torres, C. (2011). Towards an integrated multiscale simulation of turbulent clouds on petascale computers. *J. Phys.: Conf. Ser.*, 318(7):072021.

Wang, L. P., Chen, S., Brasseur, J. G., and Wyngaard, J. C. (1996). Examination of hypotheses in kolmogorov refined turbulence theory through high-resolution simulations. i. velocity field. *J. Fluid Mech.*, 309:113.

Wang, L. P. and Maxey, M. R. (1993). Settling velocity and concentration distribution of heavy particles in homogeneous isotropic turbulence. *J. Fluid Mech.*, 256:27–68.

Wang, L.-P., Wexler, A. S., and Zhou, Y. (2000). Statistical mechanical description and modeling of turbulent collision of inertial particles. *J. Fluid Mech.*, 415:117–153.

Wang, Q. and Squires, K. (1996a). Large eddy simulation of particle deposition in a vertical turbulent channel flow. *Int. J. Multiphase Flow*, 22(4):667 – 683.

Wang, Q. and Squires, K. D. (1996b). Large eddy simulation of particle-laden turbulent channel flow. *Phys. Fluids*, 8:1207–1223.

Warhaft, Z. (2009). Laboratory studies of droplets in turbulence: towards understanding the formation of clouds. *Fluid Dyn. Res.*, 41:011201.

Weisstein, E. W. (2013). Sphere point picking. *MathWorld – A Wolfram Web Resource. http://mathworld.wolfram.com/SpherePointPicking.html*.

Wilkinson, M., Mehlig, B., and Bezuglyy, V. (2006). Caustic activation of rain showers. *Phys. Rev. Lett.*, 97:048501.

Witkowska, A., Brasseur, J. G., and Juvé, D. (1997). Numerical study of noise from isotropic turbulence. *J. Comput. Acoust.*, 5:317–336.

Yao, H.-D. and He, G.-W. (2009). A kinematic subgrid scale model for large-eddy simulation of turbulence-generated sound. *J. Turb.*, 10(19):1–14.

Zaichik, L. I. and Alipchenkov, V. M. (2003). Pair dispersion and preferential concentration of particles in isotropic turbulence. *Phys. Fluids*, 15:1776–1787.

Zaichik, L. I. and Alipchenkov, V. M. (2007). Refinement of the probability density function model for preferential concentration of aerosol particles in isotropic turbulence. *Phys. Fluids*, 19(11):113308.

Zaichik, L. I. and Alipchenkov, V. M. (2009). Statistical models for predicting pair dispersion and particle clustering in isotropic turbulence and their applications. *New J. Phys.*, 11:103018.